MOLECULAR MECHANISMS OF BIOADHESION, BIOFOULING, AND ANTI-BIOFOULING

by

Chuan Leng

A dissertation submitted in partial fulfilment
of the requirements for the degree of
Doctor of Philosophy
(Chemistry)
in the University of Michigan
2016

Doctoral Committee:

Professor Zhan Chen, Chair
Professor Kristina I. Hakansson
Associate Professor Kenichi Kuroda
Professor Michael D. Morris

To my wife Shuwen Sun,
my parents Xiaoning Leng and Feng Xu,
and my daughter Melody

ACKNOWLEDGEMENTS

I would like to thank my research advisor Professor Zhan Chen for the wonderful experience of being his graduate student, and for his support and guidance through my PhD study. Professor Zhan Chen sets a great model for me as an excellent scientist, teacher, and supervisor. I learned from him not only how to do science, but also how to make plans and efforts for the development of my career and life.

I would like to thank Professors Michael Morris, Kristina Hakansson, and Kenichi Kuroda for their time and effort of being my committee members and for their insightful comments and advice on my PhD work.

I would like to express my gratitude to all members in the Chen lab. I cherish their help with my experiments and all the discussions. Especially, I want to thank Dr Yuwei Liu for guiding me into the research area of the lab and her extensive help with the start of the projects, and Drs Chi Zhang, Xiaofeng Han, Pei Yang, and Xingquan Zou for their expertise in laser optics and their help with the laser maintenance and alignment, which made my experiments much smoother.

I would also like to thank my collaborators, Professors Jon Wilker (Purdue University), Shaoyi Jiang (University of Washington), Greg Tew (University of Massachusetts), Dayang Wang (Royal Melbourne Institute of Technology), Rachel Segalman (UC Santa Barbara), Drs Bret Chisholm (North Dakota State University), Qing

Shao (University of Washington), Roger Hung (University of Washington), Katie Gibney (University of Massachusetts), Chelsey A Del Grosso (Purdue University), and Hilda Buss (UC Berkeley) for their expertise in materials science, and the novel polymers and biological samples they provided.

The financial supports from Office of Naval Research, Rackham Travel Grant, and George Ashworth Analytical Chemistry Fellowship are highly appreciated.

Finally, I want to thank my wife and my family. My wife, Shuwen Sun, offers me a happy and relaxed environment at home, which makes me mentally relieved at all times and is very important to keep my efficiency at work. She encourages me when there is a challenge, shares the happiness when I make an achievement, and works together with me to make life better. I also thank my parents for supporting my PhD study and making every effort to help me over the years. I am grateful for their unconditional love and support. My little daughter, Melody, has brought me so much joy since she was born in 2014. A happy and harmonious family is a strong support for me to keep confident and enthusiastic now and in the future.

TABLE OF CONTENTS

LIST OF FIGURES

LIST OF TABLES

CHAPTER 1 INTRODUCTION

1.1 Biofouling and Antifouling Polymers

Biofouling is the accumulation of biomolecules, microorganisms, algae, or animals to underwater surfaces. Such accumulation causes many issues. For naval industry, animals sticking to ship hulls can damage the surfaces, slow the ships, and cost extra fuel, which places a heavy financial burden to surface cleaning, replacement, and energy consumption.[1] For industrial engineering, biofouling on membranes, pipelines, and chemical reactors greatly impairs the efficiency of manufacturing and production.[2] Biofouling can also occur on biomedical devices being applied inside human body, because cells and microorganisms accumulate on the surfaces in body fluid, which may lead to malfunction of the devices and health complications.[3]

Antifouling materials can prevent surface adsorption of molecules and organisms and have a wide range of applications.[4] A variety of antifouling materials have been developed recently, which have different molecular structures and antifouling mechanisms. For example, biocides that can deter or kill microorganisms have been used to modify coatings to form antimicrobial surfaces (Figure 1.1A).[5] Such coatings can prevent the initial formation of biofilms created by microorganisms to prevent successive attachment of larger organisms. However, biocide based coatings may degrade overtime, which may result in leaking of the biocides and contamination of the environment.

Alternative approaches have been pursued to develop environmental benign coatings to prevent anything from sticking to the surfaces (Figure 1.1B).[6-8] For example, hydrophilic nonfouling zwitterionic materials have been developed recently, which can prevent the adsorption of biomolecules, cells, and organisms to their surfaces in complex environments. They have wide applications in marine industry and biomedical engineering.[9-12] It is believed that strong surface hydration is critical for the nonfouling property of the zwitterionic materials. The surfaces bind water molecules so strongly that other molecules cannot replace the water molecules and adsorb onto the surfaces.[13] Other antifouling materials include amphiphilic polymers. Usually hydrophilic zwitterionic or poly(ethylene glycol) (PEG) groups and hydrophobic silicone or fluorocarbon are incorporated into one polymer,[14-19] which demonstrates surface restructuring from air to water.[20] Due to the presence of both hydrophilic and hydrophobic groups, amphiphilic coatings are generally both antifouling and fouling release (Figure 1.1C), i.e., even if something attaches to the surface, it is easily washed off. In addition, bio-inspired omniphobic surfaces have been developed to combat biofouling.[21,22] These coatings take advantage of liquid fluorocarbon molecules trapped in a porous material and are super slippery.

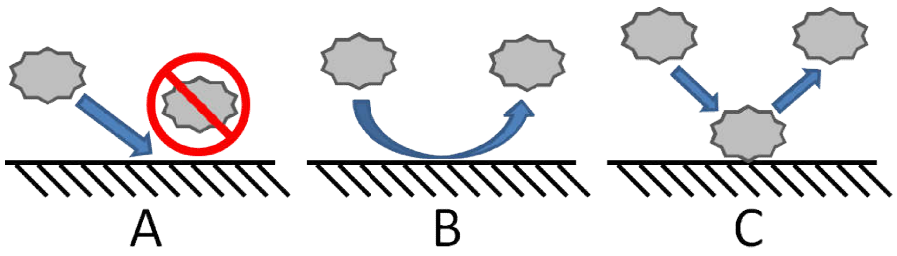

Figure 1.1 Schematic showing antifouling surfaces with different mechanisms: (A) antimicrobial, (B) nonfouling, and (C) fouling release surfaces.

As mentioned above, antifouling materials can be designed with many different molecular structures which determine their antifouling mechanisms and performances. However, detailed molecular level studies of the material surfaces have been proved challenging because commonly used surface sensitive techniques such as X-ray photoelectron spectroscopy (XPS) and electron microscopy often require vacuum to operate. Vacuum is a completely different environment compared to that where antifouling materials are being applied. Alternatively, sum frequency generation (SFG) vibrational spectroscopy is an intrinsically surface sensitive technique, which can be used to probe material surfaces in water and provide molecular-level structural information.[23] In this thesis, SFG has been applied to study the surfaces of various antifouling materials in contact with aqueous environments in situ. The SFG results have revealed the molecular mechanisms of the antifouling materials. Specifically, the surface molecular structures (i.e. the presence and orientation of certain functional groups) of the antifouling materials were investigated in air and aqueous environments. The configuration of such functional groups on the material surfaces were correlated to their antifouling properties. Because antifouling materials are expected to be used in aqueous environments, we focused on the surface structures of the materials in various aqueous solutions (with different pH and ions). Further, the critical role of the water molecules at the material surfaces under various conditions was examined and then related to the antifouling properties of the materials. The specific antifouling materials to be examined in this thesis are presented in Section 1.4 with more details, and the surface structures of these materials were for the first time revealed using SFG spectroscopy and correlated to the antifouling properties. The SFG results will guide the design of new and effective

antifouling materials. The background of SFG spectroscopy is discussed in more detail in Section 1.3.

1.2 Bio-inspired Adhesive Materials

Although biofouling causes many troubles, it presents a good model for underwater adhesion. Inspired by marine organisms that cause biofouling such as mussels and barnacles, a number of adhesive polymers have been synthesized that can adhere in a wet environment.[24-26] Particularly, the amino acid 3,4-dihydroxyphenylalanine (DOPA) (Figure 1.2) found in mussel foot proteins (MFPs) has been proven essential for mussel adhesion, and DOPA has been extensively incorporated into polymers for adhesion purposes.[27-29]

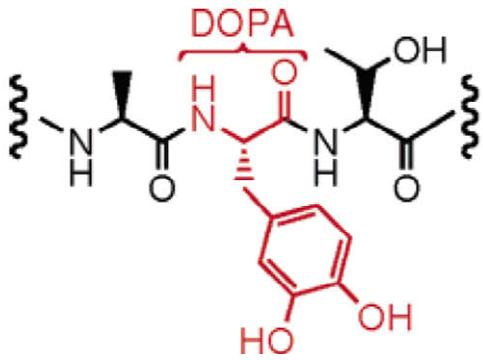

Figure 1.2 Molecular structure of DOPA.

The adhesion of DOPA has been extensively observed, but its adhesion mechanisms are challenging to study because commonly used techniques cannot probe adhesive interfaces in situ. Such interfaces generally involve buried polymer interfaces or polymer surfaces in water. In this thesis, SFG has been applied to study the molecular structures of biofouling interfaces of mussel proteins on various coatings and a DOPA

inspired polymer at various interfaces. Their underwater adhesive mechanisms will be revealed, which will guide the design of new adhesive and antifouling materials.

1.3 Sum Frequency Generation (SFG) Vibrational Spectroscopy

SFG vibrational spectroscopy is an intrinsically surface-sensitive and in situ vibrational spectroscopic method.[30,31] An SFG process involves two input photons and one outgoing photon. The outgoing photon has the sum frequency of the input photons (Figure 1.3A). Therefore, SFG signal is related to two input optical beams by a second-order nonlinear optical process. Experimentally, visible and infrared (IR) input lasers penetrate a CaF_2 or SiO_2 substrate (window or prism), and overlap spatially and temporally at the sample surface in air, water, or an aqueous solution (Figure 1.3B). The wavelength of the visible beam is 532 nm, whereas the IR beam is frequency tunable. The reflected SFG signal is collected by a monochromator along with a photomultiplier tube as a function of the wavenumber of the IR beam.

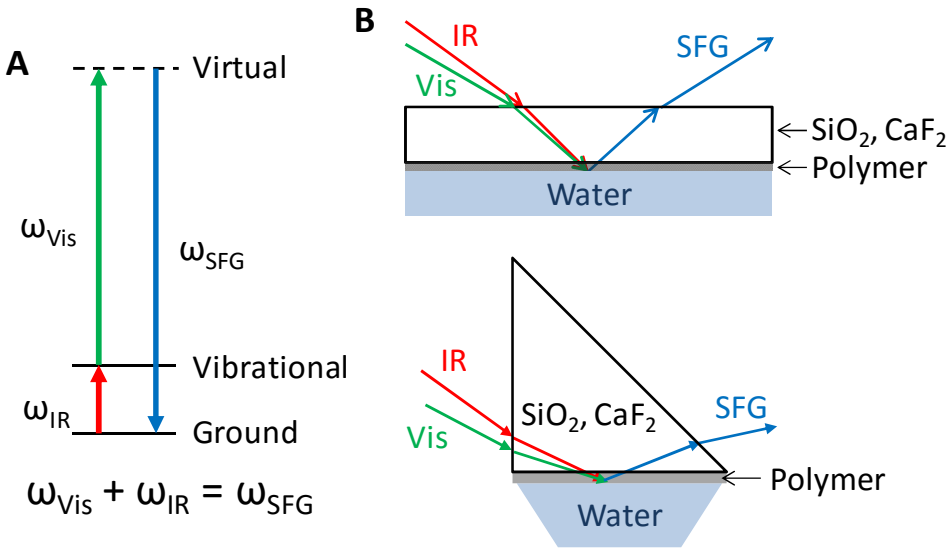

Figure 1.3 (A) SFG energy level diagram; (B) Experimental scheme of SFG vibrational spectroscopy. Top: Window geometry; Bottom: Prism geometry.

SFG is surface sensitive because of its selection rule. According to the selection rule, SFG signal intensity is proportional to the square of the second order nonlinear optical susceptibility, $\chi^{(2)}$, of the material under the electric dipole approximation. As a polar third-rank tensor, $\chi^{(2)}$ changes sign under the inversion operation: $\chi^{(2)}(r) = -\chi^{(2)}(-r)$. For materials with inversion symmetry, $\chi^{(2)}(r) = \chi^{(2)}(-r)$. The only possible solution for the above two equations is $\chi^{(2)} = 0$. Therefore, for materials with inversion symmetry, no SFG signal can be generated. Most solid polymer systems do have inversion symmetry, because the functional groups in the bulk of these polymeric materials are generally randomly oriented; therefore they would not generate SFG signals. However, because inversion symmetry is broken at the surface/interface, for molecules or functional groups on polymer surfaces or at polymer interfaces, $\chi^{(2)}(r)$ does not equal to $\chi^{(2)}(-r)$. Here, $\chi^{(2)}$ can be non-zero, and SFG signals can be detected from surfaces and interfaces. Due to this selection rule, SFG is intrinsically surface/interface sensitive. The surface/interface sensitivity of SFG is not determined by the penetration depth of the input laser beams into the sample. Even when the input laser beams can penetrate the entire sample, only molecules or functional groups on the surfaces or at the interfaces contribute to the signals due to the SFG selection rule. As signals detected in other vibrational spectroscopic methods, SFG vibrational peaks can be assigned to different vibrational modes of various functional groups in the molecules. SFG spectra can be used to determine what types of molecules/functional groups are present on the surface/at the interface according to the peak centers of the vibrational bands in the spectra.

1.4 Dissertation Overview

In this thesis, SFG spectroscopy along with other techniques was used to probe the surface structures of various antifouling materials and reveal their antifouling mechanisms. To understand biofouling, the molecular structures at the adhesion interfaces of mussel adhesives and a mussel inspired polymer were probed by SFG spectroscopy, and the adhesion mechanisms was elucidated.

The surface structures of biocide modified PDMS coatings are firstly discussed. Such coatings are able to prevent the surface growth of microorganisms underwater by killing the microorganisms on the surfaces. This work aims to optimize the formula of a biocide, quaternary amine salt (QAS), modified poly(dimethyl siloxane) (PDMS) material, and to reveal its anti-bacterial mechanism. Two different QAS silanes (methoxy and ethoxy terminated) and PDMS with two different molecular weights (18 000 and 49 000 g/mol) were mixed to prepare four different biocide coatings. The surface structures of the four coatings in air and sea water were revealed by probing their surfaces using SFG spectroscopy. The effects of the chain length of PDMS and the reactivity of the silanes on the surface structures of the coatings are discussed. The antimicrobial activity of the coatings was correlated to their surface structures. The research results of the SFG studies on the QAS modified PDMS coatings are presented in Chapter 2, Section 2.1.

Environmentally benign amphiphilic polymers provide another solution to antifouling material research. SFG spectroscopy combined with infrared spectroscopy is used to probe the surface structures of amphiphilic polymers in air and water. These amphiphilic polymer coatings were prepared with a hydrophilic betaine group and various hydrophobic or hydrophilic side chains. Their different surface structures in air

and water are discussed and correlated to their antifouling performance. The research results of the SFG studies on the polybetaines with different side chains are presented in Chapter 2, Section 2.2.

Another type of amphiphilic polymers, polypeptoids, was then investigated. Unlike most polymers, polypeptoids can be designed with specific sequence; therefore they serve as a great model for polymer physics and chemistry studies. The surface structures and hydration of a series of polypeptoids with different sequences and compositions were probed using SFG spectroscopy and correlated to their different antifouling/fouling release behaviors. This work aids in the design of polypeptoids with improved performance through optimizing the sequence and composition and is presented in Chapter 2, Section 2.3.

Polymer coatings that can resist oil fouling in water can be used for oil/water separation. In this work, the surface structures of polymer coatings for oil/water separation are examined. The coatings were prepared via layer-by-layer assembly of poly(diallyldimethylammonium chloride) (PDDA) and poly(sodium styrene sulfonate) (PSS) to form polyelectrolyte multilayer films. The oil repellency of the films in water was tested. The orientation of the functional groups on the surfaces of the films was probed by SFG spectroscopy. The surface structures of the films were correlated to their oil/water separation performance. The research results of the oil/water separation films are presented in Chapter 2, Section 2.4.

In addition to the polymer structures, surface hydration of the polymers plays an important role in resisting biofouling. Zwitterionic polymers are promising nonfouling materials, and their strong surface hydration is believed to be crucial to their nonfouling

performance. SFG spectroscopy is used to probe the surface hydration of zwitterionic materials with different molecular structures. The effects of polymer structures and environmental factors such as pH and salts on their surface hydration are discussed. The surface hydration of zwitterionic and PEG materials was compared. The interaction between the materials and proteins were investigated to further reveal their nonfouling mechanisms. Furthermore, isotopic dilution technique was applied to better interpret the SFG spectra of water and reveal the surface hydration of the materials. The correlation between the strongly hydrogen bonded water molecules at the material surfaces and their nonfouling properties are discussed. The SFG studies on the hydration of nonfouling zwitterionic materials are presented in Chapter 3.

While antifouling materials are being developed to combat biofouling, we can learn from biofouling to develop underwater adhesive materials. Mussel is one of the marine animals that can adhere to surfaces in wet environments leading to biofouling. The adhesion mechanisms of mussel have been extensively studied with isolated and purified mussel foot proteins, but the buried adhesive interfaces of live mussels have never been examined in situ. In this research, the buried interfaces between mussel adhesives and various substrates were probed in situ using SFG spectroscopy. The importance of surface dehydration to mussel adhesion underwater is discussed. The interactions between mussel proteins and the substrate materials were also examined. The research on the adhesion interfaces of mussel proteins are presented in Chapter 4, Section 4.1.

Inspired by mussel adhesion, a DOPA-containing adhesive polymer has been developed.[32] The molecular structures of this polymer at various interfaces were revealed

using combined SFG and infrared spectroscopy. The effect of oxidation of DOPA was also discussed. The interfacial structures of the polymer were related to its adhesion properties. The study on the adhesion mechanisms of the DOPA-containing polymer is presented in Chapter 4, Section 4.2.

In this thesis, we get a comprehensive understanding of biofouling and antifouling materials by using SFG spectroscopy as a main technique for probing a wide range of material surfaces and interfaces. The surface structures of novel antifouling materials at water interfaces were elucidated to interpret their antifouling performances. The adhesion interfaces underwater relevant to biofouling was studied to reveal the adhesion mechanisms.

1.5 References

(1) Schultz, M. P.; Bendick, J. A.; Holm, E. R.; Hertel, W. M. *Biofouling* **2011**, *27*, 87-98.
(2) Baker, J. S.; Dudley, L. Y. *Desalination* **1998**, *118*, 81-89.
(3) Voskerician, G.; Shive, M. S.; Shawgo, R. S.; Recum, H. v.; Anderson, J. M.; Cima, M. J.; Langer, R. *Biomaterials* **2003**, *24*, 1959-1967.
(4) Banerjee, I.; Pangule, R. C.; Kane, R. S. *Adv. Mater.* **2011**, *23*, 690-718.
(5) Kugel, A.; Stafslien, S.; Chisholm, B. J. *Prog. Org. Coat.* **2011**, *72*, 222-252.
(6) Lejars, M.; Margaillan, A.; Bressy, C. *Chem. Rev.* **2012**, *112*, 4347-4390.
(7) Callow, J. A.; Callow, M. E. *Nat. Commun.* **2011**, *2*, 244 DOI:210.1038/ncomms1251.
(8) Grozea, C. M.; Walker, G. C. *Soft Matter* **2009**, *5*, 4088-4100.
(9) Jiang, S. Y.; Cao, Z. Q. *Adv. Mater.* **2010**, *22*, 920-932.
(10) Yang, W.; Liu, S. J.; Bai, T.; Keefe, A. J.; Zhang, L.; Ella-Menye, J. R.; Li, Y. T.; Jiang, S. Y. *Nano Today* **2014**, *9*, 10-16.
(11) Zhang, L.; Cao, Z. Q.; Bai, T.; Carr, L.; Ella-Menye, J. R.; Irvin, C.; Ratner, B. D.; Jiang, S. Y. *Nat. Biotechnol.* **2013**, *31*, 553-556.
(12) Keefe, A. J.; Jiang, S. Y. *Nat. Chem.* **2012**, *4*, 60-64.
(13) Chen, S. F.; Li, L. Y.; Zhao, C.; Zheng, J. *Polymer* **2010**, *51*, 5283-5293.
(14) Sundaram, H. S.; Cho, Y.; Dimitriou, M. D.; Finlay, J. A.; Cone, G.; Williams, S.; Handlin, D.; Gatto, J.; Callow, M. E.; Callow, J. A.; Kramer, E. J.; Ober, C. K. *ACS Appl. Mater. Interf.* **2011**, *3*, 3366-3374.
(15) van Zoelen, W.; Buss, H. G.; Ellebracht, N. C.; Lynd, N. A.; Fischer, D. A.; Finlay, J.; Hill, S.; Callow, M. E.; Callow, J. A.; Kramer, E. J.; Zuckermann, R. N.; Segalman, R. A. *ACS Macro Lett.* **2014**, *3*, 364-368.
(16) Dimitriou, M. D.; Zhou, Z. L.; Yoo, H. S.; Killops, K. L.; Finlay, J. A.; Cone, G.; Sundaram, H. S.; Lynd, N. A.; Barteau, K. P.; Campos, L. M.; Fischer, D. A.; Callow, M. E.; Callow, J. A.; Ober, C. K.; Hawker, C. J.; Kramer, E. J. *Langmuir* **2011**, *27*, 13762-13772.
(17) Krishnan, S.; Ayothi, R.; Hexemer, A.; Finlay, J. A.; Sohn, K. E.; Perry, R.; Ober, C. K.; Kramer, E. J.; Callow, M. E.; Callow, J. A.; Fischer, D. A. *Langmuir* **2006**, *22*, 5075-5086.
(18) Weinman, C. J.; Gunari, N.; Krishnan, S.; Dong, R.; Paik, M. Y.; Sohn, K. E.; Walker, G. C.; Kramer, E. J.; Fischer, D. A.; Ober, C. K. *Soft Matter* **2010**, *6*, 3237-3243.
(19) Colak, S.; Tew, G. N. *Biomacromolecules* **2012**, *13*, 1233-1239.
(20) Amadei, C. A.; Yang, R.; Chiesa, M.; Gleason, K. K.; Santos, S. *ACS Appl. Mater. Interf.* **2014**, *6*, 4705-4712.
(21) Wong, T.-S.; Kang, S. H.; Tang, S. K. Y.; Smythe, E. J.; Hatton, B. D.; Grinthal, A.; Aizenberg, J. *Nature* **2011**, *477*, 443-447.
(22) Leslie, D. C.; Waterhouse, A.; Berthet, J. B.; Valentin, T. M.; Watters, A. L.; Jain, A.; Kim, P.; Hatton, B. D.; Nedder, A.; Donovan, K.; Super, E. H.; Howell, C.; Johnson, C. P.; Vu, T. L.; Bolgen, D. E.; Rifai, S.; Hansen, A. R.; Aizenberg, M.; Super, M.; Aizenberg, J.; Ingber, D. E. *Nat. Biotechnol.* **2014**, *32*, 1134-1140.
(23) Shen, Y. R. *Nature* **1989**, *337*, 519-525.
(24) Sedó, J.; Saiz-Poseu, J.; Busqué, F.; Ruiz-Molina, D. *Adv. Mater.* **2013**, *25*, 653-701.
(25) Ye, Q.; Zhou, F.; Liu, W. *Chem. Soc. Rev.* **2011**, *40*, 4244-4258.

(26) Lee, H.; Dellatore, S. M.; Miller, W. M.; Messersmith, P. B. *Science* **2007**, *318*, 426-430.
(27) Matos-Perez, C. R.; White, J. D.; Wilker, J. J. *J. Am. Chem. Soc.* **2012**, *134*, 9498-9505.
(28) Ahn, B. K.; Lee, D. W.; Israelachvili, J. N.; Waite, J. H. *Nat. Mater.* **2014**, *13*, 867-872.
(29) Holten-Andersen, N.; Harrington, M. J.; Birkedal, H.; Lee, B. P.; Messersmith, P. B.; Lee, K. Y. C.; Waite, J. H. *Proc. Natl. Acad. Sci. USA* **2011**, *108*, 2651-2655.
(30) Lambert, A. G.; Davies, P. B.; Neivandt, D. J. *Appl. Spectrosc. Rev.* **2005**, *40*, 103-145.
(31) Shen, Y. R. *J. Phys. Chem. C* **2012**, *116*, 15505-15509.
(32) Westwood, G.; Horton, T. N.; Wilker, J. J. *Macromolecules* **2007**, *40*, 3960-3964.

CHAPTER 2 SURFACE STRUCTURES AND HYDRATION OF NOVEL POLYMERS FOR ANTIFOULING/FOULING RELEASE AND OTHER APPLICATIONS

2.1 Surface Structures of Poly(dimethyl siloxane) (PDMS) Coatings Modified with Quaternary Amine Salts (QAS) for Antifouling and Fouling Release Applications

2.1.1 Introduction

Marine biofouling is generally defined as the undesirable attachment and growth of macro- and micro-organisms on surfaces immersed in seawater. Once established, it can cause a multitude of problems for ships in operation and in the harbor. Extensive research has been performed in recent years to develop new antifouling coating technologies that possess superior antifouling efficiency, longer performance lifetimes, and non-toxic mechanisms of activity.[1]

Polydimethysiloxane (PDMS) materials have demonstrated good fouling release performance due to their low surface energy, low glass transition temperature, and low elastic modulus.[1] In addition, biocides have been incorporated into PDMS matrices to form successful antibacterial materials.[2] Thus, researchers have applied this idea to generate fouling release and antifouling coatings using PDMS with chemically bound

(i.e., tethered) biocide moieties. Quaternary ammonium salts (QAS) are one of the most widely used biocides to inhibit microbial growth. They are very effective in killing a broad spectrum of microorganisms such as Gram-positive and Gram-negative bacteria, yeast, and mold.[3,4]

Extensive research has demonstrated that QAS-incorporated PDMS materials are good candidates for coatings that possess both fouling release and antifouling capabilities.[5,6] To optimize the performance of various coating materials, it is crucial to characterize their surface chemical structures at the molecular level because such surface structures determine their antifouling properties. More importantly, because these materials are used underwater, it is crucial to monitor their surface structures in situ in water. However, most of the currently available surface sensitive analytical techniques cannot meet the above requirements simultaneously.

Sum frequency generation vibrational spectroscopy (SFG) has been shown to be a powerful tool to study polymer surface structures at the molecular level in different chemical environments. SFG can provide information such as functional group composition and orientation at surfaces/interfaces with submonolayer sensitivity.[7] In addition, SFG can be used to study in situ surface restructuring behavior of polymer materials in water.[8,9]

In this work, SFG was used to monitor the surface structures of QAS-incorporated PDMS coatings. Emphasis was placed on the effects of the types of the silanes used to incorporate QAS into PDMS and the molecular weight of the PDMS chains. A previous study indicated that PDMS materials with QAS tethered using the ethoxysilane exhibited better antifouling activity than those prepared with methoxysilane.[4] The SFG results here

indicate that densely packed alkyl chains on the coating surfaces are crucial to kill bacteria, correlating well to the previously published experimental observations in antifouling properties, thus providing an in-depth understanding on the surface structure-function relationships of PDMS materials incorporated with QAS biocides.

2.1.2 Experimental Section

Silanol-terminated PDMS with molecular weights (MW) of 18,000 and 49,000 g/mol (18K-PDMS and 49K-PDMS) were purchased from Gelest, Inc. (Tullytown, PA) and were diluted in toluene to 80 wt%. Quaternary ammonium salts, octadecyldimethyl(3-trimethoxysilylpropyl) ammonium chloride (C18-TMS) and octadecyldimethyl(3-triethoxysilylpropyl) ammonium chloride (C18-TES), were synthesized using a published protocol.[4] Tetrahydrofuran, tetrabutylammonium fluoride (TBAF) in tetrahydrofuran (1.0 M), and 4-methyl-2-pentanone (MIBK) were purchased from Aldrich (Milwaukee, WI). For coating solutions, a TBAF catalyst solution (50 mM) was prepared by dispensing 1.25 mL of 1.0 M TBAF solution in a 25 mL volumetric flask and adding MIBK volumetrically to 25 mL. Coating samples were prepared by blending 18K-PDMS or 49K-PDMS, the cross-linker methyltriacetoxysilane (MTAC), the TBAF catalyst solution, and different amounts of a methanol solution (50% w/w) of QAS (Table 2.1). The coating solutions were stirred overnight and then spin-coated on fused silica windows (1 inch in diameter, 1/8 inch thick, ESCO Products Inc.) at 3000 rpm for 30 s. The spin coated films were cured at ambient condition for 24 h followed by heated at 50 °C overnight. Molecular formulas for PDMS, cross-linker, catalyst and QAS are shown in Figure 2.1.

Table 2.1 Compositions of the PDMS coatings incorporated with QAS (all values are in grams)

Sample	PDMS		QAS		MTAC	50 mM Catalyst
	type	amount	type	amount		
A	49K	6.25	C18-TMS	1.24	0.75	0.75
B	49K	6.25	C18-TES	1.61	0.75	0.75
C	18K	5.00	C18-TMS	1.24	0.75	0.75
D	18K	5.00	C18-TES	1.61	0.75	0.75

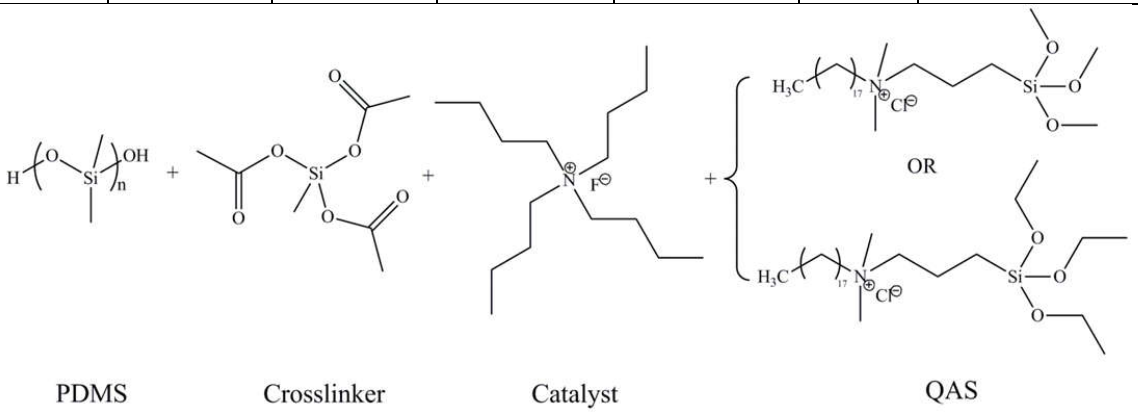

Figure 2.1 Molecular structures of the QAS incorporated PDMS system.

Details about SFG theories and instrumentation have been published elsewhere and will not be reiterated here.[7,10] SFG is a second order nonlinear optical process which selectively probes systems with no inversion symmetry. Since most bulk materials have inversion symmetry, SFG is an intrinsic surface sensitive technique and has been proven to provide submonolayer surface sensitivity. In this study, face-down sample geometry was used in which two input laser beams traveled through the fused silica windows and overlapped on the polymer/air or polymer/liquid (Millipore water or artificial sea water) interface (Figure 2.2). SFG spectra with a polarization combination of ssp (s-polarized

sum frequency output, s-polarized visible input, and p-polarized infrared input) were collected. All SFG spectra were normalized according to the intensities of the input IR and visible beams. SFG signals are dominated by the polymer/air or polymer/liquid interface, with almost no polymer/substrate or polymer bulk contributions to the spectra collected using this experimental geometry.[11]

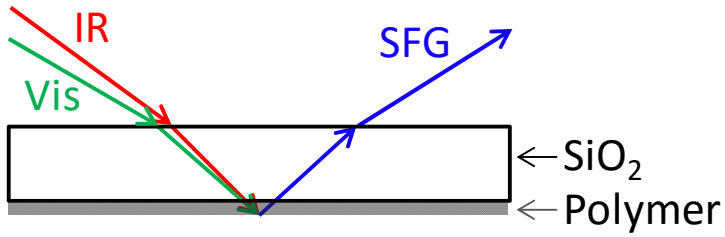

Figure 2.2 SFG experimental face-down sample geometry.

2.1.3 Results and Discussion

2.1.3.1 In air

The ssp SFG spectra collected from the surfaces of the four samples are dominated by peaks centered at 2850, 2875, 2915, 2940 and 2965 cm^{-1}, which are assigned to the CH_2 symmetric stretching, CH_3 symmetric stretching, Si-CH_3 C-H symmetric stretching, CH_3 Fermi resonance, and C-H asymmetric stretching of regular methyl and/or Si-CH_3 groups, respectively (Figure 2.3).[8,9,11-13] The 2850, 2875, 2940, and 2965 cm^{-1} peaks are contributed from QAS while the peaks at 2915 cm^{-1} and 2965 cm^{-1} are from the Si-CH_3 C-H symmetric and asymmetric stretching modes in PDMS. This was concluded because SFG spectra detected from the pure PDMS surface reported before contain only two peaks in the C-H stretching frequency region from the Si-CH_3 C-H symmetric (~2915 cm^{-1}) and asymmetric (~2965 cm^{-1}) stretching modes.[12] The four materials did not display discernible differences in their surface structures in air; both

PDMS and the QAS molecules are present on the surface and the PDMS generates the dominating signal from these surfaces. Therefore PDMS dominates the surfaces of the coatings, responsible for their fouling release property.

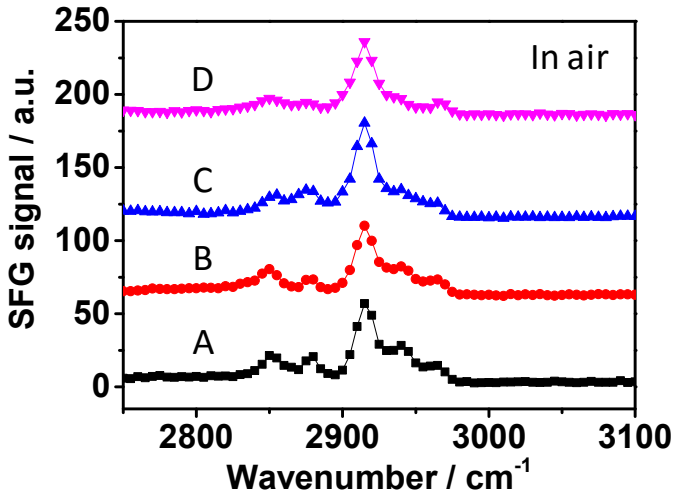

Figure 2.3 SFG ssp spectra collected from QAS-tethered PDMS systems in air. The four samples studied are (A) 49K-PDMS, C18-TMS; (B) 49K-PDMS, C18-TES; (C) 18K-PDMS, C18-TMS; (D) 18K-PDMS, C18-TES.

2.1.3.2 In artificial sea water (ASW)

SFG spectra were also collected from the material/ASW (Aldrich, Milwaukee, WI) interface. Salt ions in sea water may induce surface reorientation of the coating materials which might provide a better understanding of their antifouling performance (Figure 2.4). The ions in ASW randomize the orientation of the interfacial water molecules resulting in no detected water O-H stretching signal. As a result, only SFG spectra in the C-H stretching frequency are displayed. The spectral signatures and relative intensities are different for each of the four samples, indicating that both the silane head group on QAS and the MW of PDMS play a role in determining the surface structures of these materials

in ASW. These differences show that the QAS molecules on the surfaces, especially the alkyl chains attached to the quaternized nitrogen atoms, organized differently in ASW.

Two observations can be made from the four SFG spectra in Figure 2.4. Firstly, the materials made from C18-TES have notably stronger CH_3 signals at 2880 and 2940 cm^{-1} than the analogues made from C18-TMS. Strong SFG signals mean that the interfacial molecules or functional groups are more ordered along the surface normal. This suggests that on the coating surfaces in ASW, the alkyl chains on the QAS prepared with TES-QAS have a longer extension and protrude out farther from the surfaces (or standing up on the surface) while the alkyl chains on the QAS prepared with TMS-QAS fold back and are more disordered. Secondly, the materials made from 18K-PDMS have relatively stronger SFG signals than those made from 49K-PDMS. As a result, the alky chains on the surface of 18K-PDMS are better ordered than those on 49K-PDMS surface in ASW.

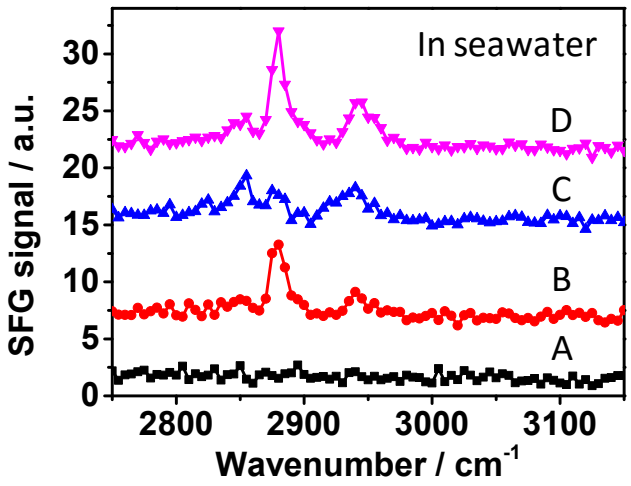

Figure 2.4 SFG ssp spectra collected from QAS-tethered PDMS systems in ASW. The four samples studied are (A) 49K-PDMS, C18-TMS; (B) 49K-PDMS, C18-TES; (C) 18K-PDMS, C18-TMS; (D) 18K-PDMS, C18-TES.

2.1.3.3 Antifouling activity

According to antifouling experiments performed previously, using various marine microorganism-based laboratory assays, the QAS-tethered PDMS materials prepared with TES-QAS were more effective in preventing microbial biofilm growth than those prepared with TMS-QAS.[4] Furthermore, the biofilms attached to the surfaces of the QAS-tethered PDMS materials prepared with TES-QAS were much easier to remove. Previous atomic force microscopic (AFM) results indicated that QAS-tethered PDMS prepared with TES-QAS leads to greater segregation of QAS groups to the coating surface than that prepared with TMS-QAS.[4] This may be attributed to the lower reactivity of the ethoxysilane groups, which resulted in additional time for the diffusion of TES-QAS to the surface.

The reported AFM results on the aggregation morphology of the surfaces are consistent with our SFG data, as QAS-tethered PDMS prepared with TES-QAS exhibited stronger methyl signals in aqueous environment, especially in ASW. As discussed above, it is necessary to have the alkyl groups of the QAS protruding out from the surface of the QAS-tethered PDMS to kill bacteria. It can be deduced from the SFG results that the alkyl chains on surfaces prepared from TES-QAS were densely packed with ordering and extended out in ASW whereas coatings from TMS-QAS do not have extended alkyl chains on the surfaces (Figure 2.5), due to the different reaction dynamics of methoxysilane and ethoxysilane.

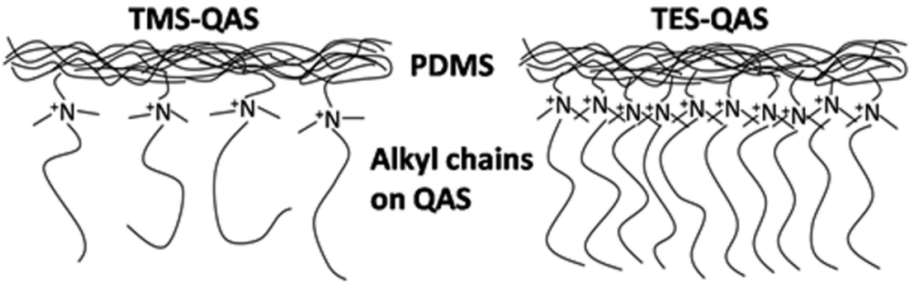

Figure 2.5 Illustration showing the surface structures of QAS-tethered PDMS system in aqueous environment. Different silane groups on QAS lead to different alkyl chain ordering of the system.

2.1.4 Conclusions

In this study, SFG has been applied to investigate surface structures of PDMS materials incorporated with QAS-based biocides *in situ* for fouling release and antifouling coatings. Polymers prepared from TES-QAS resulted in better antifouling coatings. SFG studies showed that they generated stronger signals from alkyl groups in aqueous environments, especially in ASW. This shows that the different reaction dynamics of methoxysilane and ethoxysilane can lead to different surface structures of QAS-tethered PDMS, resulting in different antifouling activities. In addition, coatings prepared from QAS-tethered 18K-PDMS generated stronger SFG signals from the QAS alkyl chains than those prepared from the QAS-tethered 49K-PDMS because 18K-PDMS could provide more end groups for QAS tethering. The degree of extension of the alkyl chains in QAS plays an important role in preventing bacterial biofilm growth. The correlations made between the SFG studies and antifouling properties in this study also agreed well with our previous studies on PDMS materials incorporated with QAS possessing different alkyl chain lengths.[6] This study provides a general set of guidelines to follow when designing PDMS materials incorporated with QAS to generate antifouling coatings: The QAS groups need to aggregate to the surface and the QAS alkyl chains

need to extend fully into the aqueous environment. As a result, the long alkyl chains can penetrate into the cell membrane and kill microorganisms.

2.2 Surface Restructuring of Antifouling Amphiphilic Polybetaines in Water

2.2.1 Introduction

Anti-biofouling materials have great use in a wide range of important applications from ship hulls to biomedical implants.[14] Poly(dimethyl siloxane) (PDMS), poly(ethylene glycol) (PEG)[15] and zwitterionic based materials[16] have been extensively studied for fouling-release and non-sticky coatings. Solely hydrophobic or hydrophilic surfaces are believed to be inadequate to completely resist biofouling, because proteins and larger organisms are intrinsically amphiphilic and can attach to surfaces with different mechanisms.[17] To address this issue, there is an increasing awareness that amphiphilic materials may offer superior anti-biofouling properties. Such materials can resist biofouling by restructuring their surfaces depending on their environment, similar to living organisms.[18]

A typical amphiphilic material combines both hydrophilic PEG and hydrophobic fluorinated polymer segments, which can resist biofouling better than the sole use of PEG or fluorinated polymers.[19] Based on the same principle, surface active block copolymers (SABC) were synthesized with amphiphilic side chains containing both PEG and fluorinated components, which showed strong resistance to the attachment of various organisms.[20-22] Polypeptoids, a non-natural bio-mimetic polymer, have also been designed for anti-biofouling. The property of the polypeptoids could be tuned by varying

the amount and sequence of PEG and fluorinated blocks.[23] Recently, an entirely new class of amphiphilic polybetaines with different side chains were synthesized via ring-opening metathesis polymerization.[24,25] These materials take advantage of the hydrophilic zwitterionic functional groups while their surface properties are further tuned by hydrophilic or hydrophobic side chains (Figure 2.6). For example, the polybetaine containing oligo(ethylene glycol) side chain (ZI-OEG) is hydrophilic, while the polymers bearing octyl or fluorinated side chains (ZI-C8 or ZI-F13) are hydrophobic. The anti-biofouling assays showed that the ZI-OEG and ZI-F13 surfaces resisted the non-specific adsorption of several types of proteins, while protein adsorption on the ZI-C8 coating was greater than the other betaines.[24]

The anti-biofouling capability of amphiphilic materials often depends on their surface structures in water. In previous reports, the surface structures of various polymers were determined by X ray spectroscopy in vacuum[20-22,26,27] and their surface restructuring in water was deduced from atomic force microscopy and dynamic water contact angle experiments.[23-25] However, none of these characterization methods provided direct evidence of the polymer surface restructuring at the molecular level in water. Hence, an in situ technique is needed to probe the polymer/water interface.

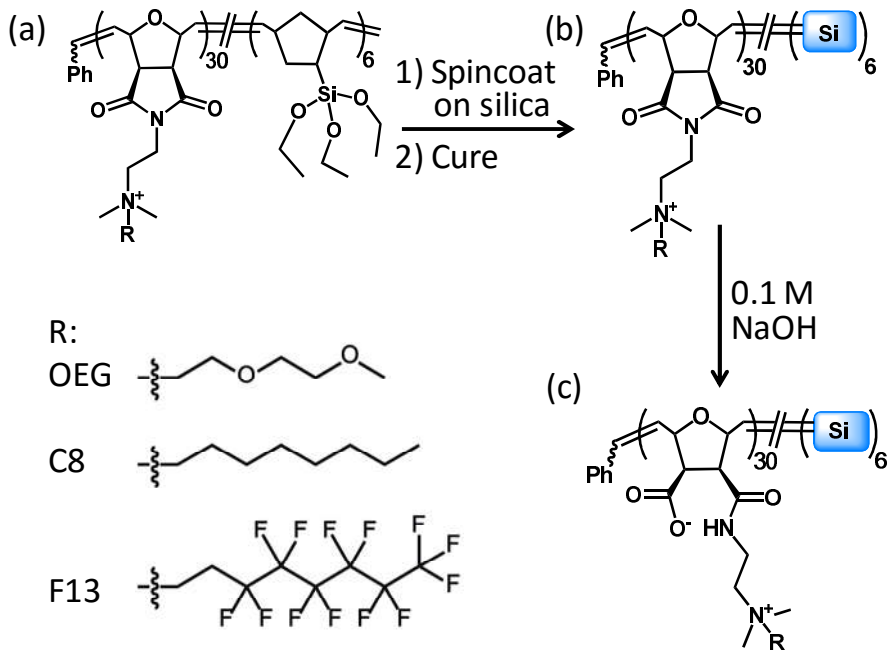

Figure 2.6 Preparation of the amphiphilic polybetaine coatings. Briefly, (a) cationic polymers were spin-coated on SiO_2 substrates and cured to form (b) cationic coatings, followed by hydrolysis in 0.1 M NaOH to form (c) amphiphilic coatings.

As discussed above, SFG has been extensively applied to study structures of polymers and biomolecules at various interfaces[28-31] and has proved to be particularly powerful in revealing polymer/water interfacial structures in ambient environments.[32-35] Here surface structures of three amphiphilic polybetaines with different side chains (Figure 2.6) were probed in air and water with SFG *in situ*. The SFG signals from the OEG, C8 and F13 side chains were obtained in air and then compared to signals from the water interface to understand their different restructuring behaviors. Moreover, the SFG signals from the betaine group showed its affinity towards water. The SFG results on the surface restructuring of the polymers in water were used to explain their anti-biofouling mechanisms.

2.2.2 Experimental Section

Cationic polymers with OEG, C8 and F13 side chains (N(+)-OEG, N(+)-C8 and N(+)-F13) (Figure 2.6a) were synthesized by our collaborators (Prof. Gregory Tew's lab at University of Massachusetts) according to the previously published method with molecular weight and compositions presented in the literature.[24,25] Millipore water (18.2 MΩ·cm) was used in all the experiments.

Right angle SiO_2 and CaF_2 prisms were purchased from Altos Photonics (Bozeman, MT). A layer of 100 nm SiO_2 was deposited onto each CaF_2 prism by an electron-beam deposition process using an SJ-26 Evaporator system at a pressure below 10^{-5} Torr. The deposition rate is 5 Å/s. The SiO_2 prisms and SiO_2 coated CaF_2 prisms were treated with O_2 plasma for 4 minutes in a PE-25-JW plasma cleaner (Plasma Etch, Carson City, NV). The amphiphilic polybetaine coatings were prepared according to our prior report (Figure 2.6).[24] The ZI-OEG and ZI-C8 coatings were prepared on SiO_2 prisms and the ZI-F13 coating was prepared on the SiO_2 coated CaF_2 prism. The thicknesses of the spin-coated films are around 30 nm measured by a LSE model Gaertner Scientific Stokes Ellipsometer.[24,25]

Attenuated total reflection Fourier transform infrared (ATR-FTIR) spectra were collected on a Thermo Scientific Nicolet 6700 spectrometer with a Harrick germanium attenuated total reflection accessory and a liquid N_2-cooled HgCdTe amplified detector. Polymer films were prepared on freshly cleaned Si surfaces, which were pressured against the germanium crystal for ATR-FTIR measurements.

We used the same SFG spectroscopic system as reported previously.[36] Briefly, the visible and infrared (IR) input beams penetrate a right angle SiO_2 or CaF_2 prism and

overlap spatially and temporally at the sample surface/interface, as shown in Figure 2.7. The incident angles of the visible and IR beams are 60° and 54° with respect to the surface normal, and the pulse energies of the visible and IR beams are 30 and 100 μJ, respectively. The reflected SFG signal is collected by a monochromator along with a photomultiplier tube. All SFG spectra were collected using the ssp (SFG output, visible input, and IR input) polarization combination.

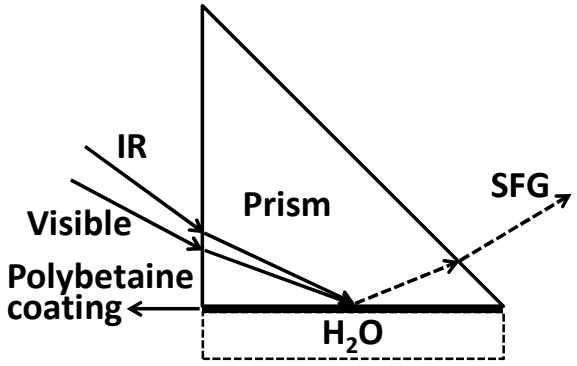

Figure 2.7 SFG sample geometry with polybetaine film on a right angle prism in contact with water.

2.2.3 Results and Discussion

The conversion from the cationic coatings (N(+)-OEG, (N+)-C8 and N(+)-F13, Figure 2.6b) to the zwitterionic coatings (Figure 2.6c) was characterized by ATR-FTIR. The ATR-FTIR spectra collected from all cationic coating samples showed a peak at 1706 cm^{-1} (Figure 2.8A, B and C) contributed from the imide group. After ring-opening in NaOH, for all coating samples, the peak at 1706 cm^{-1} disappeared and two new peaks at 1587 and 1662 cm^{-1} from the carboxylate or amide groups appeared (Figure 2.8D, E and F), indicating the complete conversion from the imide ring to the negatively charged carboxylate group. In addition, signals from the side chains for all the polymers were observed in the IR spectra. The peak at 1102 cm^{-1} for both N(+)-OEG and ZI-OEG was

assigned to the vibration of C-O-C on the OEG chain (Figure 2.8A and D). Both N(+)-C8 and ZI-C8 showed IR absorption at the range of 2850~2930 cm^{-1} due to the alkyl chain (Figure 2.8B and E). For both N(+)-F13 and ZI-F13, the peaks at 1146~1238 cm^{-1} were attributed to the C-F vibration (Figure 2.8C and F). The assignment of the IR signals will guide proper assignment of the peaks in the SFG spectra below.

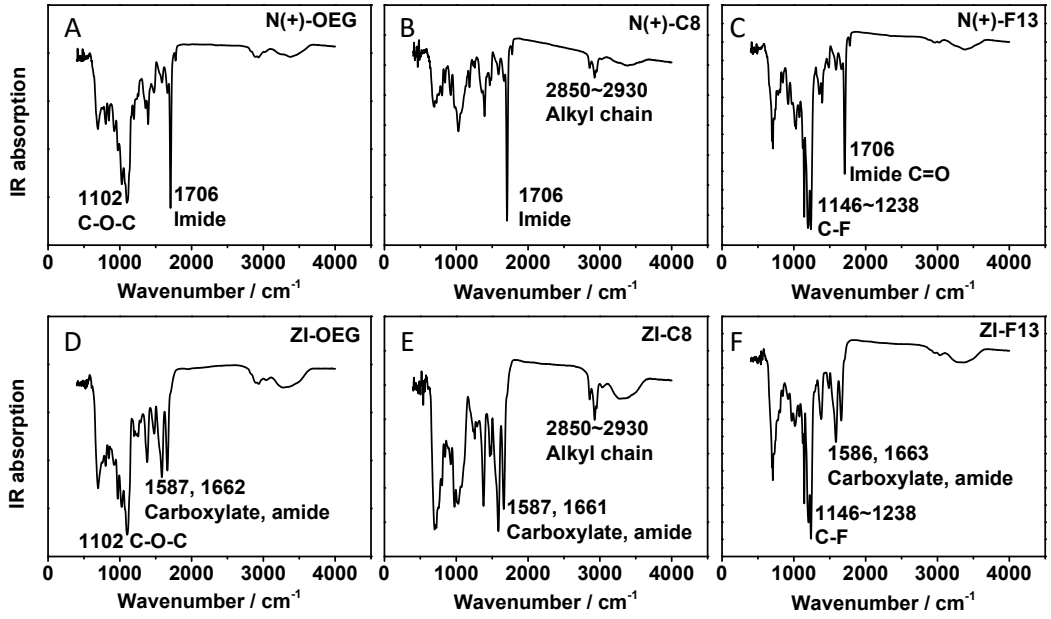

Figure 2.8 ATR-FTIR spectra of cationic (A) N(+)-OEG, (B) N(+)-C8 and (C) N(+)-F13 coatings and zwitterionic (D) ZI-OEG, (E) ZI-C8 and (F) ZI-F13 coatings.

For SFG experiments, we initially characterized the polymer surfaces in air before studying the surface restructuring in water. In the SFG spectra in the C-H stretching vibrational frequency region in air (Figure 2.9A), characteristic signals from the OEG and C8 side chains were observed. The peak at 2820 cm^{-1} was assigned to the O-CH_3 end group on the OEG chain.[37] The peaks at 2850 and 2880 cm^{-1} were contributed from the symmetric stretching of the CH_2 and CH_3 groups on the C8 chain respectively.[8] The SFG signals detected from the OEG and C8 chains indicated their presence on the coating

surfaces in air. No SFG signal was observed for the ZI-F13 coating in this frequency region, showing that no ordered CH groups were present on the surface.

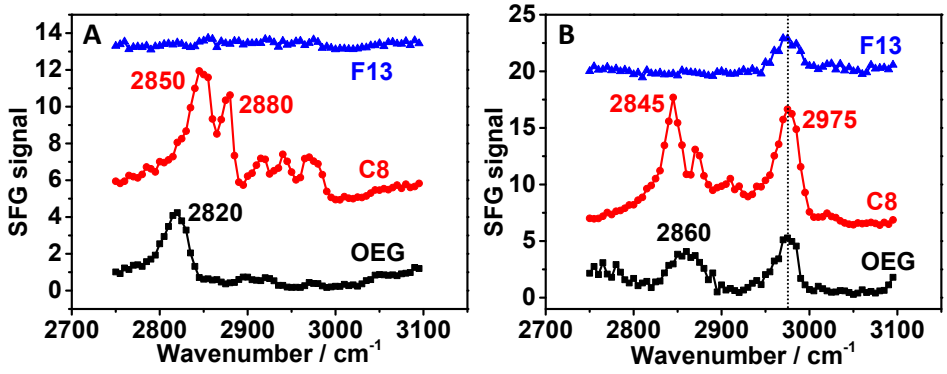

Figure 2.9 SFG spectra of ZI-OEG, ZI-C8 and ZI-F13 surfaces (A) in air and (B) in contact with D_2O in the C-H stretching vibrational frequency region.

To study the polymer/water interfaces, D_2O was used to avoid signal interference between the polymer CH groups and H_2O. Figure 2.9B displays the SFG spectra of the interfaces between the three coatings and water. All samples exhibit a peak at 2975 cm^{-1}, possibly from the N-CH_3 or N-CH_2 groups, indicating that the cationic quaternary amine might migrate to the surface in contact with water.

The ZI-OEG sample showed a peak at 2860 cm^{-1}, which was contributed from the O-CH_2 group on the OEG chain,[37] indicating the presence of the OEG chain at the water interface. PEG has been extensively used to prepare anti-biofouling materials due to its hydrophilicity.[15,38-40] Here, the OEG chain at the surface is critical to resist biofouling on the ZI-OEG coating. The ZI-C8 sample showed peaks at 2845 and 2880 cm^{-1}, assigned to the symmetric stretching of the CH_2 and CH_3 groups, indicating that the C8 chain was presence on the surface in water. The hydrophobic C8 chain was present at the water interface most likely because the C8 chain was directly connected to the quaternary

amine which has strong affinity towards water. The C8 chain at the water interface could lead to protein adsorption by hydrophobic interactions, which explains the reported fouling properties of the ZI-C8 material.[25] It is worth mentioning that the 2975 cm^{-1} signal detected from ZI-OEG and ZI-C8 may also contain some contribution from the asymmetric C-H stretching of the OCH_3 and CH_3 groups respectively.

In addition, SFG spectra were taken for the ZI-F13 coating between 1000 and 1350 cm^{-1} to study the C-F vibrational signals (Figure 2.10A). In air, a peak at 1235 cm^{-1} was detected. According to the IR spectra (Figure 2.8C and F), this peak was assigned to C-F stretching from the F13 chain, again confirming the surface presence of the F13 chain in air. When the film was in contact with water, this peak disappeared, indicating that the fluorinated chain either became random or withdrew from the water interface due to the unfavorable interactions between the hydrophobic fluorinated chain and water. This result is well correlated to the SFG C-H studies of the ZI-F13 sample, where no CH groups were observed on the surface in air, however CH signals were detected on the surface in water.

In order to study the surface behavior of the carboxylate group in the ZI-F13 sample, SFG spectra were collected from 1500 to 1800 cm^{-1} in the C=O stretching vibration frequency range (Figure 2.10B). In air, a peak at 1660 cm^{-1} was detected, while in water, a stronger peak around 1610 cm^{-1} was observed. The signals here were contributed from the carboxylate group. The higher signal intensity in water than in air indicated that the carboxylate group was present and had better ordering at the water interface. The red shift of the peak from air to water could be caused by hydration or hydrogen bonding of the carboxylate group with water. The signal at 1610 cm^{-1} could not

be contributed by the amide, because the hydrogen bonding between amide and water would not shift the signal of amide to as low as 1610 cm^{-1}.[41] Therefore, combining the SFG results of the ZI-F13 sample in water (Figure 2.9B and Figure 2.10), we believe that the betaine group containing the quaternary amine and the carboxylate groups moved to the water interface while the F13 chain withdrew from water. Previously, zwitterionic polymers have been reported as promising anti-biofouling materials due to their surface hydration.[16,42-44] Here, the exposure of the betaine group to the water interface and its hydration were responsible for resisting biofouling, as detected previously.[24,25]

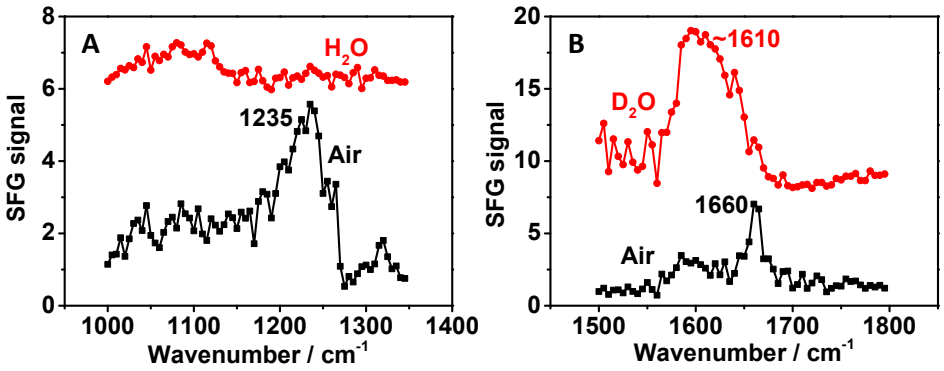

Figure 2.10 SFG spectra of the ZI-F13 coating in air and water in the (A) C-F and (B) C=O vibrational frequency region.

SFG studies indicated that the three polymers with the same backbone but different side chains exhibit different surface structures in water. Surface restructurings of polymers were observed using SFG in situ. The schematics of the three polymer surfaces in water are depicted in Figure 2.11. The SFG results on surface restructurings are consistent with the dynamic water contact angle data reported previously.[24] The contact angle hysteresis of the ZI-F13 surface is much larger than that of the ZI-OEG and ZI-C8 surfaces, indicating its more distinct surface restructuring upon contacting water.

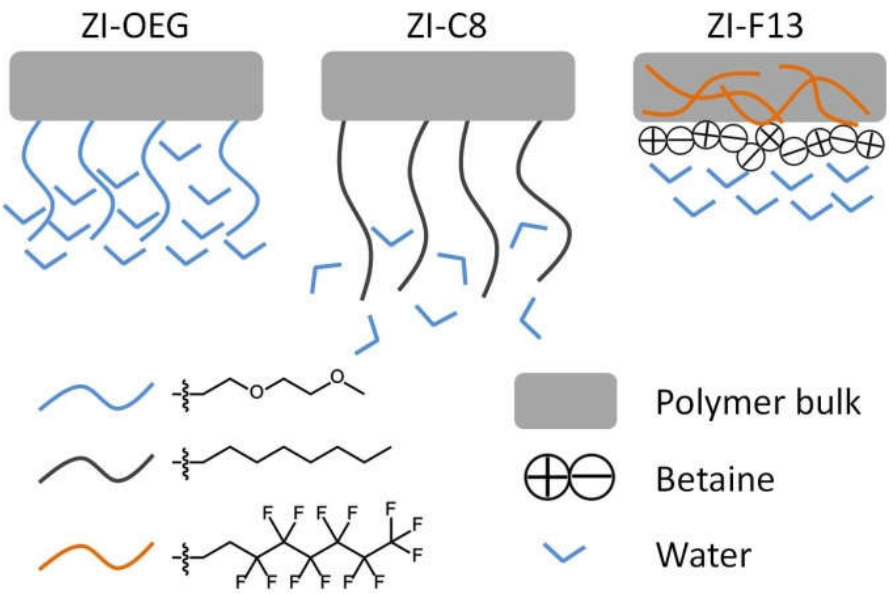

Figure 2.11 Schematic representation of the polymer surface structures in water.

2.2.4 Conclusions

In this work, we probed the surface restructuring behavior of three polybetaines with different side chains in water using SFG spectroscopy. The SFG results showed that the side chains of the three polymers were all present on the surface in air. In water, the OEG and C8 chains remained on the coating surface, while the F13 chain withdrew from water. For ZI-F13, both the quaternary amine group and the carboxylate group were present at the water interface, where the carboxylate group formed hydrogen bonds with water molecules. The surface restructuring information obtained from the SFG data provides direct experimental evidence of the anti-biofouling mechanisms of the amphiphilic materials: The good anti-fouling properties of ZI-OEG were due to the surface presence of the OEG groups on the surface; it has been extensively shown that the surface OEG groups lead to improved anti biofouling activity. The poor anti-fouling performance of the ZI-C8 was due to the surface presence of the C8 side chain, which resulted in protein adsorption due to hydrophobic interactions. The ZI-F13 also exhibited

good anti-fouling performance, because the F13 side chain retreated to the bulk in water so that the zwitterionic groups were exposed at the surface. It has been demonstrated that zwitterionic materials can be good anti-biofouling materials. This research indicates that side chains can greatly influence the polymer surface structures in water, resulting in different surface properties and thus different anti-biofouling properties.

2.3 Surface Structures and Hydration of Sequence-Specific Amphiphilic Polypeptoids for Antifouling/Fouling Release Applications

2.3.1 Introduction

For antifouling purposes, amphiphilic polymers can be designed with different molecular structures. Usually hydrophilic poly(ethylene glycol) (PEG) and hydrophobic perfluorinated carbon chains or poly(dimethyl siloxane) (PDMS) are incorporated into one polymer, which shows good antifouling or fouling release of proteins and living organisms.[19-22,26,45-48] However, precise control of the amounts and positions of the hydrophilic and hydrophobic moieties in one polymer remains a challenge.[49] Because the antifouling performance of a polymer coating depends on its surface structure, which is in turn determined by the molecular formula, there is an increasing awareness of controlling the polymer sequence and composition for optimized antifouling property.[50]

Biological polymers such as polypeptides exhibit specific amino acid sequence, which affects their folding and biofunction. Inspired by nature, polypeptoids (or N-substituted glycines) have emerged as a class of sequence-specific materials that are interesting for polymer physics studies.[51] Because the monomer type and sequence can be precisely controlled, study of the polypeptoid systems can provide insights into the

structure-property relationship of the materials.[23] For antifouling purposes, polypeptoids can be designed into amphiphilic polymers by incorporating both hydrophilic and hydrophobic peptoid units into one polymer. The surface structure and antifouling ability of the materials can be tuned by even a subtle change in the number or position of the structural units.[23,52]

The antifouling property of polymer coatings depends on their surface structures in water. In previous reports, the surfaces of amphiphilic polymers were characterized in water with atomic force microscopy and dynamic water contact angle measurements to deduce their antifouling mechanisms, [23,25,45,53] but they did not provide molecular structural information. The surface chemical compositions of the polymers were often investigated by X-ray spectroscopy in vacuum,[20-23,26,27,52] which is a different environment from real antifouling applications. Recently, carbon edge near edge X-ray absorption fine structure (NEXAFS) spectroscopy was used to characterize a series of amphiphilic polypeptoids with different compositions and sequences, and revealed that the changes in the amount or position of the fluorinated units in the polymers greatly affect their surface composition.[23,52] The sequence-dependent antifouling/fouling release mechanism was further proposed from the NEXAFS data. Whereas X-ray spectroscopy methods provide valuable information about the surface distribution of elements and functional groups, the antifouling ability of the polymers is more closely related to their surface structures in water. Further, the water structures at the material surfaces also play an important role in determining the antifouling performance.[54]

To understand the relationship between the molecular structure, surface structure, and hydration of the sequence-specific polypeptoids, here we applied sum frequency

generation (SFG) vibrational spectroscopy to probe the material surfaces at the molecular level in air and in water in situ. As we discussed above in this thesis, SFG vibrational spectroscopy is intrinsically surface sensitive, providing information about molecular structures at surfaces and interfaces.[10,55-57] It has been extensively applied to study the structures of polymers and biomolecules at various interfaces[31,58-61] and has proven particularly powerful in revealing polymer/water interfacial structures in ambient environments.[32-35,62] Furthermore, detailed structural information of interfacial water can be extracted from SFG spectra.[63-68]

In this work, we examined the surface structures and hydration of a series of amphiphilic polypeptoids with different sequences (with their abbreviations shown in Figure 2.12) using SFG spectroscopy. SFG signals of the polymer surfaces in air are well-correlated with the previously reported NEXAFS data, showing inverse surface amounts of the hydrophilic N-(2-methoxyethyl)glycine (Nme) units and the hydrophobic N-(heptafluorobutyl)glycine (NF) units, which are also dependent on the polymer sequences. The SFG signals of water at the polymer surfaces are sensitive to the number and position of the fluorinated units. In addition, the underwater restructuring behaviors of the polymer surfaces were evaluated with time evolution contact angle measurements. The SFG and contact angle data revealed that the strongly hydrogen-bonded water at the polymer surfaces is critical for good antifouling property and the underwater surface restructuring rate deduced from contact angle data determines their fouling release performance, demonstrating the sequence-dependent hydration and antifouling/fouling release properties of the amphiphilic polypeptoids.

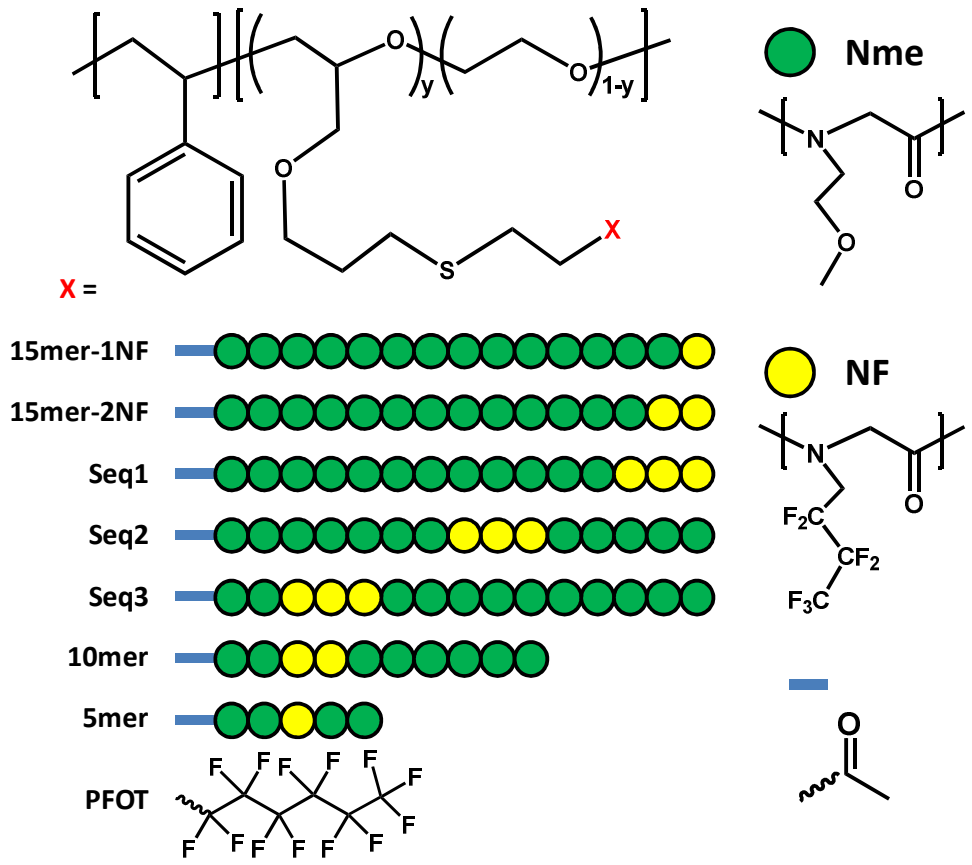

Figure 2.12 Molecular structures of the amphiphilic polymers investigated in this work.

2.3.2 Experimental Section

The polypeptoids (Figure 2.12) were synthesized according to the previous published method with molecular weights and compositions presented in the literature by our collaborators (Prof. Rachel Segalman's lab at UC-Berkeley and UC-Santa Barbara).[52] The polymer backbone contains 23 kDa (Mn) of polystyrene and 46 kDa (Mn) of poly(ethylene oxide).[52] The polymers were coated on silica windows (1 inch in diameter, 1/8 inch thick, from ESCO Optics) via spin-coating and annealing, with a thickness of approximately 80 nm.[52] The density of the polymers is around 1.2 g/cm^3.[69] Millipore water was used in all the experiments.

The hydrophilicity and underwater surface restructuring of the polymer coatings were assessed by time-dependent water contact angles measured with a CAM 100 contact angle goniometer (KSV Instruments). The SFG spectroscopy was implemented according to the protocol reported previously.[54] Briefly, the visible and infrared (IR) input beams penetrated a SiO_2 window and overlapped spatially and temporally at the polymer surface/interface (Figure 2.13). The incident angles of the visible and IR beams were 60° and 54° with respect to the surface normal, and the pulse energies of the visible and IR beams were 50 and 100 μJ, respectively. The reflected SFG signal was collected by a monochromator along with a photomultiplier tube. All SFG spectra were shown using the ssp (SFG output, visible input, and IR input) polarization combination. The SFG signals of the polypeptoids were normalized by the strong peak at 2955 cm^{-1} generated from a spin-coated poly(methyl methacrylate) (PMMA) film[11] on a silica window. Average spectra of three repetitions were shown and standard deviations were presented as error bars for quantitative comparison.

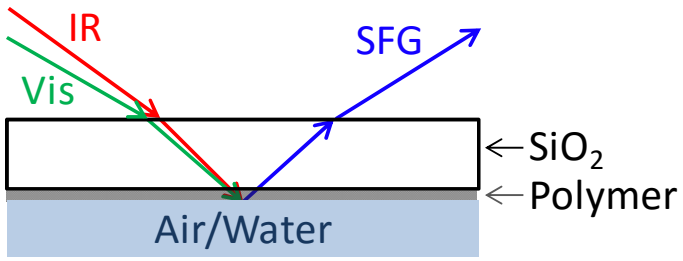

Figure 2.13 SFG measurement of a polymer coating on a silica window in air or water.

2.3.3 Results and Discussion

Figure 2.14A shows the SFG spectra of the polymer coatings in air. A distinct peak at 2815 cm^{-1} assigned to the O-CH_3 group[37,70] on Nme was observed for all the Nme-containing polypeptoids, indicating that the O-CH_3 end group is present at the

polymer surfaces in air. As expected, the spectrum of PFOT does not show any peak at 2815 cm^{-1}, verifying that the 2815 cm^{-1} signal for the other polymers is contributed from Nme. Because the polymers have similar structures and they are all exposed to the same environment (e.g. air), we assume that the ordering of the O-CH_3 group at the polymer surfaces in air is similar.[8,12] Thus, the intensity of the peak at 2815 cm^{-1} can be used to estimate the surface coverage of the Nme unit.

For comparison, Figure 2.14B summarizes the intensity of the peak at 2815 cm^{-1} detected from the polymer surfaces in air, which shows a clear trend as a function of the polypeptoid sequence. The strongest intensity was detected for 15mer-1NF, in which one NF unit is attached to the outer edge of the peptoid (farthest from the polymer backbone). The surface presence of Nme is owing to the migration of the adjacent hydrophobic NF unit to the polymer surface in air, which has been observed in other C-F containing amphiphilic polymers.[70] In other words, the NF unit can "drag" the adjacent peptoid units to the air interface.[23] As the number of the NF units at the outer edge of the peptoid increases from one to three (comparing 15mer-1NF, 15mer-2NF, and Seq1), the SFG signal of Nme decreases. Because fluorocarbon chain is known to have low surface tension, it tends to stay at the surface in air. Thus the increase of the NF components suppresses the surface coverage of Nme. For Seq1, Seq2, and Seq3, in which the number of the NF units stays constant at three in the peptoid chain, the O-CH_3 signal increases when the NF units are moved from the outer edge to the middle of the peptoid close to the polymer backbone. Unlike those at the end of the peptoid, the three NF units in the middle of peptoid can drag the Nme units at both sides to the surface, thereby increasing the surface coverage of Nme. Comparing Seq3, 10mer, and 5mer, in which peptoid chain

becomes shorter but the ratio of Nme to NF and the position of NF are kept the same, the O-CH_3 signal increases as the length of peptoid chain decreases. Although the absolute amount of Nme is lower in the shorter peptoid chains, the decrease of the NF content at the same time allows more surface coverage of Nme. For all the polymers, no signal of the phenyl ring above 3000 cm^{-1} was detected (Figure 2.14A), indicating the absence of the polystyrene component at the polymer surfaces in air or the surface phenyl groups lie down on the surface. According to the previous research, surface phenyl groups in air always tilt on the surface, instead of lying down.[71-75] Because no SFG signal of phenyl ring could be obtained using sps polarization as well, we believe that indeed here the polystyrene component is absent on the surface and present only in the polymer bulk. This is consistent with a previous report which showed that the NF units in peptoid could effectively suppress the surface presence of the phenyl rings.[23]

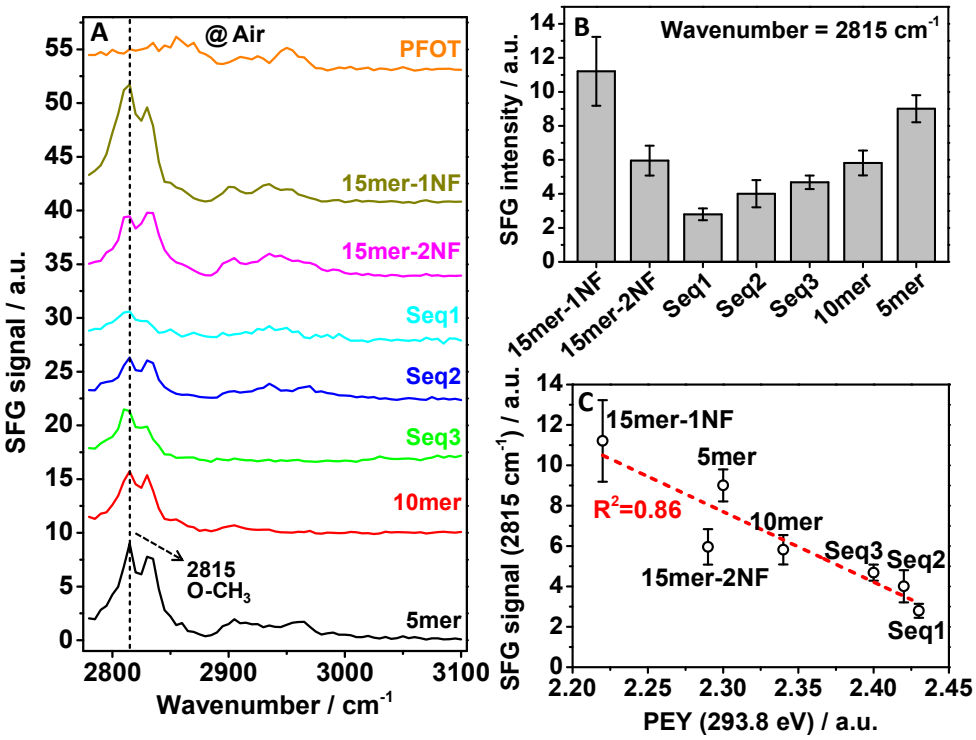

Figure 2.14 (A) SFG spectra of the polymers in air. (B) Peak intensity at 2815 cm^{-1} from the spectra of the polypeptoids in (A). (C) The SFG intensity at 2815 cm^{-1} assigned to O-CH_3 of Nme is negatively correlated to the partial electron yield (PEY) at 293.8 eV from NEXAFS assigned to the fluorine element on NF.[52]

The surface coverage of the Nme units is dependent on both the sequence of the peptoids and the surface presence of the NF units. Figure 2.14C shows a negative correlation between the SFG signal at 2815 cm^{-1} in air detected in this work and the NEXAFS signal at 293.8 eV that was published previously.[52] Here, the partial electron yield (PEY) at 293.8 eV of NEXAFS is proportional to the amount of the surface fluorine element at the top 2 nm.[76] This negative correlation indicates the inversely related surface coverage between the Nme and NF units due to their different surface energies, meanwhile demonstrating the consistency between the results from SFG and NEXAFS measurements.

Whereas SFG data of the amphiphilic polymers collected in air provides insight into the relationship between the polypeptoid materials' molecular formulas and surface structures in air, marine antifouling/fouling release properties are determined by the surfaces in aqueous environments, thereby we need to probe the surfaces of the polypeptoid coatings in contact with water with SFG. As shown in Figure 2.15A, the SFG spectra of all the polymers in water show little C-H stretching signals from the polymers, indicating a lack of ordering of the polymer surface structures in water. The random orientation of the surface functional groups may result from the surface restructuring processes that amphiphilic polymers are expected to experience underwater.[45,53] Water signals dominate the SFG spectra at the polymer/water interfaces, with a stronger band at 3200 cm^{-1} and a weaker signal at 3400 cm^{-1}, assigned to strongly hydrogen bonded and weakly hydrogen bonded water respectively.[63,64] While the shape of the water spectra is similar for all the polymers, the signal intensity varies depending on the polymer surface structures, indicating the different ordering of the interfacial water molecules on different polymer surfaces.

Comparing SFG spectra collected from 15mer-1NF, 15mer-2NF, and Seq1 in water, an increase in the number of the NF units at the outer edge of the peptoid leads to a decrease of water signal due to the unfavorable interaction between the hydrophobic fluorocarbon chains and water molecules, which disrupts the ordering of the interfacial water molecules. For Seq1, Seq2, and Seq3, the water signal increases as the NF units are moved from the outer edge to the middle of the peptoid close to the polymer backbone. Compared to the NF units at the end of the polymer, when NF units are placed in the middle of the polymer, they facilitate the migration of the hydrophilic parts of the

polymer (e.g. Nme) at both sides of the NF block to the surface. These hydrophilic components can interact more favorably with water, order the interfacial water molecules, and induce strong hydrogen bonding formation. When both the length of the peptoid chain and the number of the NF units decrease, for Seq3, 10mer, and 5mer, the water signal is similar for Seq3 and 5mer, and is weaker for 10mer. Whereas three NF units effectively drag the Nme chain to the surface and one NF unit allows more surface coverage of Nme, the dragging effect of the block containing two NF units in 10mer is weaker than that of Seq3, and meanwhile its suppression of the Nme surface coverage is stronger than 5mer, resulting in less surface coverage of Nme and the weaker water signal of 10mer than Seq3 and 5mer. These SFG water signals demonstrate that the hydration of the polymer surfaces is sensitively dependent on the sequence of the peptoid (the number and the position of the fluorocarbon chains), revealing a subtle tradeoff between the dragging effect on and the surface suppression of the hydrophilic components by the NF units.

To further understand the surface hydration and underwater restructuring of the amphiphilic polypeptoids, their water contact angles were measured as a function of time. As shown in Figure 2.15B, the water contact angles of 5mer and 15mer-1NF, which contain one NF unit in each peptoid chain, are similar and demonstrate faster surface restructuring than the other polymers, as evidenced by the sharp decrease of the contact angle ($>10^{o}$) within the first 10 s. This is consistent with a previous report which showed that polypeptoids containing longer NF blocks tend to crystallize and reorganize more slowly.[23] Comparing 15mer-1NF, 15mer-2NF, and Seq1, when the NF units locate at the outer edge of the peptoid, more NF units result in higher water contact angles. When the

block containing three NF units is moved into the middle of the polymer, the surface becomes more hydrophilic. To better interpret the contact angle trend, a negative correlation between the SFG signal of the polymers in water at 3200 cm^{-1} and the water contact angles at 50 s was drawn in Figure 2.15C. Thus, the affinity of water to the polymers results in the ordering of interfacial water molecules and strong hydrogen bonding.

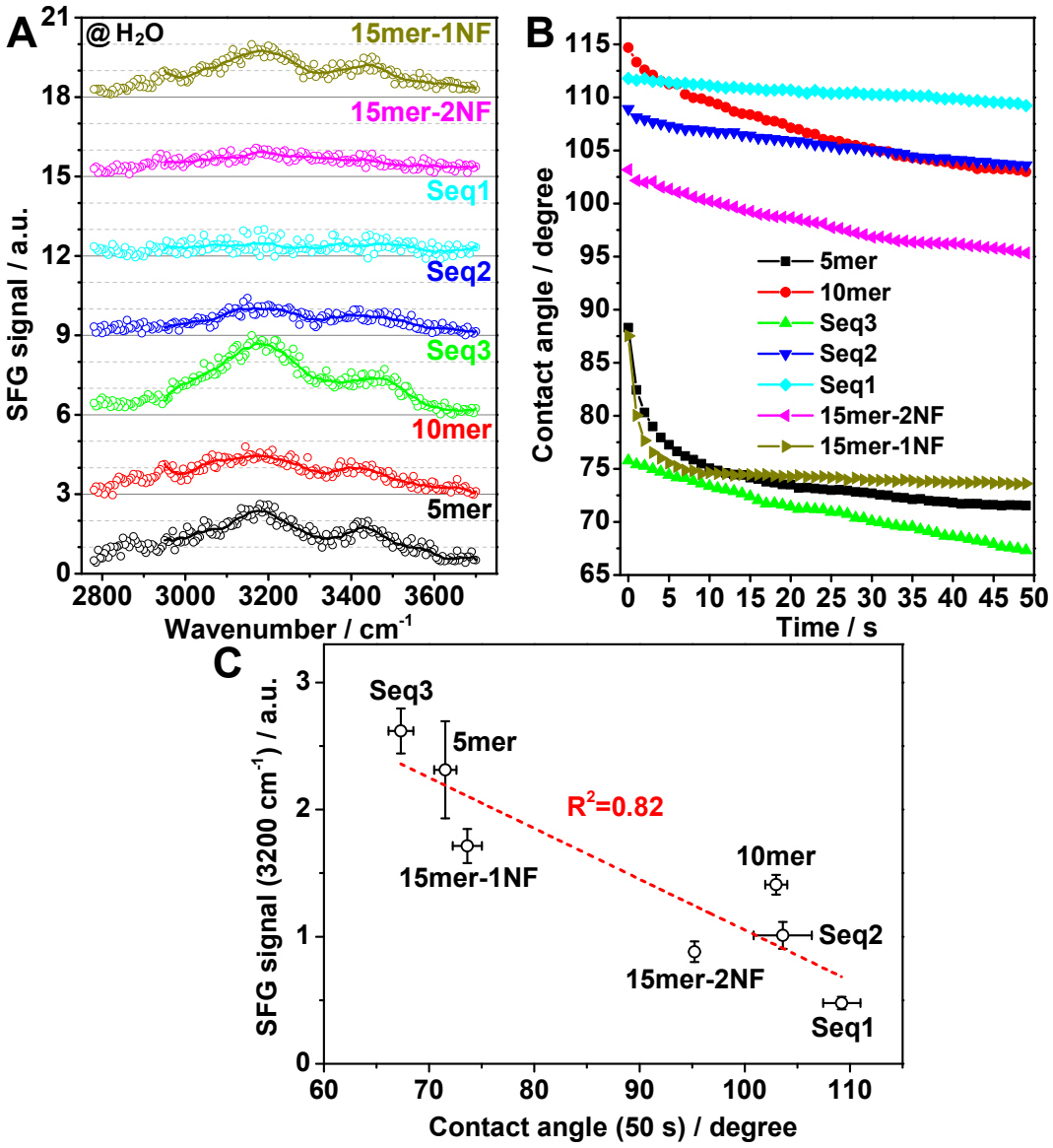

Figure 2.15 (A) SFG spectra of the polymer/water interfaces (Solid curves are smoothed spectra using 10 points adjacent averaging). (B) Time evolution of the water contact angles at the polymer surfaces. (C) The SFG intensity of the polymer/water interfaces at 3200 cm^{-1} is negatively correlated to the water contact angles of the polymer surfaces at 50 s.

As shown in Figure 2.16, the above SFG data of the polymers in air and water can be correlated to the antifouling (spore attachment) and fouling release (spore removal) test results published previously.[52] For 15mer-1NF, 15mer-2NF, and Seq1, in which the

peptoid chains are of the same length with an increasing number of the NF units at the outer edge of each peptoid chain, the most spore attachment was detected on Seq1 and the most spore removal was achieved on 15mer-1NF. For these three polymers, the SFG signal intensity detected from both Nme and water shows the same order --- 15mer-1NF>15mer-2NF>Seq1, indicating that limiting the suppression of the surface hydrophilic groups by the fluorinated moieties and the ability of the hydrophilic components at the polymer surfaces to order and to hydrogen-bond strongly with water are important for antifouling/fouling release performances. Comparing Seq1, Seq2, and, Seq3, with the same number of NF units at different positions, Seq3 is best to resist spore attachment. Similarly, SFG spectra of Seq3 show the strongest signal intensity from both Nme and water among the three polymers. The fouling release performances of the three polymers, however, are weaker than the other polymers, probably due to the slow surface restructuring process as suggested by the water contact angle data. For Seq1, 10mer, and 5mer, the strongest SFG signals from both Nme and water were detected at the 5mer surface, where the most spore removal and the least spore attachment was achieved, again demonstrating the relationship between the surface hydrophilicity and antifouling/foul-release property. Further, water contact angle results suggest that efficient surface restructuring plays an important role in facilitating fouling release at the 15mer-1NF and 5mer surfaces, which contain only one NF unit in each peptoid chain.

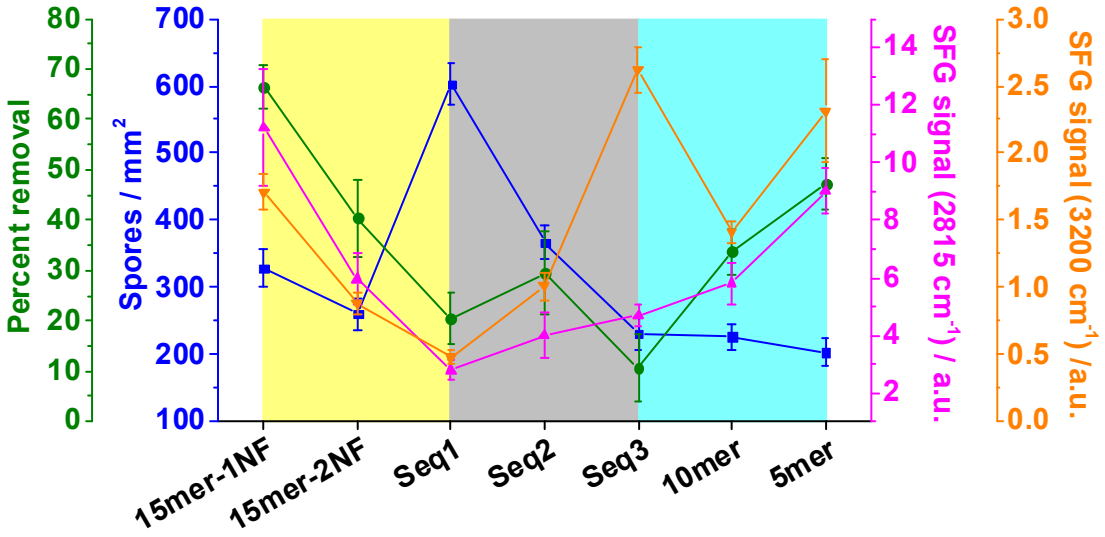

Figure 2.16 Correlation between the antifouling/fouling release data and the SFG signals of Nme and water for the polypeptoids. The density of the spores on peptoid surfaces was measured after 45 min of attachment. The percent removal of sporelings from surface was measured after exposure to an impact pressure of 160 kPa, generated by a calibrated water jet. The plot was divided into three areas to guide the comparison among three materials with similar structures at a time.

2.3.4 Conclusions

In this chapter, the surface structure and hydration of a series of sequence-specific amphiphilic polypeptoids were investigated with SFG spectroscopy and correlated to their antifouling/fouling release performances. SFG spectra of the polymer surfaces in air revealed the sequence-dependent surface coverage of the hydrophilic Nme units as a function of the number and position of the hydrophobic NF units in the peptoid chain, which also has an inverse relation to the surface fluorine concentration. The SFG results of the polymer/water interfaces indicate that the ability of the polymer surfaces to orient and form strongly hydrogen bonded water is sensitively dependent on the sequence of the peptoids, which determines their hydrophilicity and surface restructuring rate underwater. The surface coverage of the hydrophilic Nme groups and strong interactions between the

polymers and water are well-correlated to their antifouling properties. We have investigated interfacial water structure on other anti-biofouling polymer surfaces, e.g., zwitterionic polymers.[54] Similarly, it was found that strongly hydrogen bonded water is important for the antifouling behavior of the zwitterionic polymers. This research also shows that the surface restructuring rate is well-correlated with the fouling-release properties of the peptoid surfaces.

2.4 Surface Wetting and Restructuring Behavior of Polyelectrolyte Multilayers for Oil/Water Separation

2.4.1 Introduction

Studies of water wetting on charged surfaces will not only advance our knowledge of many important surface functions, such as lubrication, anti-fouling, and self-cleaning, which are encountered in biological systems, but also enhance our ability to translate these surface functions into innovative technical applications.[77] In general, charged surfaces are easily wetted by water, which is a macroscopic expression of strong hydration of the surface ionic groups. For a solid surface, air drying is obviously inevitable in practice, even if is not required technically. Upon contact with air, charged surfaces, like many other polar surfaces with high surface free energy, must orient the ionic groups inwards to lower the surface free energy, thus resulting in a noticeable increase in surface hydrophobicity. As such, wetting charged surfaces with water, characterized by the water contact angle in air ($\theta_{w/a}$), has little dependence on the surface ionic group, though the interaction of ions or ionic groups with water (hydration) is known to be ion-specific.[78] In contrast, the present work demonstrates a prominent

dependence of the surface hydrophilicity of polyelectrolyte multilayers (PEMs) on the molecular nature of the uncompensated ionic groups presented at the surface.

Herein we study surface wetting of the PEMs, which are obtained by layer-by-layer (LbL) deposition of polydiallyldimethylammonium chloride (PDDA) and poly(styrene sulfonate) (PSS), mainly in water-solid-oil systems. Our results demonstrate that the surface hydrophilicity of the resulting PEMs is correlated primarily to the molecular configuration. According to a newly developed theory on the correlation between the water contact angle and surface polarity,[79] the surface hydrophilicity of PEMs should be determined by the surface charge density, which can be defined by the surface area occupied by the surface ionic groups. For PSS-capped surfaces, the uncompensated benzenesulfonate (BS^-) groups on the surfaces comprise rigid and hydrophobic phenyl (Ph) moieties and hydrophilic, anionic sulfonate (SO_3^-) moieties, which are well separated in space. Our spectroscopic results show that in water, the surface BS^- groups orient their Ph moieties in an orderly and upright position out of the surface of the plane. This orientation maximizes surface charge density and transforms the surface hydration of the SO_3^- moieties into oil repellency with an oil contact angle in water ($\theta_{o/w}$) of greater than 165°. Upon contact with air or oil, the Ph moieties are randomly distributed and orient parallel to the surface plane, and thus significantly reduce the surface charge density. As a result, the PSS-capped surfaces become poorly wetted by water, as evidenced by the water contact angle in oil ($\theta_{w/o}$) of greater than 90°. In contrast, the uncompensated quaternary amine (QA^+) groups on PDDA-capped surfaces have their cationic (N^+) center enveloped by four alkyl moieties in each pyrrolidine ring. Owing to this configuration, the surface charge density and surface hydrophilicity of the PDDA

capped surfaces are insensitive to the orientation of the quaternized pyrrolidine ring. They remain well wetted by water in air and in oil ($\theta_{w/o}$=42°), though the weak hydration of the surface QA^+ groups cannot effectively prevent oil adhesion in water ($\theta_{o/w}$=ca. 133°). Thus, our results demonstrate a pronounced dependence of the wetting behavior of charged surfaces on the molecular nature and geometric configuration of the surface ionic groups. This dependence will also provide a better model to describe how ionic species interact with water, air, and oil at interfaces where a marked conformational change is essential for adsorption and translocation.

Surface wetting is conventionally studied in water-solid-air systems, and our study mainly focused on water-solid-oil systems because of the academic importance and strong relevance in industry. In this context, oil/water separation is an important technical application. To date, the prevailing strategy is to make hydrophilic nanostructures on the surfaces of separation membranes, inspired by the oil-repellent skins of fish and other aquatic organisms.[80,81] Such surface nanostructures are designed for water trapping, and can effectively offset the potential surface hydrophilicity loss because of their air-drying-induced surface reconstruction, thus ensuring underwater surface superoleophobicity. Here we discover that upon immersion into water, PSS-capped PEMs exhibit excellent oil-repellency regardless of aging treatment in air. This repellency has encouraged us to coat conventional steel meshes with PSS-capped PEMs, thus enabling highly efficient separation of water from oil/water mixtures at high flux, and opening promising prospects in the oil-water separation industry.

2.4.2 Experimental Section

PDDA (M_w 100 000-200 000), PSS (M_w 70 000), n-hexadecane, oil red O, and methylene blue were purchased form Sigma-Aldrich. NaCl, acetone, isopropanol, ethanol, chloroform and cyclohexane were purchased from Chem-Supply, Australia. All the chemicals were used as received without purification. Stainless steel meshes with aperture of 25 μm were purchased from Sefar Pty Ltd, Australia. Si wafers were purchased from Si-Mat Silicon Materials, Germany. CaF_2 prisms were purchased from Altos Photonics (Bozeman, MT).

Silicon wafers were cleaned by immersing in Piranha solution (1:3 (v/v) mixture of 30% H_2O_2 and 98% H_2SO_4), followed by heating until no bubbles were released. *Note that Piranha solution reacts violently with organic materials and should be handled carefully.* Afterwards, the Si wafers were thoroughly rinsed with water and dried with N_2 flow. $(PDDA/PSS)_n$ PEMs were readily grown on the freshly cleaned silicon wafers via alternatingly immersing the wafers into the aqueous solutions of PDDA and PSS, respectively, for 20 min, followed by thorough rinsing with water. After the desired layer number was reached, the resulting PEMs were thoroughly rinsed by water and gently dried with N_2 flow. The concentration of PDDA and PSS in water were 1.0 mg/mL in the presence of 1.0 M NaCl. With the same method, PEMs were also prepared on plasma cleaned CaF_2 prisms for sum frequency generation (SFG) vibrational spectroscopy measurements.

Stainless steel meshes were cleaned by successive sonication in acetone, isopropanol, ethanol and water. The cleaned stainless steel meshes were further cleaned by oxygen plasma to enhance the surface hydrophilicity and ionization. The freshly

hydrophilized stainless steel meshes were modified by $(PDDA/PSS)_4$ PEMs following the protocol described above.

Contact angle measurements were implemented on a Dataphysics OCA 20 contact angle system at ambient temperature using a 2 μL liquid droplet as an indicator. Colorimeter glass cells, purchased from Starna, were used for measurement of the $\theta_{o/w}$ on solid surfaces. Atomic force microscopy (AFM) imaging was performed with a MultiMode 8 AFM from Bruker in a ScanAsyst mode at ambient condition using Si cantilevers. X-ray photoelectron spectroscopy (XPS) analysis was carried out on a Kratos Axis Ultra with a Delay Line Detector photoelectron spectrometer using an Al monochromatic X-ray source. Scanning electron microscopy (SEM) images were obtained on FEI Quanta 450 operated at 10-20 kV. SFG vibrational spectroscopy measurement was conducted according to the method reported by Chen et al.[54] Typically, the visible and infrared (IR) input beams penetrate a right angle CaF_2 prism and overlap spatially and temporally at the sample surfaces. The incident angles of the visible and IR beams are 60° and 54° with respect to the surface normal, and the pulse energies of the visible and IR beams are 30 and 100 μJ, respectively.

2.4.3 Results and Discussion

PDDA and PSS are the most commonly used, permanently charged polyelectrolytes. Here they were alternatingly deposited onto Si wafers in the presence of 1.0 M NaCl, and the resulting PEMs were denoted as $(PDDA/PSS)_n$ where "n" represents the bilayer numbers. In this work, we mainly studied $(PDDA/PSS)_3$-PDDA and $(PDDA/PSS)_4$ PEMs (Figure 2.17) with a surface roughness of less than 3 nm as shown

in their AFM images (Figure 2.18), so the impact of the surface roughness on surface wetting could be ignored.

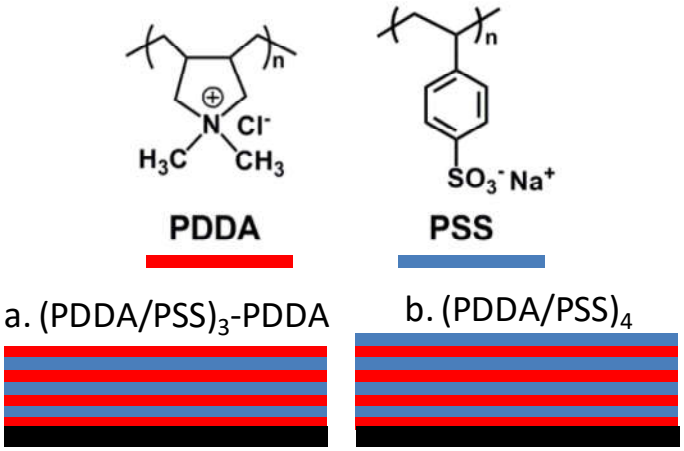

Figure 2.17 Molecular structures of PDDA and PSS, and the (a) PDDA and (b) PSS capped PEMs prepared from LbL assembly.

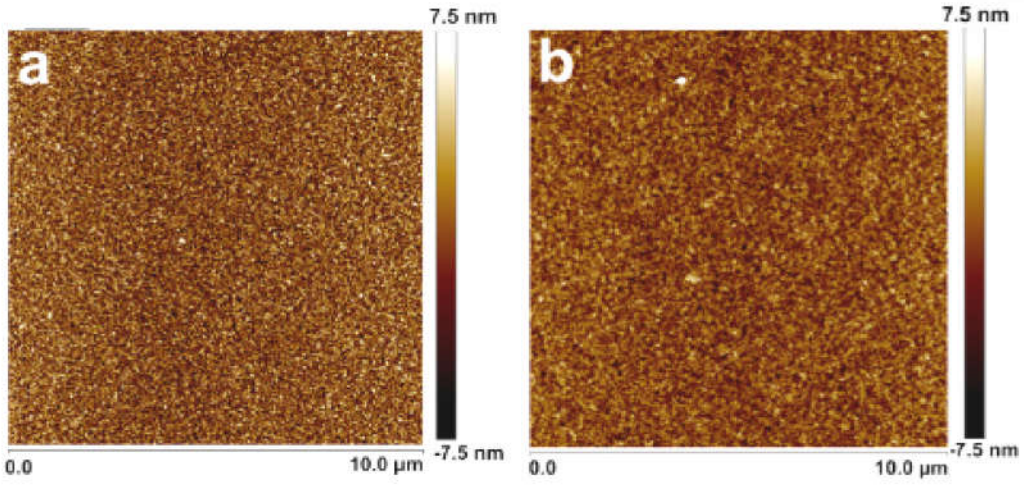

Figure 2.18 AFM images of (a) $(PDDA/PSS)_3$-PDDA and (b) $(PDDA/PSS)_4$ films.

We also studied oil wetting on $(PDDA/PSS)_3$-PDDA and $(PDDA/PSS)_4$ PEMs in water (Figure 2.19). When the PEMs were brought in contact with a pendant droplet of hexadecane (2 µL) in water, both $(PDDA/PSS)_3$-PDDA and $(PDDA/PSS)_4$ PEMs initially exhibit a $\theta_{o/w}$ value above 150°. With the prolonged contact time, however, the $\theta_{o/w}$ value

of the PDDA-capped surfaces gradually dropped from 152° to 133° in 30 minutes while that of the PSS-caped surfaces remained as high as 165° with no detectable change. When the PEMs were removed from the hexadecane droplet, the oil droplets stayed on the PDDA-capped surfaces, whereas complete oil detachment was observed on the PSS-capped surfaces, even after the surfaces were kept in tight contact with the oil droplets for 12 hours.

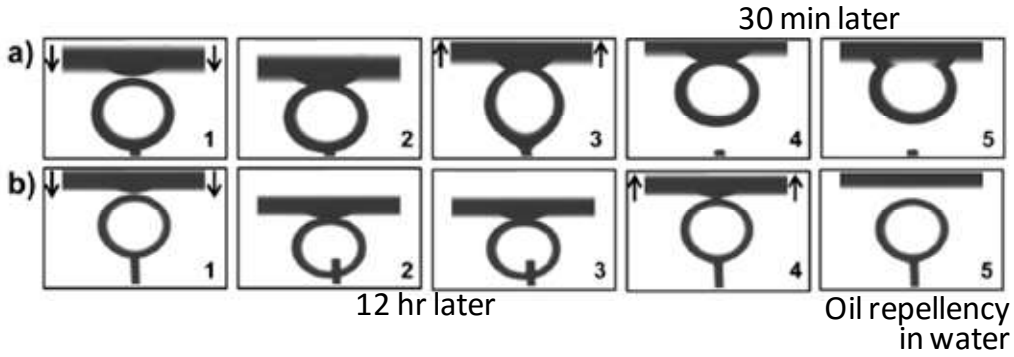

Figure 2.19 Photographs taken when the (a) $(PDDA/PSS)_3$-PDDA and (b) $(PDDA/PSS)_4$ surfaces were approaching (a1, a2, b1, b2) and leaving (a3, a4, b4, b5) a droplet of n-hexadecane (2 μL) pending on a needle in water. a5 is 30 min after a4, b3 is 12 h after b2. The arrows indicate the directions of the sample movement.

To reveal the molecular rationale for their complicated wetting behavior, the surface molecular structures of the $(PDDA/PSS)_3$-PDDA and $(PDDA/PSS)_4$ PEMs were investigated by SFG vibrational spectroscopy (Figure 2.20). Figure 2.20a shows that in water the uncompensated QA^+ groups on the $(PDDA/PSS)_3$-PDDA PEMs exhibit fairly strong $C\text{-}N^+$ stretching vibrational signal, thus indicating the surface QA^+ groups preferentially orient perpendicular to the surface plane (Figure 2.21b). The strong CH_3 stretching signal in water suggests that each QA^+ group has two CH_3 moieties normal to the surface in direct contact with water. The CH_2 stretching signal is also strong in water (compared to that in air), though weaker than the CH_3 one, thus indicating that the two

CH_2 moieties of the pyrrolidine ring are also ordered on the surface and directly in contact with water. Note that the CH_2 moieties of the PDDA backbone should have a small contribution to the CH_2 stretching vibration signal as they may be either shielded by the pyrrolidine ring of the QA^+ groups or randomly oriented within the surface plane This orientational configuration agrees with the molecular structures of the surface QA^+ groups where the N^+ center isotropically enveloped by two CH_3 and two CH_2 moieties in each pyrrolidine ring, and accounts for the wetting behavior of the PDDA-capped surface in water. This alkyl envelopment greatly lowers the hydration effectiveness of the N^+ center and, at the same time, facilitates oil adhesion on the PDDA-capped surface in water. When the PDDA-capped surface is exposed to air, the CH_3 stretching signal becomes weaker than that of CH_2 (Figure 2.20a), thus indicating that the surface QA^+ groups orient parallel to the surface plane with two CH_2 moieties of the pyrrolidine ring protruding more from the surface plane than the two CH_3 moieties (Figure 2.21a). This orientation change may just slightly change the surface area occupied by each QA^+ group and in turn the surface charge density on the PDDA capped surface, because quaternized pyrrolidine rings are inserted as bulky repeating units in the PDDA backbone and the N^+ center of each ring is enveloped by two CH_3 and two CH_2 moieties. The distinct C-N^+ stretching signal in air, albeit weaker than that in water, indicates that the surface QA^+ groups point the N^+ centers towards air, and facilitates the surface hydration. Hence the surface charge density on the PDDA-capped surfaces is little altered and, therefore, the water wetting remains effective regardless of the orientation of the surface QA^+ groups in response to the environmental change.

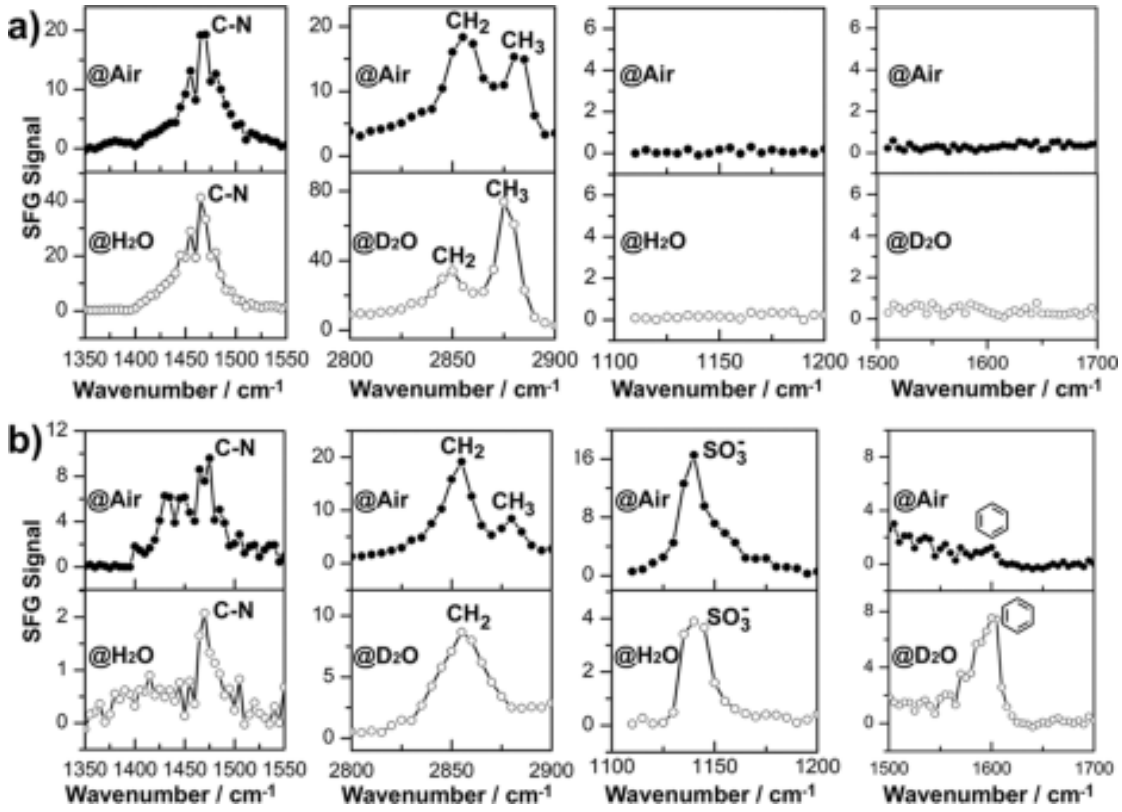

Figure 2.20 SFG spectra of (a) $(PDDA/PSS)_3$-PDDA and (b) $(PDDA/PSS)_4$ PEMs measured in air (upper panel) and water (lower panel). Deuterated water is used instead of water to distinctly reveal the vibration signal of alkyl and phenyl moieties.

Figure 2.20b shows that the SO_3^- moieties of the uncompensated BS^- groups on the $(PDDA/PSS)_4$ PEMs are present both in air and water, but the aromatic C=C stretching signal of the Ph moieties appears only in water, thus indicating the different orientation and ordering of the Ph moieties in air and water. Since surface BS^- groups have the SO_3^- and Ph moieties placed side by side, and when their Ph moieties orient perpendicular to the surface plane with ordering in water, individual surface BS^- groups on the PSS-capped surfaces will occupy minimal surface area (Figure 2.21b), thus maximizing the surface charge density and transforming the strong surface hydration of the SO_3^- moieties into strong oil repellency in water. In air, however, the Ph moieties randomly orient parallel to the surface plane, so the surface area occupied by each surface

BS^- group is maximized (Figure 2.21a), thus significantly reducing the surface charge density and in turn the surface hydrophilicity. This arrangement explains the poor water wetting on PSS-capped surfaces in oil/air.

Whereas neither SO_3^- nor Ph moieties of BS^- groups are visible in the SFG spectra collected from the $(PDDA/PSS)_3$-PDDA PEM, the C-N^+ and CH_3 signals of the QA^+ groups were detected in the SFG spectra of the $(PDDA/PSS)_4$ PEM (Figure 2.20b). This detection implies that despite the surface charge overcompensation upon PSS adsorption in 1.0 M NaCl, a small number of the QA^+ groups from the PDDA layer beneath, as evidenced by their weaker intensities compared to those observed on the PDDA-capped PEM surface, remain exposed to the environment, along with the BS^- groups of the PSS capping layer. This finding inspires us to focus on understanding the internal structure of $(PDDA/PSS)_n$ PEMs, as it is still under debate. Figure 2.20b indicates the absence of the CH_3 stretching vibrational signal of the QA^+ groups in water. This is reasonable because the surface BS^- groups stand up on the surfaces in water, which is beneficial for the PSS-capped surfaces to keep hydrated and repel oil in water.

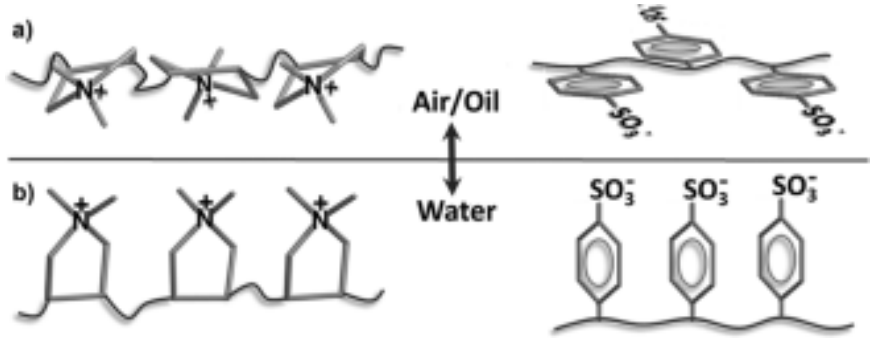

Figure 2.21 Schematic illustration of the orientational configuration of the uncompensated QA^+ groups on $(PDDA/PSS)_3$-PDDA PEMs and the uncompensated BS^- groups on $(PDDA/PSS)_4$ PEMs in response to the surrounding environmental change.

Encouraged by the surface hydration of PSS-capped surfaces, our collaborators (Prof. Dayang Wang's lab at University of South Australia) coated stainless steel meshes with apertures of 25 μm by $(PDDA/PSS)_4$ PEMs for oil/water separation . The $(PDDA/PSS)_4$ PEMs film is thick enough to fully cover the stainless steel mesh surface, as evidenced by the disappearance of metal signals in the XPS spectra (Figure 2.22a). The resulting meshes allow easy filtration of water from an oil/water mixture at high flux of about 610 L m^{-2} s^{-1} (Figure 2.22b) with high separation efficiency. The surface roughness of the $(PDDA/PSS)_4$ coating is less than 3 nm, and the notches and scratches present on the steel meshes are on the scale of tens to hundreds of micrometers. Thus, the contribution of the surface roughness to the high oil/water separation efficiency can be ignored. Since the $(PDDA/PSS)_4$ coating were produced by LbL deposition in 1.0 M NaCl, its superior oil-repellency in water exhibited long term stability against acid, alkaline, and salt at high concentrations, and will be advantageous for technical applications such as oil-spill cleanup in seawater.

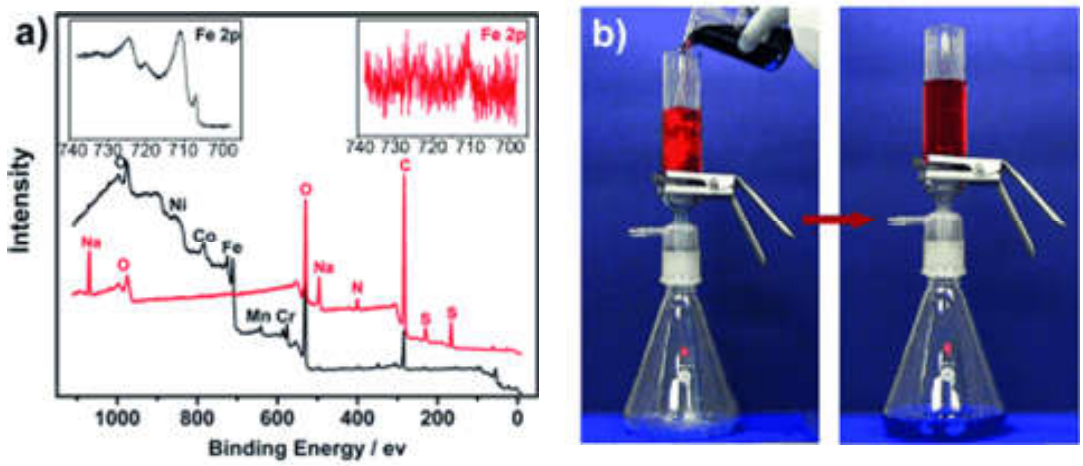

Figure 2.22 (a) XPS wide scan spectra of a stainless steel mesh with (red) and without (black) $(PDDA/PSS)_4$ film. The insets show the corresponding high-resolution spectra of Fe in the steel mesh. (b) Photos shot during filtration of the mixtures of hexadecane, stained by Oil Red O, and water, stained by methylene blue, through a $(PDDA/PSS)_4$-

coated stainless steel mesh (left panel) and after the filtration (right panel), in which water is selectively filtered through the steel mesh while hexadecane is retained on the top of the mesh. The aperture of the steel mesh is 25 μm.

2.4.4 Conclusions

In summary, we demonstrate a prominent impact of the nature of the surface ionic groups on the surface wetting behavior of $(PDDA/PSS)_n$ PEMs, which hinges mainly on the configurational geometry of the uncompensated ionic groups on the surfaces. For PDDA-capped surfaces, the orientation of the surface QA^+ groups with isotropic configuration with respect to the surface plane hardly affect the surface hydrophilicity. For PSS-capped surfaces, the strong hydration of the surface BS^- groups with anisotropic configuration can be translated into excellent oil-repellency in water (poor water de-wetting) depending on the orientational order and directionality of the BS^- groups with respect to the surface plane. This configurational effect should be a better framework to interpret the wetting behavior of a charged surface according to the molecular nature of surface ionic groups. We hope that it will stimulate studies to revisit experimental and theoretical molecular design of surface wetting, and that future research will focus more on the molecular features of the substituents next to the ionic centers of surface groups, such as size, shape, flexibility, and spatial arrangement with regard to the ionic centers rather than simply on the hydration strength of the ionic centers alone.

Further, the lessons learnt from the correlation between the surface wetting behavior of PEMs and their surface local structures will shed light on the study of the PEM internal structures, which are still under debate. Thanks to the operational simplicity and versatility of LbL deposition, our success in using $(PDDA/PSS)_4$-coated meshes for

efficient oil-water separation also endorses the technical significance of PEMs in self-cleaning applications.

2.5 References

(1) Lejars, M.; Margaillan, A.; Bressy, C. *Chem. Rev.* **2012**, *112*, 4347-4390.
(2) Stafslien, S.; Daniels, J.; Mayo, B.; Christianson, D.; Chisholm, B.; Ekin, A.; Webster, D.; Swain, G. *Biofouling* **2007**, *23*, 45-54.
(3) Kugel, A.; Stafslien, S.; Chisholm, B. J. *Prog. Org. Coat.* **2011**, *72*, 222-252.
(4) Majumdar, P.; Crowley, E.; Htet, M.; Stafslien, S. J.; Daniels, J.; VanderWal, L.; Chisholm, B. J. *ACS Comb. Sci.* **2011**, *13*, 298-309.
(5) Ye, S. J.; McClelland, A.; Majumdar, P.; Stafslien, S. J.; Daniels, J.; Chisholm, B.; Chen, Z. *Langmuir* **2008**, *24*, 9686-9694.
(6) Ye, S. J.; Majumdar, P.; Chisholm, B.; Stafslien, S.; Chen, Z. *Langmuir* **2010**, *26*, 16455-16462.
(7) Chen, Z. *Prog. Polym. Sci.* **2010**, *35*, 1376-1402.
(8) Wang, J.; Woodcock, S. E.; Buck, S. M.; Chen, C. Y.; Chen, Z. *J. Am. Chem. Soc.* **2001**, *123*, 9470-9471.
(9) Wang, J.; Paszti, Z.; Even, M. A.; Chen, Z. *J. Am. Chem. Soc.* **2002**, *124*, 7016-7023.
(10) Shen, Y. R. *J. Phys. Chem. C* **2012**, *116*, 15505-15509.
(11) Wang, J.; Chen, C. Y.; Buck, S. M.; Chen, Z. *J. Phys. Chem. B* **2001**, *105*, 12118-12125.
(12) Chen, C. Y.; Wang, J.; Chen, Z. *Langmuir* **2004**, *20*, 10186-10193.
(13) Clarke, M. L.; Chen, C. Y.; Wang, J.; Chen, Z. *Langmuir* **2006**, *22*, 8800-8806.
(14) Banerjee, I.; Pangule, R. C.; Kane, R. S. *Adv. Mater.* **2011**, *23*, 690-718.
(15) Ma, H. W.; Hyun, J.; Stiller, P.; Chilkoti, A. *Adv. Mater.* **2004**, *16*, 338-341.
(16) Zhang, Z.; Chao, T.; Chen, S. F.; Jiang, S. Y. *Langmuir* **2006**, *22*, 10072-10077.
(17) Ramsden, J. J. *Chem. Soc. Rev.* **1995**, *24*, 73-78.
(18) Krishnan, S.; Weinman, C. J.; Ober, C. K. *J. Mater. Chem.* **2008**, *18*, 3405-3413.
(19) Gudipati, C. S.; Finlay, J. A.; Callow, J. A.; Callow, M. E.; Wooley, K. L. *Langmuir* **2005**, *21*, 3044-3053.
(20) Weinman, C. J.; Gunari, N.; Krishnan, S.; Dong, R.; Paik, M. Y.; Sohn, K. E.; Walker, G. C.; Kramer, E. J.; Fischer, D. A.; Ober, C. K. *Soft Matter* **2010**, *6*, 3237-3243.
(21) Weinman, C. J.; Finlay, J. A.; Park, D.; Paik, M. Y.; Krishnan, S.; Sundaram, H. S.; Dimitriou, M.; Sohn, K. E.; Callow, M. E.; Callow, J. A.; Handlin, D. L.; Willis, C. L.; Kramer, E. J.; Ober, C. K. *Langmuir* **2009**, *25*, 12266-12274.
(22) Krishnan, S.; Ayothi, R.; Hexemer, A.; Finlay, J. A.; Sohn, K. E.; Perry, R.; Ober, C. K.; Kramer, E. J.; Callow, M. E.; Callow, J. A.; Fischer, D. A. *Langmuir* **2006**, *22*, 5075-5086.
(23) van Zoelen, W.; Zuckermann, R. N.; Segalman, R. A. *Macromolecules* **2012**, *45*, 7072-7082.
(24) Colak, S.; Tew, G. N. *Biomacromolecules* **2012**, *13*, 1233-1239.
(25) Colak, S.; Tew, G. N. *Langmuir* **2012**, *28*, 666-675.
(26) Dimitriou, M. D.; Zhou, Z. L.; Yoo, H. S.; Killops, K. L.; Finlay, J. A.; Cone, G.; Sundaram, H. S.; Lynd, N. A.; Barteau, K. P.; Campos, L. M.; Fischer, D. A.; Callow, M.

E.; Callow, J. A.; Ober, C. K.; Hawker, C. J.; Kramer, E. J. *Langmuir* **2011**, *27*, 13762-13772.
(27) Sundaram, H. S.; Cho, Y.; Dimitriou, M. D.; Finlay, J. A.; Cone, G.; Williams, S.; Handlin, D.; Gatto, J.; Callow, M. E.; Callow, J. A.; Kramer, E. J.; Ober, C. K. *ACS Appl. Mater. Interf.* **2011**, *3*, 3366-3374.
(28) Gracias, D. H.; Chen, Z.; Shen, Y. R.; Somorjai, G. A. *Acc. Chem. Res.* **1999**, *32*, 930-940.
(29) Liu, Y. W.; Jasensky, J.; Chen, Z. *Langmuir* **2012**, *28*, 2113-2121.
(30) Howell, C.; Diesner, M. O.; Grunze, M.; Koelsch, P. *Langmuir* **2008**, *24*, 13819-13821.
(31) Zhang, C.; Myers, J. N.; Chen, Z. *Soft Matter* **2013**, *9*, 4738-4761.
(32) Hankett, J. M.; Liu, Y. W.; Zhang, X. X.; Zhang, C.; Chen, Z. *J. Polym. Sci., Part B: Polym. Phys.* **2013**, *51*, 311-328.
(33) Li, G. F.; Ye, S.; Morita, S.; Nishida, T.; Osawa, M. *J. Am. Chem. Soc.* **2004**, *126*, 12198-12199.
(34) Ye, S. J.; Liu, G. M.; Li, H. C.; Chen, F. G.; Wang, X. W. *Langmuir* **2012**, *28*, 1374-1380.
(35) Leung, B. O.; Yang, Z.; Wu, S. S. H.; Chou, K. C. *Langmuir* **2012**, *28*, 5724-5728.
(36) Leng, C.; Liu, Y. W.; Jenkins, C.; Meredith, H.; Wilker, J. J.; Chen, Z. *Langmuir* **2013**, *29*, 6659-6664.
(37) Even, M. A.; Chen, C. Y.; Wang, J.; Chen, Z. *Macromolecules* **2006**, *39*, 9396-9401.
(38) Lee, B. S.; Lee, J. K.; Kim, W. J.; Jung, Y. H.; Sim, S. J.; Lee, J.; Choi, I. S. *Biomacromolecules* **2007**, *8*, 744-749.
(39) Li, L. Y.; Chen, S. F.; Zheng, J.; Ratner, B. D.; Jiang, S. Y. *J. Phys. Chem. B* **2005**, *109*, 2934-2941.
(40) Zheng, J.; Li, L. Y.; Chen, S. F.; Jiang, S. Y. *Langmuir* **2004**, *20*, 8931-8938.
(41) Ye, S. J.; Nguyen, K. T.; Boughton, A. P.; Mello, C. M.; Chen, Z. *Langmuir* **2009**, *26*, 6471-6477.
(42) Keefe, A. J.; Brault, N. D.; Jiang, S. Y. *Biomacromolecules* **2012**, *13*, 1683-1687.
(43) Zhang, Z.; Vaisocherova, H.; Cheng, G.; Yang, W.; Xue, H.; Jiang, S. Y. *Biomacromolecules* **2008**, *9*, 2686-2692.
(44) Yang, W.; Xue, H.; Li, W.; Zhang, J. L.; Jiang, S. Y. *Langmuir* **2009**, *25*, 11911-11916.
(45) Pollack, K. A.; Imbesi, P. M.; Raymond, J. E.; Wooley, K. L. *ACS Appl. Mater. Interf.* **2014**, *6*, 19265-19274.
(46) Zhao, X. T.; Su, Y. L.; Li, Y. F.; Zhang, R. N.; Zhao, J. J.; Jiang, Z. Y. *J. Membr. Sci.* **2014**, *450*, 111-123.
(47) Zhou, Z. L.; Calabrese, D. R.; Taylor, W.; Finlay, J. A.; Callow, M. E.; Callow, J. A.; Fischer, D.; Kramer, E. J.; Ober, C. K. *Biofouling* **2014**, *30*, 589-604.
(48) Krajangpan, S.; Kalita, H.; Chisholm, B. J.; Bezbaruah, A. N. *Environ Sci Technol* **2012**, *46*, 10130-10136.
(49) Badi, N.; Lutz, J.-F. *Chem. Soc. Rev.* **2009**, *38*, 3383-3390.
(50) Lutz, J.-F.; Ouchi, M.; Liu, D. R.; Sawamoto, M. *Science* **2013**, *341*, 1238149.
(51) Rosales, A. M.; Segalman, R. A.; Zuckermann, R. N. *Soft Matter* **2013**, *9*, 8400-8414.

(52) van Zoelen, W.; Buss, H. G.; Ellebracht, N. C.; Lynd, N. A.; Fischer, D. A.; Finlay, J.; Hill, S.; Callow, M. E.; Callow, J. A.; Kramer, E. J.; Zuckermann, R. N.; Segalman, R. A. *ACS Macro Lett.* **2014**, *3*, 364-368.
(53) Amadei, C. A.; Yang, R.; Chiesa, M.; Gleason, K. K.; Santos, S. *ACS Appl. Mater. Interf.* **2014**, *6*, 4705-4712.
(54) Leng, C.; Han, X. F.; Shao, Q.; Zhu, Y. H.; Li, Y. T.; Jiang, S. Y.; Chen, Z. *J. Phys. Chem. C* **2014**, *118*, 15840-15845.
(55) Shen, Y. R. *Nature* **1989**, *337*, 519-525.
(56) Lambert, A. G.; Davies, P. B.; Neivandt, D. J. *Appl. Spectrosc. Rev.* **2005**, *40*, 103-145.
(57) Lis, D.; Backus, E. H. G.; Hunger, J.; Parekh, S. H.; Bonn, M. *Science* **2014**, *344*, 1138-1142.
(58) Roy, S.; Covert, P. A.; FitzGerald, W. R.; Hore, D. K. *Chem. Rev.* **2014**, *114*, 8388-8415.
(59) Yan, E. C. Y.; Fu, L.; Wang, Z. G.; Liu, W. *Chem. Rev.* **2014**, *114*, 8471-8498.
(60) Lu, X. L.; Shephard, N.; Han, J. L.; Xue, G.; Chen, Z. *Macromolecules* **2008**, *41*, 8770-8777.
(61) Holinga, G. J.; York, R. L.; Onorato, R. M.; Thompson, C. M.; Webb, N. E.; Yoon, A. P.; Somorjai, G. A. *J. Am. Chem. Soc.* **2011**, *133*, 6243-6253.
(62) Chen, Q.; Zhang, D.; Somorjai, G.; Bertozzi, C. R. *J. Am. Chem. Soc.* **1998**, *121*, 446-447.
(63) Richmond, G. L. *Chem. Rev.* **2002**, *102*, 2693-2724.
(64) Shen, Y. R.; Ostroverkhov, V. *Chem. Rev.* **2006**, *106*, 1140-1154.
(65) Perry, A.; Neipert, C.; Space, B.; Moore, P. B. *Chem. Rev.* **2006**, *106*, 1234-1258.
(66) Du, Q.; Freysz, E.; Shen, Y. R. *Science* **1994**, *264*, 826-828.
(67) Nihonyanagi, S.; Ishiyama, T.; Lee, T.; Yamaguchi, S.; Bonn, M.; Morita, A.; Tahara, T. *J. Am. Chem. Soc.* **2011**, *133*, 16875-16880.
(68) Gopalakrishnan, S.; Liu, D. F.; Allen, H. C.; Kuo, M.; Shultz, M. J. *Chem. Rev.* **2006**, *106*, 1155-1175.
(69) Rosales, A. M.; McCulloch, B. L.; Zuckermann, R. N.; Segalman, R. A. *Macromolecules* **2012**, *45*, 6027-6035.
(70) Leng, C.; Gibney, K. A.; Liu, Y. W.; Tew, G. N.; Chen, Z. *ACS Macro Lett.* **2013**, *2*, 1011-1015.
(71) Johnson, W. C.; Wang, J.; Chen, Z. *J. Phys. Chem. B* **2005**, *109*, 6280-6286.
(72) Chen, C. Y.; Wang, J.; Woodcock, S. E.; Chen, Z. *Langmuir* **2002**, *18*, 1302-1309.
(73) Woodcock, S. E.; Chen, C. Y.; Chen, Z. *Langmuir* **2004**, *20*, 1928-1933.
(74) Zhang, D.; Dougal, S. M.; Yeganeh, M. S. *Langmuir* **2000**, *16*, 4528-4532.
(75) Gautam, K. S.; Schwab, A. D.; Dhinojwala, A.; Zhang, D.; Dougal, S. M.; Yeganeh, M. S. *Phys. Rev. Lett.* **2000**, *85*, 3854-3857.
(76) Sohn, K. E.; Dimitriou, M. D.; Genzer, J.; Fischer, D. A.; Hawker, C. J.; Kramer, E. J. *Langmuir* **2009**, *25*, 6341-6348.
(77) Raviv, U.; Giasson, S.; Kampf, N.; Gohy, J.-F.; Jerome, R.; Klein, J. *Nature* **2003**, *425*, 163-165.
(78) Scheu, R.; Chen, Y.; de Aguiar, H. B.; Rankin, B. M.; Ben-Amotz, D.; Roke, S. *J. Am. Chem. Soc.* **2014**, *136*, 2040-2047.

(79) Giovambattista, N.; Debenedetti, P. G.; Rossky, P. J. *J. Phys. Chem. B* **2007**, *111*, 9581-9587.
(80) Liu, M.; Wang, S.; Wei, Z.; Song, Y.; Jiang, L. *Adv. Mater.* **2009**, *21*, 665-669.
(81) Jung, Y. C.; Bhushan, B. *Langmuir* **2009**, *25*, 14165-14173.

CHAPTER 3 SURFACE HYDRATION OF NONFOULING ZWITTERIONIC POLYMERS

3.1 Structural and Environmental Effects on the Surface Hydration of Zwitterionic Polymers

3.1.1 Introduction

Nonfouling materials have a wide range of applications for biosensors, biomedical implants, and marine industry.[1-6] Recently, zwitterionic polymer brushes synthesized on gold or glass substrates have been reported as promising materials to resist biofouling in complex environments.[7,8] It is believed that the non-fouling ability of zwitterionic polymers is closely related to an electrostatically induced hydration layer at the surface, because the tightly bound water molecules form a physical and energy barrier to prevent non-specific adsorption of biomolecules and organisms.[9]

However, zwitterionic materials can be designed with different molecular structures which change their non-fouling properties. For example, poly(carboxybetaine acrylamide)s (pCBAAs) have been synthesized with one to five carbon atoms (pCBAA1~5) between the positively charged quaternary amine and the negatively charged carboxyl groups. When the number of carbon atoms is greater than two, protein adsorption will start to occur on pCBAA, particularly in complex media.[10] In addition,

environmental parameters like pH and ionic strength alter their non-fouling performances. Carboxybetaine polymers can resist non-specific protein adsorption at pH>5 but have protein adsorption at low pH values, while anti-fouling performance of sulfobetaine materials is insensitive to pH.[11] Meanwhile, the increase of ionic strength up to 200 mM leads to low protein adsorption on zwitterionic polymer surfaces.[12] As surface hydration is proposed to play a key role to prevent biofouling, *in situ* examination of the polymer/water interface is highly desired.

As we presented above, sum frequency generation (SFG) vibrational spectroscopy is an intrinsically surface sensitive and *in situ* vibrational spectroscopic method, providing information about chemical structures at a molecular level.[13-16] It has been extensively applied to study the structures of polymers and biomolecules at various interfaces[17-24] and has proved particularly powerful in revealing polymer/water interfacial structures in ambient environments.[25-29] Furthermore, detailed structural information of interfacial water can be extracted from SFG spectra.[30-36]

In this work, we applied SFG spectroscopy to study the surface hydration of three zwitterionic polymer brushes, pCBAA1, pCBAA2 and poly(sulfobetaine methacrylate) (pSBMA) prepared on silica substrates (Figure 3.1). The surface structures of the materials in air and water were characterized by SFG. The effects of ions and pH on the interfacial water structures were investigated and the different binding affinities of the ions to the polymers were deduced from the water signals. The SFG results indicate that the surface hydration properties of zwitterionic materials are mediated by the chemical structures of the materials as well as the environmental parameters including ionic strength, ionic size and charge, and pH.

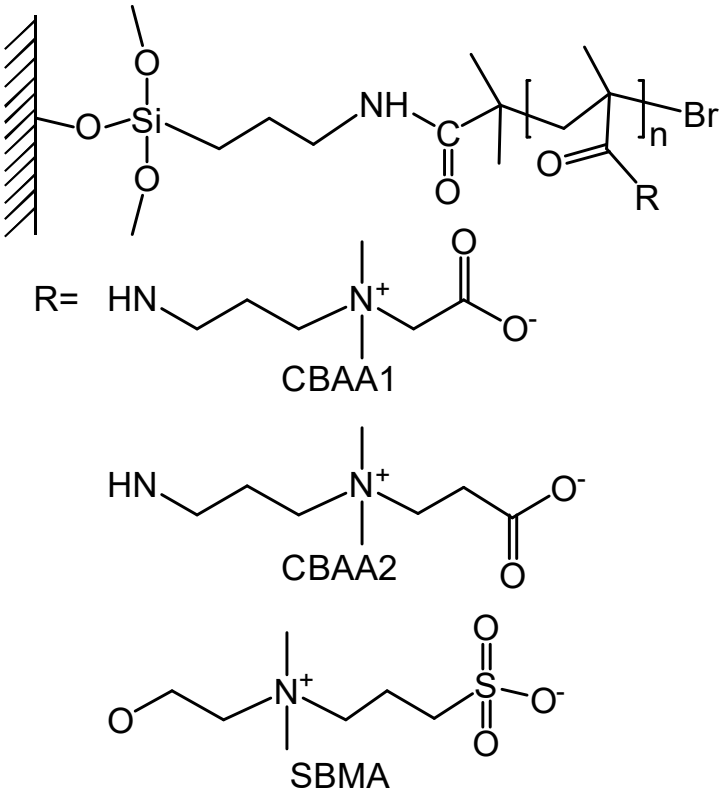

Figure 3.1 Molecular structures of pCBAA1, pCBAA2 and pSBMA polymer brushes synthesized on silica substrates. These materials were provided by Prof. Shaoyi Jiang's lab at the University of Washington.

3.1.2 Experimental Section

The polymer brushes were synthesized on SiO_2 prisms (Altos Photonics, Bozeman, MT) according to the previous reports with thicknesses of 20-30 nm, which showed good non-fouling properties (Figure 3.1).[12,37] To probe the polymer/water interfacial structures, the surfaces of the polymer brushes were placed in contact with Millipore water. Various amounts of NaCl, KCl, $MgCl_2$ and $CaCl_2$ were added to water to study the ion effect at the polymer surfaces. The pH of water was adjusted to 5, 7 and 9 with HCl or NaOH to study the pH effect.

We used the same SFG spectrometer as reported previously.[38] Briefly, the visible and infrared (IR) input beams penetrate a right angle SiO_2 prism and overlap spatially and

temporally at the sample (zwitterionic polymer on prism) surface/interface (Figure 3.2). The incident angles of the visible and IR beams are 60° and 54° with respect to the surface normal, and the pulse energies of the visible and IR beams are 30 and 100 μJ, respectively. The reflected SFG signal is collected by a monochromator along with a photomultiplier tube. All SFG spectra were collected using the ssp (SFG output, visible input, and IR input) polarization combination.

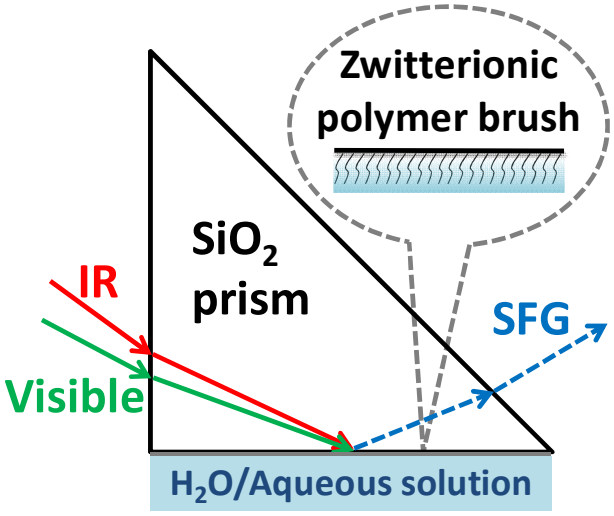

Figure 3.2 SFG measurement of a zwitterionic polymer on a right-angle SiO_2 prism in contact with water or an aqueous solution.

3.1.3 Results and Discussion

Before studying the zwitterionic polymer/water interfaces, the surface structures of pCBAA1, pCBAA2 and pSBMA in air were characterized using SFG spectroscopy. All three polymers showed almost the same spectra in air, with a stronger peak at 2845 cm^{-1} and a weaker peak at 2920 cm^{-1} (Figure 3.3). The common 2845 and 2920 cm^{-1} peaks are most likely from the symmetric and asymmetric stretching of the CH_2 groups in the backbone and/or side chains.[39] Nevertheless, the SFG spectra indicate the similar good ordering of the three polymer brushes in air. Besides, no water signal above 3000

cm^{-1} could be detected in air, showing that either no water molecule is present on the zwitterionic polymer surface in air, or the water molecules on the zwitterionic polymer surfaces in air are disordered.

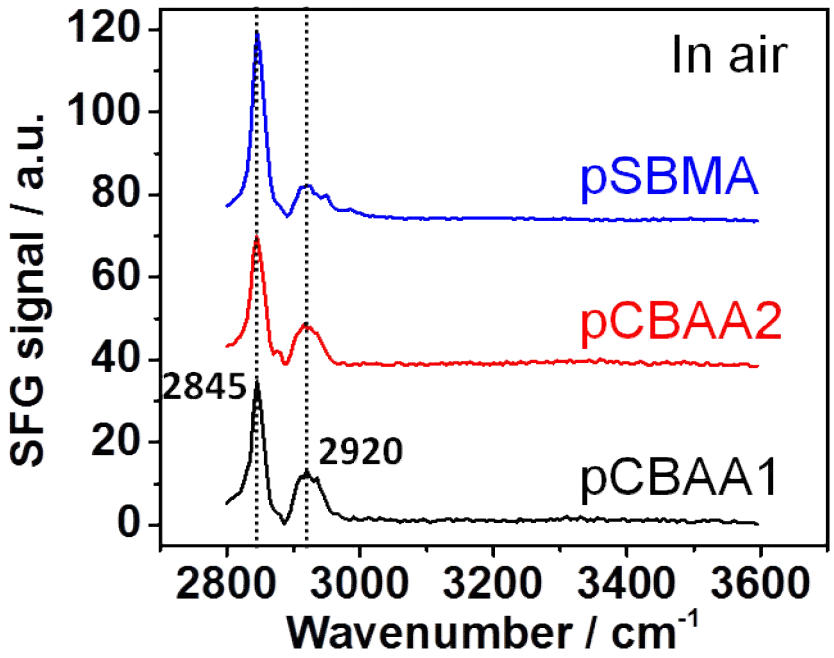

Figure 3.3 SFG spectra of pCBAA1, pCBAA2 and pSBMA in air.

When contacting H_2O, the spectra of all three materials showed strong C-H vibration signals below 3000 cm^{-1} (Figure 3.4A-F, black lines), indicating good ordering of the polymer brushes in water, due to the electrostatic attraction of the positive and negative charges. Here we noticed that all spectra under water showed new peaks at 2895 cm^{-1} and 2950 cm^{-1} (Figure 3.4A-F) compared to those in air (Figure 3.3), which may come from the $N\text{-}CH_3$, $N\text{-}CH_2$ or $O\text{-}CH_2$ groups in the polymer structures, indicating the surface restructuring of the polymers in water. The bands centered at 3180 cm^{-1} in the spectra were contributed from interfacial water molecules. Prior SFG studies on water

showed that water peaks around 3200 cm^{-1} and 3400 cm^{-1} are contributed by the strongly hydrogen bonded and relatively weakly hydrogen bonded water, respectively.[32,33,40] Here, the water molecules form strong hydrogen bonding at the zwitterionic polymer surfaces. Such strong bonding was likely induced by electrostatic attraction, and the tightly immobilized hydration layer is crucial to resist biofouling.

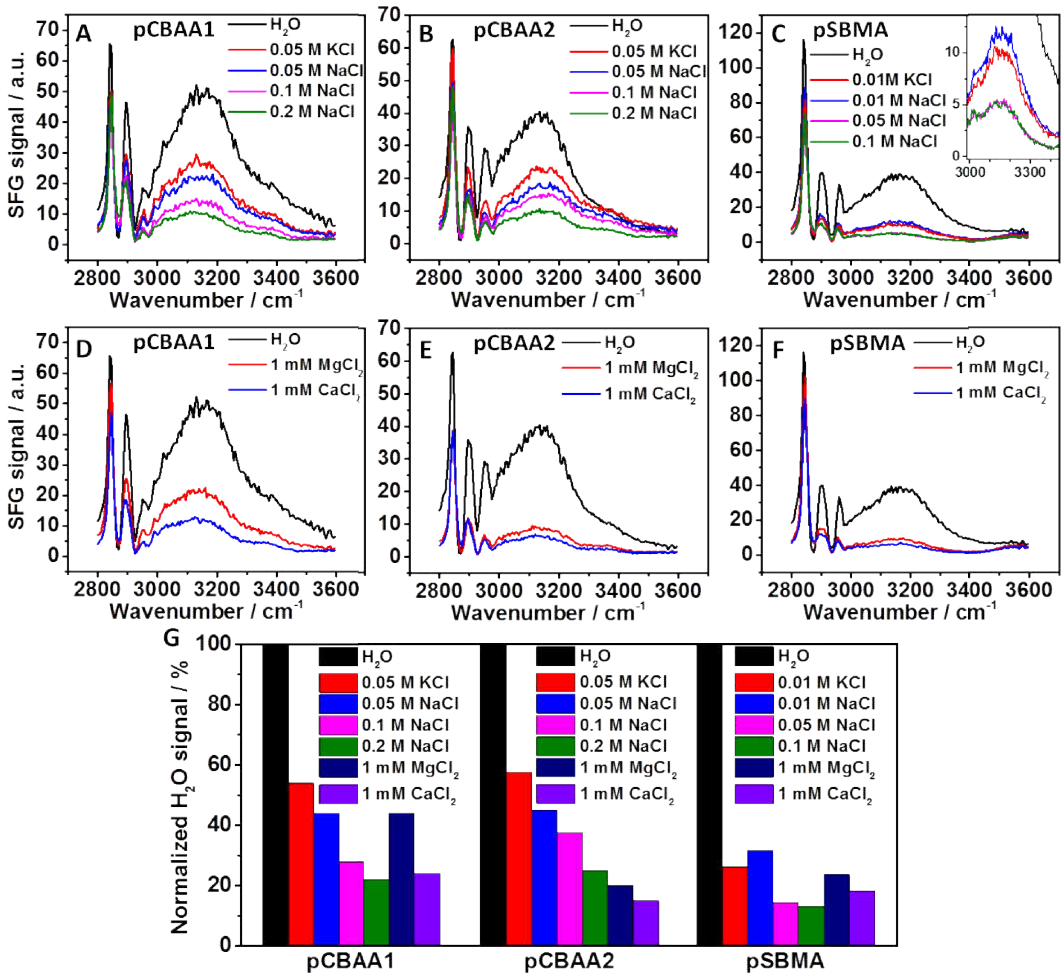

Figure 3.4 SFG spectra of (A)(D) pCBAA1, (B)(E) pCBAA2 and (C)(F) pSBMA in contact with (A)(B)(C) NaCl or KCl solutions and (D)(E)(F) $MgCl_2$ or $CaCl_2$ solutions. The NaCl solutions were prepared with various concentrations. Inset of (C) is an enlarged figure of water spectra in (C) for a clear comparison. (G) The corresponding normalized H_2O signal intensity (Each intensity was measured at least three times and the error is less than 2%).

Since the zwitterionic materials will be used in complex environments such as seawater and body fluid, we investigated the binding and hydration effects of several ions onto the pCBAA1, pCBAA2 and pSBMA polymer brushes by contacting the materials with the salt solutions. Ion binding at various surfaces could be characterized by SFG through the signal of interfacial water.[41-47] Figure 3.4A-F showed the SFG spectra of the polymers in contact with the salt solutions and Figure 3.4G summarized the normalized intensity of the water signals, in which the water signal intensity detected without the salt addition was set to 100% for the three polymers. Firstly, we placed the polymer brushes in the NaCl solutions with various concentrations. The water signal decreased as the concentration of NaCl increased, as shown in Figure 3.4A-C, indicating the increasing amount of Na^+ and Cl^- binding to the surfaces which disrupted the ordering of interfacial water molecules. Secondly, we tested the KCl solution with the same concentration as the NaCl solution to compare binding affinity of K^+ with Na^+. For pCBAA1 and pCBAA2, the decrease of the water signal in the KCl solution was smaller than that in the NaCl solution, showing that they both bind K^+ more weakly than Na^+. In contrast, for pSBMA, the decrease of the water signal in the KCl solution was slightly greater than that in the NaCl solution, showing that pSBMA binds K^+ more strongly than Na^+. The SFG results on the binding of monovalent cations to pCBAAs and pSBMA polymer brushes are consistent with prior simulation results on the ion binding properties of small carboxybetaine (CB) and sulfobetaine (SB) molecules.[48] Thirdly, we tested the $MgCl_2$ and $CaCl_2$ solutions to compare the divalent cations with the monovalent cations. For all three materials, the decrease of the water signal in the $MgCl_2$ and $CaCl_2$ solutions is greater than that in the NaCl or KCl solutions (Figure 3.4D-F), indicating that all

polymers bind divalent cations more strongly than monovalent cations. In addition, we observed that pCBAA2 binds Mg^{2+} and Ca^{2+} stronger than pCBAA1. This is reasonable because the CB-2 molecule has a higher pKa than CB-1[49] thus tends to have greater affinity towards Lewis acids. The difference between pCBAA1 and pCBAA2 in binding divalent cations is well-correlated with a previous report on the different polysaccharide adsorption at zwitterionic surfaces.[50] Overall, the difference in the binding of cations to the polymers originates from a combination of cation hydration energy, size of the cation and the size of the polymer headgroups. Besides, as shown in Figure 3.4A-F, all three materials showed strong C-H vibration signals below 3000 cm^{-1} in the presence of salts, indicating that the good ordering of the polymer brushes was not disrupted by salt addition.

In addition to ions, the pH of the aqueous environment is also an important parameter that affects the surface hydration of zwitterionic materials with different structures. Here, we investigated pCBAA1, pCBAA2 and pSBMA in contact with water at various pH. As shown in Figure 3.5A-C, sharp peaks from C-H vibrations below 3000 cm^{-1} indicated the good ordering of all polymers in contact with water with pH ranging from 5 to 9. For both pCBAA1 and pCBAA2, the SFG water signal decreased as the pH of the water decreased from 9 to 5 due to reduced ordering of the interfacial water (Figure 3.5A and B). At pH 5, while water signal is still observable for pCBAA1, no water signal was detected at the pCBAA2/water interface, indicating complete loss of the interfacial water ordering at the latter interface. The difference between pCBAA1 and pCBAA2 at pH 5 could be attributed to their different pKa's. The pKa values of CB-1 and CB-2 molecules are 1.8 and 3.3 respectively,[49] therefore CB-2 is more easily protonated

(Figure 3.5D). Because the ordering of water molecules around the positively charged quaternary amine is much weaker than that around the negatively charged carboxyl group,[51] neutralization of the carboxyl group could weaken the electrostatically induced hydrogen bonding and reduce the ordering of the interfacial water.

We also compared pSBMA with pCBAAs. Figure 3.5C showed the SFG spectra of pSBMA in contact with water at pH 5, 7 and 9. Different from pCBAAs, the intensity of water signal did not change with pH varying from 5 to 9, indicating that the interfacial water ordering at the pSBMA/water interface is not affected by pH. Generally, sulfonic acid has a negative pKa and is a much stronger acid than carboxylic acid, therefore sulfobetaine is harder to protonate compared to carboxybetaine even when there is an extra methylene group present in the molecule. When pH is in the range of 5 to 9, the sulfonate group cannot be protonated and the charge balance of pSBMA does not change. As a result, the ordering of interfacial water stays the same.

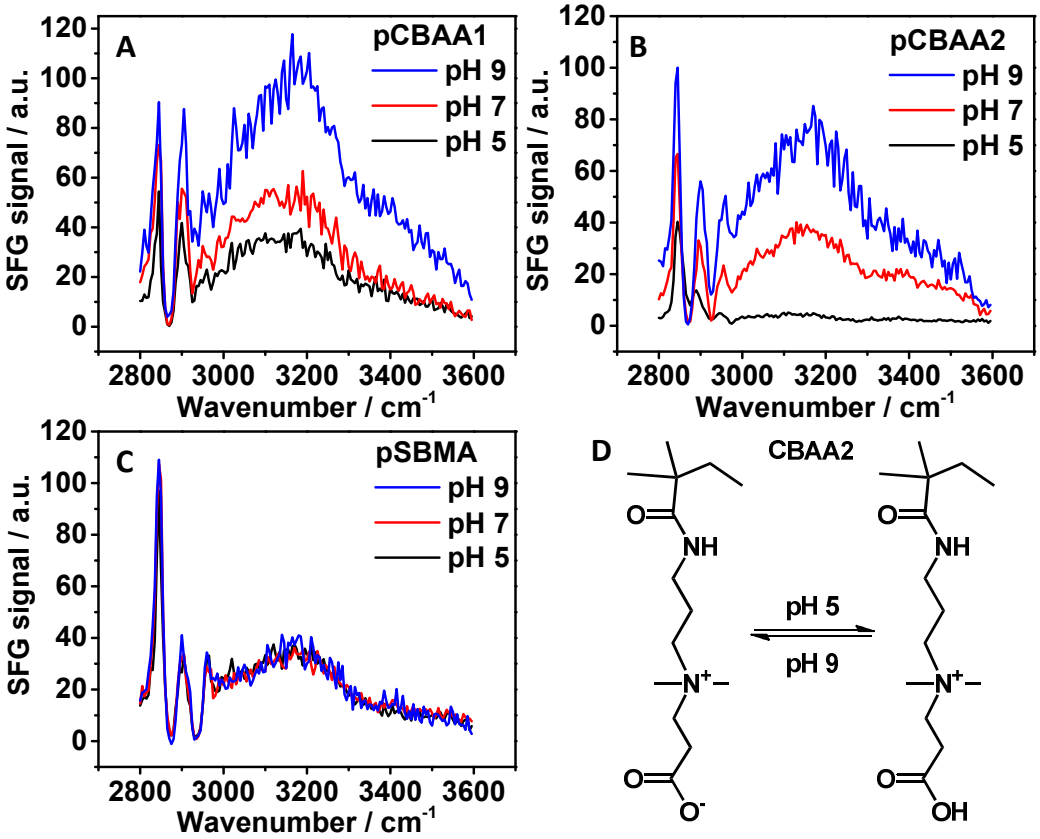

Figure 3.5 SFG spectra of (A) pCBAA1, (B) pCBAA2 and (C) pSBMA in contact with water at pH 5, 7 and 9. (D) Protonation and deprotonation of a pCBAA2 unit.

For the above pH experiments, pure water with varied pH adjusted by very small amount of HCl or NaOH was used instead of buffers to exclude the interference of salt. Since biofouling tests were generally done in phosphate buffer saline (PBS) solutions, we repeated the pH experiments using 10 mM PBS at pH 4.8, 7.0 and 9.1 prepared from sodium phosphates. The water signals at the polymer/PBS interfaces showed exactly the same trend as a function of pH as in pure water but were weaker due to salt screening (Figure 3.6).

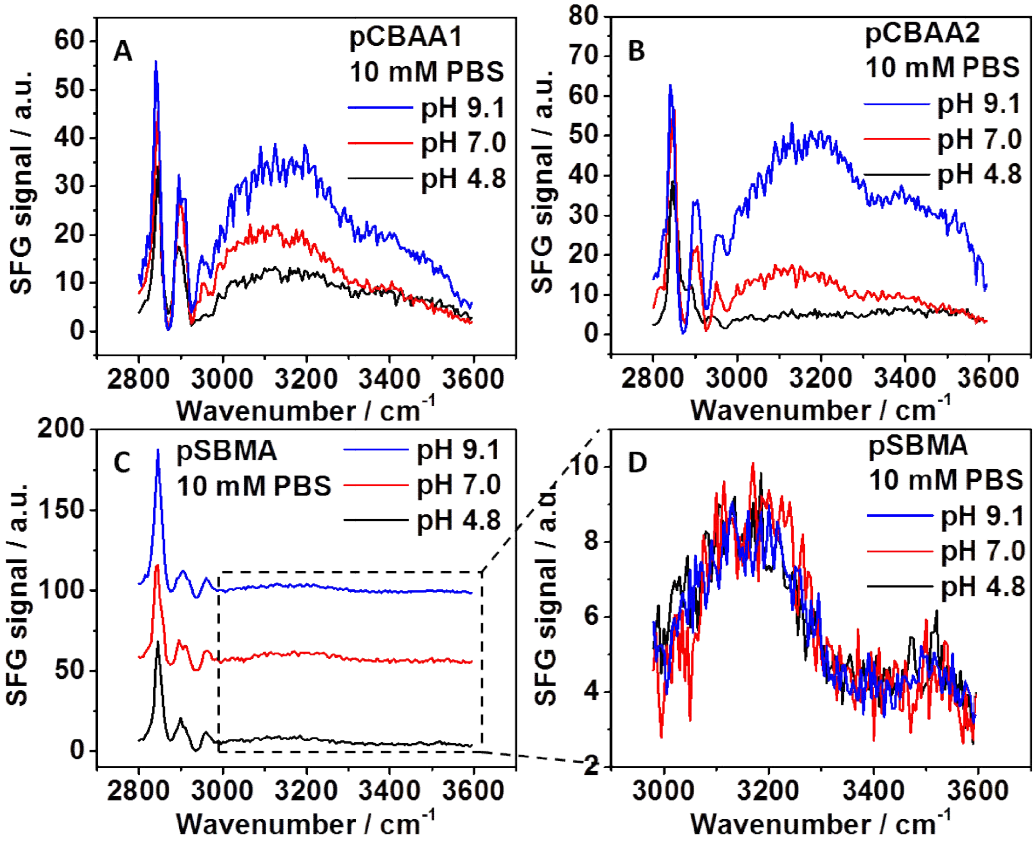

Figure 3.6 SFG spectra of (A) pCBAA1, (B) pCBAA2 and (C) pSBMA in 10 mM PBS. (D) Enlarged H_2O spectra for pSBMA.

3.1.4 Conclusions

In this work, we examined the effects of ions and pH on the surface hydration of three zwitterionic polymer brushes using SFG spectroscopy. The SFG results indicated good ordering of the polymer brushes in water and the strongly hydrogen bonded water structure at polymer/water interfaces. Ions have different binding affinities to the polymers as indicated by the reduced ordering of interfacial water. For example, pCBAAs bind Na^+ more strongly than K^+ while pSBMA binds K^+ more strongly than Na^+. It is worth mentioning that the zwitterionic surfaces are highly hydrated, therefore

interfacial binding of ions like Na^+ and K^+ at low salt concentrations would not cause the loss of non-fouling property of the zwitterionic polymer materials. All three materials bind divalent cations more strongly than monovalent cations and pCBAA2 binds Mg^{2+} and Ca^{2+} more strongly than pCBAA1. Furthermore, for pCBAAs, lower pH of water leads to weaker ordering of the interfacial water molecules. At pH 5, water was still ordered at the pCBAA1/water interface but was completely random at the pCBAA2/water interface. Different from pCBAAs, the ordering of water at the pSBMA/water interface was not affected by pH in the same range. Recently, significant biomedical and engineering applications of CB materials have been reported and CB materials were shown to have excellent properties because they are derived from naturally occurring betaines and have excellent bio-compatibility.[52,53] We believe that zwitterionic polymers will be more and more widely used in many important applications in the future. Therefore it is important to elucidate their surface hydration behavior in different chemical environments.

3.2 Surface Hydration of Zwitterionic and PEG Materials in Contact with Proteins

3.2.1 Introduction

Nonfouling materials have been extensively investigated for a wide spectrum of applications ranging from marine industry to biomedical engineering.[3,5,6,54-56] Two types of most widely studied nonfouling materials are zwitterionic polymers[7] and poly(ethylene glycol) (PEG).[57] It is believed that the nonfouling property of these materials results from their strong surface hydration, which is formed at the zwitterionic polymer surfaces through electrostatic induced hydrogen bonding, and at the PEG surfaces through

hydrogen bonding between water molecules and the ether oxygen atoms.[9,28,58] The tightly bound hydration layer is theorized to act as a physical and energy barrier and the water molecules are difficult to be replaced by biomolecules and organisms. However, this straightforward correlation between the nonfouling behavior of a material and its surface hydration may be questionable, because the presence of biological molecules such as proteins or organisms complicates the adsorption behavior and the interfacial water structure.[59] Deeper understanding of the nonfouling performance of a material needs a comprehensive molecular picture of the hydration at the material surface and the protein surface, which, however, has not been completely established. Therefore, it is imperative to probe the local water structures at both nonfouling material and protein surfaces and especially their temporal evolution when the nonfouling materials are brought to interact with the proteins in water or vice versa.

Zwitterionic polymers and PEG differ in molecular structure, which may result in their different hydration properties. Molecular dynamics simulation results suggested that there are hydrophobic interactions between PEG and proteins.[60] Due to the hydrophobic interactions, PEG can block the active sites of enzymes, leading to reduction in the catalytic activity of PEG-enzyme conjugates. In contrast, the bioactivity of enzymes can be retained or even improved after conjugation with zwitterionic polymers, because the superhydrophilicity of the zwitterionic polymers offers a hydration environment that favors enzyme-substrate interaction.[53] Further, the surface coatings of zwitterionic polymers exhibit better in vivo performance than PEG, including minimal biomolecule binding,[61] resistance to foreign body reaction,[52] and long circulation.[62] Because their molecular structures are distinctly different, it is not a surprise that zwitterionic polymers

and PEG have different mechanisms to interact with water, proteins, and organisms. This hypothesis is plausible but has not been validated by direct experimental evidence so far. In this context, it is of essential importance to probe the local water structures at the zwitterionic polymer and PEG surfaces and their responses to the presence of protein molecules. We believe that this fundamental study will allow better design and tailoring of the nonfouling performance of materials in a variety of technical applications, for instance in biomedicine, where contact with biological environments containing proteins or organisms is inevitable at the material surfaces.

In this work, SFG spectroscopy was applied to systematically study the surface hydration of the polymer brushes of sulfobetaine methacrylate (SBMA) and oligo(ethylene glycol) methacrylate (OEGMA), denoted as pSBMA and pOEGMA, anchored on silica surfaces (Figure 3.7A) in the absence and presence of proteins (Figure 3.7B). The SFG spectra of water at the polymer surfaces were taken before, during, and after contacting several protein solutions, and the time-dependent SFG signals of the interfacial water were monitored to probe the structural changes of water upon contact with the protein solutions. The SFG results revealed that pSBMA and pOEGMA surfaces showed different surface hydrations upon contact with the protein solutions. In addition, the effects of sulfobetaine (SB), PEGs with molecular weight of 300 and 2000 (PEG-300 and PEG-2000), and PEG-2000-coated gold nanoparticles (PEG-2000-AuNP) (Figure 3.7C) on the surface hydration of proteins were investigated (Figure 3.7D) with SFG spectroscopy, which further elucidated the different hydration behaviors between SB and PEG in contact with proteins.

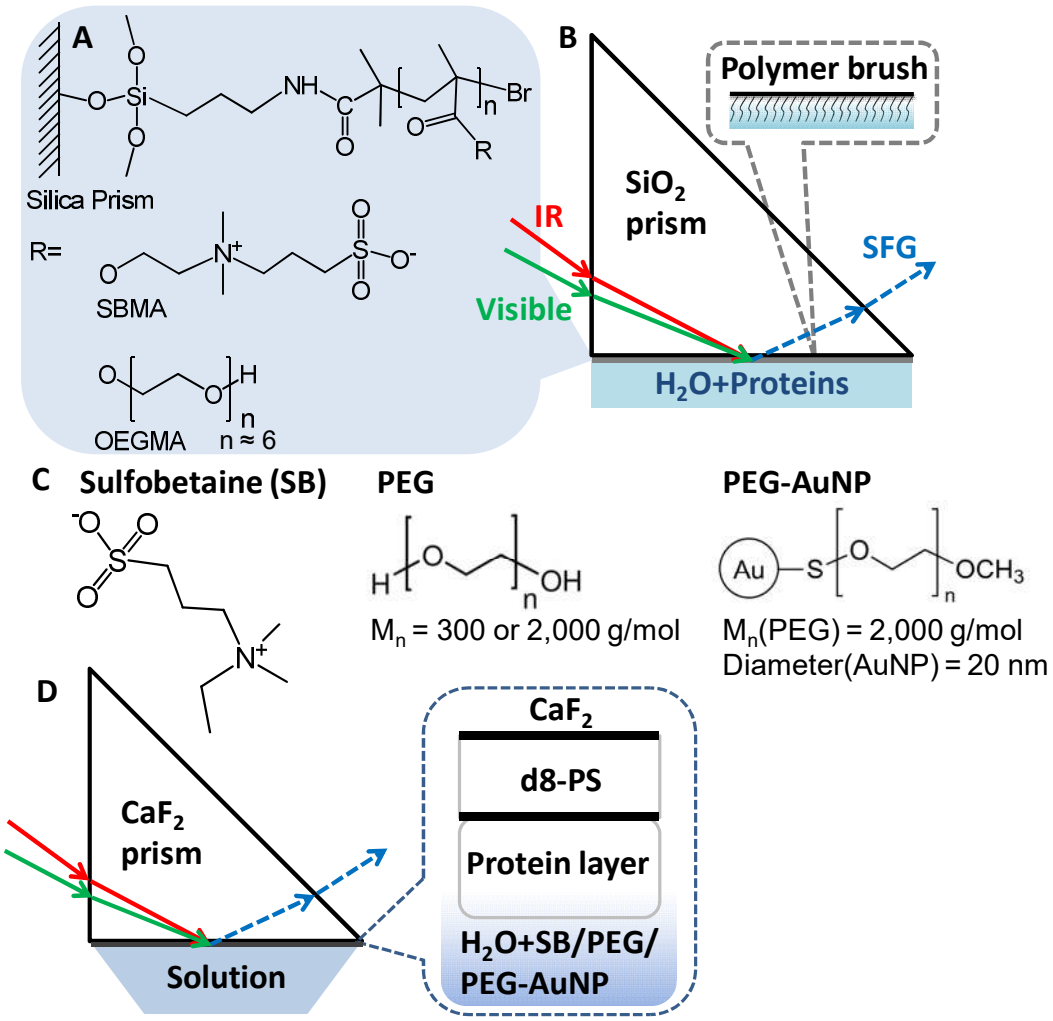

Figure 3.7 (A) Molecular structures of pSBMA and pOEGMA brushes anchored on silica surfaces. (B) SFG measurement of a polymer coating on a right-angle SiO_2 prism in contact with a protein solution. (C) Molecular structures of SB, PEG-300, PEG-2000, and PEG-2000-AuNPs. (D) SFG measurement of a protein layer physically adsorbed on a deuterated polystyrene (d8-PS) coated CaF_2 prism in contact with an SB, PEG-300, PEG-2000, or PEG-2000-AuNP solution.

3.2.2 Experimental Section

Bovine serum albumin (BSA, 99%), lysozyme (90%), fibrinogen (Type I-S, 65-85%, may contain 10% sodium citrate and 15% sodium chloride), fluorescein isothiocyanate labeled BSA (FITC-BSA), dimethylethylammoniumpropane sulfonate (sulfobetaine, SB), PEG-300, PEG-2000, PEG-2000-AuNP (diameter = 20 nm, optical density (OD) = 50) dispersed in water, and phosphate buffered saline (PBS, prepared

from Na_2HPO_4 and KH_2PO_4, contains 11.9 mM phosphates, 137 mM NaCl, and 2.7 mM KCl, pH = 7.4±0.1) were purchased from Sigma-Aldrich. Deuterated polystyrene (d8-PS) (M_w = 207,500 g/mol) was purchased from Polymer Source Inc. Right angle SiO_2 and CaF_2 prisms were purchased from Altos Photonics. Millipore water was used in all experiments.

The brushes of pSBMA and pOEGMA were grown on SiO_2 prisms (Figure 3.7A) via atomic transfer radical polymerization (ATRP) according to previous reports by our collaborators (Prof. Shaoyi Jiang's lab at University of Washington).[63,64] The thicknesses of the identical polymer brushes prepared on silicon wafers were measured to be 25-30 nm by an alpha-SE ellipsometer (J. A. Woollam). The hydrophilicity of the polymer coatings was assessed by static water contact angles measured with a CAM 100 contact angle goniometer (KSV Instruments).

To test the protein adsorption on the polymer surfaces, the pSBMA and pOEGMA samples were immersed into the PBS solution of FITC-BSA (5 mg/mL) for 1 hr, followed by rinsing with water and drying with N_2 flow. The surface adsorption of FITC-BSA molecules was assessed with an inverted fluorescence microscope (Olympus, Melville, NY) equipped with a Xenon arc lamp (Sutter instrument company, Novato, CA) and an electron multiplier CCD camera (Hamamatsu, Bridgewater, NJ). A bare silica substrate was used as a control.

To probe the water structure at the polymer brush/water interfaces in the absence and presence of proteins, the polymer brush samples were placed in water and the aqueous solutions of BSA, lysozyme, and fibrinogen (1.0 mg/mL), respectively (Figure

3.7B). SFG spectra were collected from the polymer brush/water (with or without protein) interfaces.

To study the effects of proteins on the surface hydration of the polymers, we adopted the following procedure. The polymer sample was first measured with SFG in air from 2800 to 3100 cm^{-1} (for C-H signal) and then placed in water for another SFG measurement from 2800 to 3600 cm^{-1} (for C-H and O-H signals). Then time-dependent SFG signal at the wavenumber of OH stretching vibration (around 3200 cm^{-1}) was monitored while water was switched to a protein solution in situ. When the OH signal at the protein solution interface was stable, an SFG spectrum was taken from 2800 to 3600 cm^{-1}. Finally, the sample was rinsed with water with a regular wash bottle, dried under N_2 and measured with SFG in air and water again.

To study the effects of SB, PEG-300, PEG-2000, and PEG-2000-AuNPs in water on the surface hydration of proteins, a protein layer was physically adsorbed on a prism. Firstly, a d8-PS solution in toluene (1% w/w) was spin-coated on a clean CaF_2 prism at 3000 rpm for 30 sec with a P-6000 spin coater (Speedline Technologies). Secondly, the d8-PS coated prisms were immersed in the PBS solutions of BSA, lysozyme, and fibrinogen (5.0 mg/mL), respectively, for 30 min. Thirdly, the protein coatings on the prisms were rinsed with water and dried under N_2. The presence of d8-PS and the proteins was confirmed by water contact angle measurements (Table 3.1). The protein surfaces were then measured with SFG in contact with water and the aqueous solutions of SB (0.5 M), PEG-300 (0.5 M), PEG-2000 (0.08 M), or PEG-2000-AuNP (OD = 5) (Figure 3.7D).

Table 3.1 Water contact angles of the surfaces of CaF_2, d8PS coated CaF_2 (d8PS-CaF_2), and BSA, lysozyme, and fibrinogen adsorbed on d8PS-CaF_2 (BSA-d8PS-CaF_2, lysozyme-d8PS-CaF_2, and fibrinogen-d8PS-CaF_2).

Surface	Water contact angle
CaF_2	<5°
d8PS-CaF_2	89±1 °
BSA-d8PS-CaF_2	39±1 °
Lysozyme-d8PS-CaF_2	54±2 °
Fibrinogen-d8PS-CaF_2	37±1 °

3.2.3 Results and Discussion

3.2.3.1 Surface Characterization and Hydration of pSBMA and pOEGMA

To study the surface hydration of nonfouling materials, the as-prepared pSBMA and pOEGMA were selected in this work considering the following factors: Firstly, proteins can adsorb onto charged surfaces through Coulomb interaction.[11,65-68] Both pSBMA and pOEGMA herein are overall neutral, so Coulomb interaction induced protein adsorption is excluded. Secondly, the hydrophilicity and nonfouling properties of the polymer brushes are affected by their thicknesses.[63,64,69] The pSBMA and pOEGMA films with a thickness of 25-30 nm herein demonstrated strong resistance to protein adsorption.[63,64] Thirdly, high packing density is crucial to the nonfouling performance of the polymer brushes.[63,70] Here, to ensure the high packing density, the initiators were anchored on the silica surface to form a self-assembled monolayer with high density.[63,64] Fourthly, the polymer chemical composition influences their nonfouling properties. For example, ethylene glycol (EG) oligomer molecules anchored on surfaces with six or more EG units demonstrate strong protein resistance.[71] The nonfouling property of polymers

made from carboxybetaine is affected by environmental pH, whereas that of sulfobetaine is independent of pH.[11] Therefore, pSBMA and pOEGMA (EG unit = 6) were selected for study in this work.

The surface hydrophobic/hydrophilic properties of the polymer brushes studied here were characterized by sessile drop contact angle measurements. As shown in Figure 3.8, the static water contact angles of the pSBMA and pOEGMA brushes anchored on silica substrates were measured to be 20±1° and 42±1°, respectively, which agree with those reported in the literature,[63,69,72-74] and were smaller than those of the commonly used polymers such as poly(methyl methacrylate),[75] polyethylene terephthalate,[75] polycarbonate,[75] polyvinyl chloride,[76] poly(dimethyl siloxane),[76] or polystyrene.[77] The water contact angle of the pSBMA surfaces is noticeably smaller than that of the pOEGMA surfaces, suggesting that the zwitterionic groups of the pSBMA brushes can interact more strongly with water for more effective surface hydration than the ethylene oxide groups of the pOEGMA brushes.

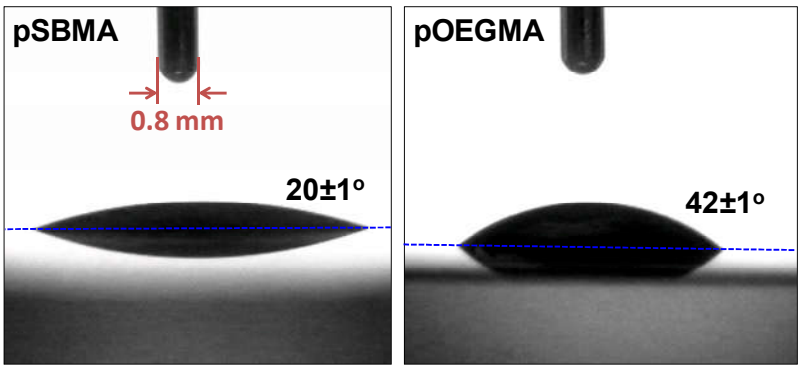

Figure 3.8 Images of the static water contact angles on the pSBMA and pOEGMA brushes anchored on silica substrates. The blue dashed lines indicate the surface plane. The diameter of the syringe needle is 0.8 mm.

The resistance of pSBMA and pOEGMA to protein adsorption determined by surface plasmon resonance and ellipsometry measurements has been well-documented.[57,63,64,78,79] To verify the nonfouling performance of the as-prepared pSBMA and pOEGMA, FITC-BSA was used as a model protein and its adsorption on the polymer brushes and a bare silica substrate (as a control sample) was measured with fluorescence microscopy. As shown in Figure 3.9, whereas strong FITC-BSA adsorption on bare silica surface was detected, no protein adsorption was observed on pSBMA or pOEGMA, indicating that both of the polymer surfaces were effectively resistant to protein adsorption in water as reported.[63,64] This provides the basis for the interpretation of the SFG results below.

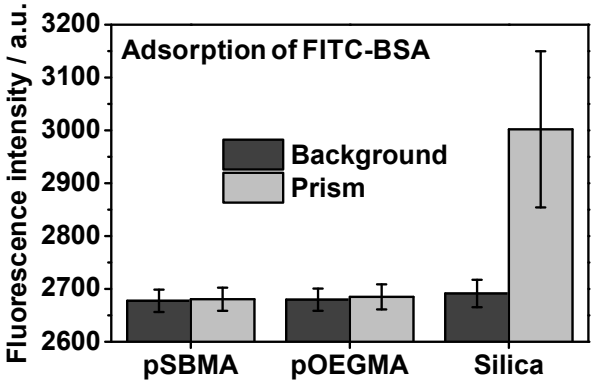

Figure 3.9 Summary of the average fluorescence intensities of FITC-BSA adsorbed on pSBMA, pOEGMA, and bare silica surfaces compared to the background.

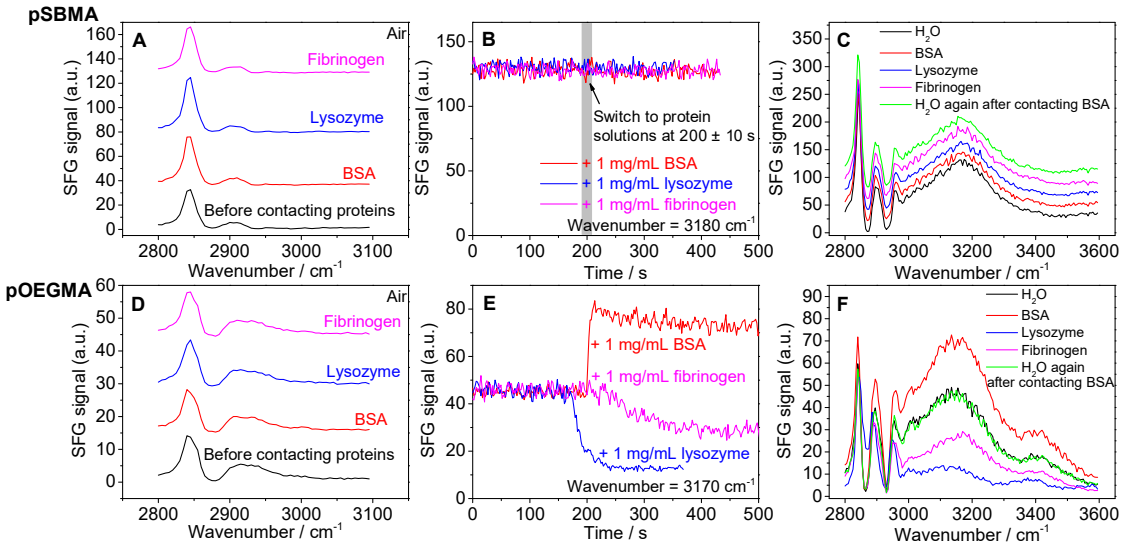

Figure 3.10 SFG signals of (A~C) pSBMA and (D~F) pOEGMA before, during, and after contacting the solutions of BSA, lysozyme, and fibrinogen. SFG spectra of (A) pSBMA and (D) pOEGMA were collected in air before and after contacting each protein solution. Time-dependent water signals of (B) pSBMA and (E) pOEGMA were monitored in situ as the aqueous phase was switched from water to each protein solution. SFG spectra of (C) pSBMA and (F) pOEGMA in contact with water and the protein solutions were also collected. The spectra in (A), (C), and (D) are stacked and offset by vertical translation for a clear view.

Figure 3.10 shows the SFG spectra collected from the pSBMA and pOEGMA surfaces in air, in water, and in various protein solutions. The time dependent SFG signals detected from the interfaces between the polymers and aqueous media before and after the addition of the proteins to the aqueous media are also shown. In air, both the pSBMA and pOEGMA surfaces show a strong peak at 2845 cm^{-1} and a weak peak at 2920 cm^{-1} from symmetric and asymmetric stretching modes of the methylene groups[80] in the polymer backbone and/or side chains (Figure 3.10A and D, black curves), indicative of good ordering of the polymers at the polymer/air interfaces. The polymer surfaces also show strong C-H signal below 3000 cm^{-1} in water, indicative of good ordering of the polymers at the polymer/water interfaces as well (Figure 3.10C and F, black curves). The water signal above 3000 cm^{-1} at the pSBMA surface consists only one band centered

around 3180 cm^{-1} with hardly observable signal at 3400 cm^{-1}. Differently, the water signal at the pOEGMA surface is dominated by the band centered around 3170 cm^{-1} with a shoulder around 3400 cm^{-1}, which are assigned to strongly and weakly hydrogen-bonded water molecules,[40] respectively. Thus, the majority of the ordered water molecules are associated via strong hydrogen bonding at both the pSBMA and pOEGMA surfaces, but some water molecules via weak hydrogen bonding at the pOEGMA surface. The different water structures at the pSBMA and pOEGMA surfaces may reflect the differences in hydrogen bonding mechanisms. Water molecules form hydrogen bonds with the hydrophilic zwitterionic groups in pSBMA or the oxygen atoms in the repeating units of the OEG chains, while the former is enhanced by electrostatic attraction.

3.2.3.2 Impact of Proteins on the Surface Hydration of pSBMA and pOEGMA

To study the impact of proteins on polymer hydration, proteins were prepared in water instead of PBS because the ionic strength of PBS is high enough to change the interfacial water structure and affect the SFG water signal (Figure 3.11). Moreover, we excluded the possibility that the low concentration of salts in the protein solutions (e.g., 150 mg/L (2.6 mM) sodium chloride and 100 mg/L (0.47 mM) monosodium citrate) may affect the SFG signal of water (Figure 3.11). Here, we selected BSA, lysozyme, and fibrinogen to represent typical proteins because they have a wide range of molecular weight and isoelectric point (Table 3.2).

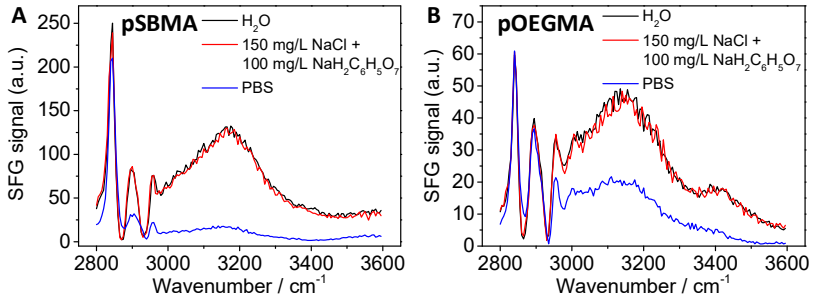

Figure 3.11 SFG spectra of (A) pSBMA and (B) pOEGMA in contact with water, an aqueous solution of 150 mg/L (2.6 mM) NaCl and 100 mg/L (0.47 mM) $NaH_2C_6H_5O_7$ (monosodium citrate), and PBS.

Table 3.2 Molecular weight (MW) and isoelectric point (pI) of BSA, lysozyme, and fibrinogen.

Protein	MW (g/mol)	pI
BSA	69,000	4.8
Lysozyme	14,000	11.1
Fibrinogen	340,000	5.5

The SFG signal intensity of water was monitored in real time when the aqueous phase was switched from water to a protein solution at the polymer surface (Figure 3.10B and E). For pSBMA, the intensity of the water SFG signal at 3180 cm^{-1} remains the same when the aqueous phase is switched from water to different protein solutions (Figure 3.10B), indicating that the strongly hydrogen-bonded water structure is hardly disturbed by proteins. The SFG spectra collected from the pSBMA/protein solution interfaces are almost identical to those taken at the pSBMA/water interface, indicating the same interfacial polymer and water structures at the pSBMA/protein solution and pSBMA/water interfaces (Figure 3.10C). This indicates that the interfacial water molecules are strongly bonded with pSBMA and cannot be disturbed by the protein molecules under the current experimental condition. After the surface was rinsed with

water, the SFG spectra of the pSBMA surface collected in air and water are identical to those obtained from the original pSBMA surface before contacting protein solutions, indicating no change of the polymer surface structure and no adsorption of the proteins onto the pSBMA surface (Figure 3.10A, C, and Figure 3.12A).

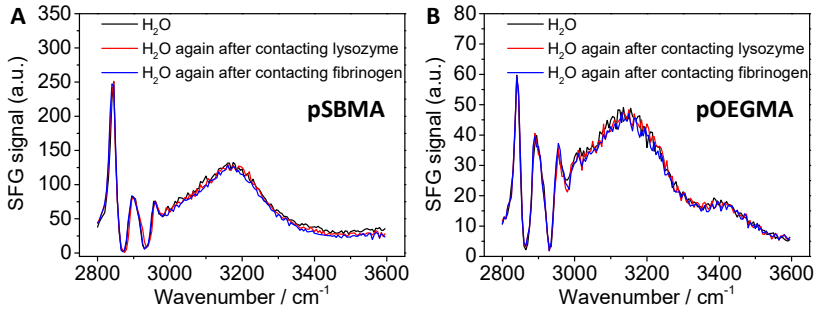

Figure 3.12 SFG spectra of (A) pSBMA and (B) pOEGMA in contact with water before and after contacting lysozyme and fibrinogen solutions and rinsing with water.

Different from pSBMA, the water signal at 3170 cm^{-1} at the pOEGMA surface becomes either stronger or weaker upon contacting protein solutions, indicating a noticeable impact of the presence of proteins on the water molecules at the pOEGMA surface (Figure 3.10E). After about 150 sec, the water signal at the pOEGMA surface in the protein solutions reaches plateau. When the water signal did not exhibit further change, SFG spectra were taken at the pOEGMA/protein solution interfaces. The C-H stretching signals taken at the pOEGMA/protein solution interfaces are similar to those at the pOEGMA/water interface (Figure 3.10F), indicative of little change in the polymer structures upon contact with the proteins and no preferred ordering of the proteins at the polymer surface. However, the contact with proteins causes noticeably different changes in the water signal intensity, suggesting that the ordering of the water molecules adjacent to the polymer surface is very sensitive to the presence of proteins and the protein nature.

Note that whereas the water signal intensity at 3170 cm^{-1} greatly changes upon contacting each protein solution, the change of the peak area of the 3400 cm^{-1} component is much smaller than that of the 3170 cm^{-1} component. This suggests that protein molecules near the pOEGMA surface primarily disturb the structural ordering of the strongly hydrogen-bonded water molecules that most likely hydrogen-bonded with the oxygen atoms on the OEG chains. After the pOEGMA surface was removed from the protein solutions and rinsed with water, their SFG spectra in air show the same signals as that taken before contacting the protein solutions (Figure 3.10D). Furthermore, the water signal at the pOEGMA surface is completely recovered when the surface was placed in pure water again (Figure 3.10F and Figure 3.12B). These data demonstrate little change in the polymer structures and negligible protein adsorption, which is consistent with the aforementioned fluorescence measurements.

A clean silica surface interacting with the proteins was monitored as a control. The water contact angle of the silica surface was measured to be less than 5^{o}. As shown in Figure 3.13, there was no SFG signal visible in the C-H stretching frequency region in air. After contacting the protein solutions and rinsed with water, the surface in air showed the peaks at 2880 and 2925 cm^{-1}, which were assigned to the hydrophobic groups of the proteins at air interface (Figure 3.13A), indicating the protein adsorption on the silica surface.[81,82] The water signal was monitored when the aqueous phase in contact with the silica surface was switched from water to the protein solutions. As shown in Figure 3.13B, the time-dependent SFG water signal intensity increased or decreased upon contacting protein solutions, due to the disturbance of the interfacial water structure by the proteins. These data were similar to those obtained with pOEGMA (Figure 3.10E). However, after

the surface was rinsed with water and placed in water again, the interfacial water signal detected at the silica/water interface could not be recovered to its original intensity due to the irreversible protein adsorption (Figure 3.13C).

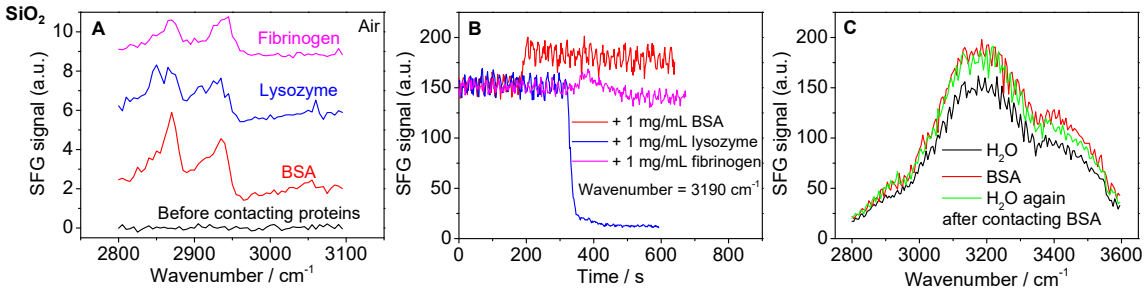

Figure 3.13 (A) SFG spectra of a silica surface in air before and after contacting the aqueous solution of BSA, lysozyme, and fibrinogen. (B) Time-dependent water signals of the silica surface monitored in situ when the aqueous phase is switched manually from water to protein solutions. Due to manual operation, the switching time may vary. (C) SFG spectra of the silica surface in contact with the BSA solution and with water before and after contacting the BSA solution.

The above SFG results highlight that pSBMA, pOEGMA, and silica surfaces exhibit different surface hydration and protein adsorption behavior. A layer of strongly hydrogen-bonded interfacial water molecules protects the pSBMA surface from protein contact. At the pOEGMA surface, the proteins can disturb the interfacial water structure and may possibly directly interact with the polymer surface. However, proteins can be rinsed off from the pOEGMA surface, suggesting that the OEG chains interact with water more strongly than with the proteins, leaving behind no proteins adsorbed on the pOEGMA surface. For silica, the proteins change the interfacial water structure and irreversibly adsorb onto the surface.

3.2.3.3 Impact of SB and PEG on Protein Surface Hydration

To further reveal the difference in surface hydration between zwitterionic materials and PEG, we applied SFG to investigate the effects of the structural unit of

pSBMA and pOEGMA, SB and PEG-300 (Figure 3.7C), on the surface hydration of proteins. Figure 3.14 demonstrates that the water structures at the protein surfaces are dependent on the protein nature. The signal centered at about 3200 cm^{-1} dominates the SFG water spectra at the BSA and fibrinogen surfaces, whereas the signal around 3500 cm^{-1} is stronger at the lysozyme/water interface. The observation on the lysozyme surface is consistent with the results presented in Figure 3.10E and F, which shows that lysozyme (originally with weak hydration) affects the hydration layer of pOEGMA more than BSA and fibrinogen. The different features of the water spectra should be correlated with the different conformation and charge of the proteins and the different ways in which the proteins orient surface water molecules. For example, lysozyme is known to be more rigid than the other two proteins and has a higher isoelectric point. The detailed study of the correlation of the water structures with the protein nature, however, is beyond the scope of this work. The present work focuses on the water signal change at the protein surfaces after SB and PEG are introduced into the surrounding environment of the protein surfaces. Regardless of the different water structures at the protein surfaces, the surface hydration of different types of proteins is affected by SB or PEG-300 in a rather similar way, as discussed below.

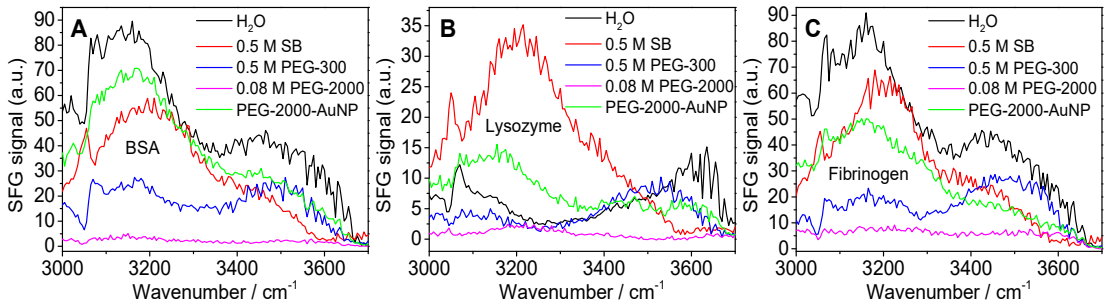

Figure 3.14 SFG spectra of (A) BSA, (B) lysozyme, and (C) fibrinogen adsorbed on d8-PS coatings in contact with water and aqueous solutions of SB (0.5 M), PEG-300 (0.5 M), PEG-2000 (0.08 M), and PEG-2000-AuNPs (OD = 5).

When the protein surfaces are placed in contact with a 0.5 M SB solution, the SFG water spectra are dominated by the signal centered at about 3200 cm^{-1} for all three proteins (Figure 3.14, red curves), which is assigned to strongly hydrogen-bonded water molecules.[40] As suggested by Figure 3.10C, strongly hydrogen-bonded water molecules are present at the pSBMA/water and pSBMA/protein solution interfaces, which are hardly affected by the proteins. Similarly, free SB molecules are expected to have strongly hydrogen-bonded water molecules in their hydration shells. When they are in close proximity to the protein layers, their hydration shells remain hardly changed. The strong hydration shells on the SB molecules effectively prevent the near-surface contact between the proteins and SB molecules. This agrees with the results presented in Figure 3.10. To further reveal the importance of a zwitterion (inner salt) in surface hydration rather than independent ions, a salt solution of ammonium sulfate with the same concentration (0.5 M) was investigated as a control. As shown in Figure 3.15, for all the proteins, the interfacial water signals decreased to almost zero while in contact with the ammonium sulfate solution. Different from SB, here the ammonium and sulfate ions can separately interact with the charged domains of the proteins; therefore the hydration of the proteins is significantly disrupted.

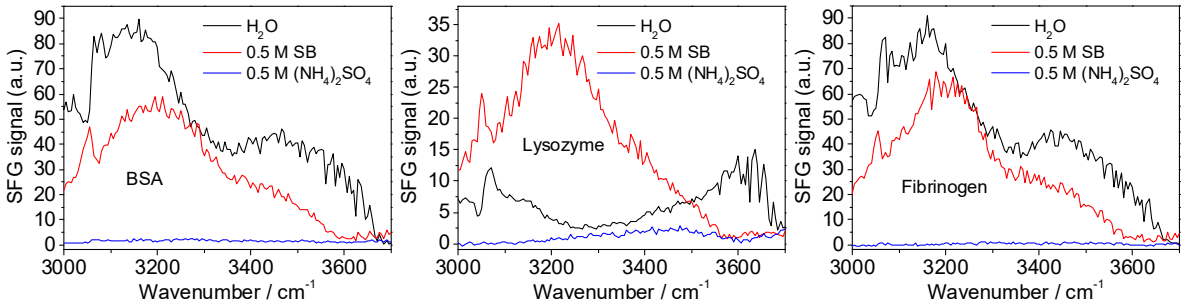

Figure 3.15 SFG spectra of BSA, lysozyme, and fibrinogen adsorbed on d8-PS coatings in contact with water and aqueous solutions of SB (0.5 M) and $(NH_4)_2SO_4$ (0.5 M).

However, when the protein surfaces were in contact with the PEG-300 solution, the SFG signal centered at ca. 3500 cm^{-1}, contributed from weakly hydrogen-bonded or less coordinated water,[40] becomes noticeably stronger than the signal around 3200 cm^{-1} (Figure 3.14, blue curves) for all three types of proteins, though both of these signals were largely reduced. This is different from the water signals observed at the BSA/water and fibrinogen/water interfaces (Figure 3.14A and C, black curves), and is also different from that observed from the pOEGMA/water interface (Figure 3.10F, black curves). PEG is a hydrogen bond acceptor, and it can be envisioned that PEG/water hydrogen bonds are formed at the cost of the hydrogen bonds between water molecules. Comparison of the SFG signals at 3200 cm^{-1} at the protein/water interfaces in the absence and presence of PEG-300 suggests that PEG-300 effectively breaks the strongly hydrogen-bonded water, but has less effect on the weakly hydrogen-bonded water. Distinct from the pOEGMA/water interface in the presence of proteins in water, at which the majority of water molecules are strongly hydrogen-bonded, at the protein/water interfaces in the presence of PEG-300 molecules, the majority of water molecules are weakly hydrogen-bonded. Thereby, we believe that free PEG molecules in water behave differently from PEG molecules anchored on a solid surface.

Free PEG molecules are expected to interact with proteins via hydrophobic interaction between the CH_2 moieties on their backbones and the hydrophobic parts of proteins.[60,83] To confirm the effect of the hydrophobic interaction between PEG and proteins, here the protein layers were brought into contact with the aqueous solution of PEG-2000, the concentration of which was 0.08 M to achieve the same concentration of ethylene glycol unit of PEG-300 at 0.5 M. Figure 3.14 shows that the water signals at the protein/water interfaces decrease to almost zero upon contact with PEG-2000. This suggests that PEG-2000 substantially disrupts the hydration layer(s) around the proteins and interacts with the proteins more strongly than PEG-300. It is possible that the long PEG chains can even wrap the protein molecules. Taking into account the results shown in Figure 3.10E and F, the studies of the hydration at the pOEGMA surface and at the protein layers confirm the direct interaction between PEG and proteins.

The comparison between Figure 3.10 and Figure 3.14 indicates that free PEG and surface-bound PEG may affect the protein hydration differently. To further test this, PEG-2000-AuNP was introduced to interact with the protein layers in water to compare with free PEG-300 and PEG-2000 molecules. As shown in Figure 3.14 (green curves), the water signal at 3200 cm^{-1} remains stronger than that at 3400 cm^{-1}, particularly for the lysozyme surface, at which the original signal at 3200 cm^{-1} is weaker in contact with water (Figure 3.14B, black curves). This result indicates that different from free PEG, the PEG chains tethered on the nanoparticles can form and align strongly hydrogen-bonded water molecules adjacent to the protein surfaces, which is similar to the pOEGMA surface (Figure 3.10F). Similar to those coated on planar surfaces, the PEG chains tethered on nanoparticles are closely packed with most of the hydrophobic CH_2 groups

buried in the film, and have limited freedom to change conformation to interact with proteins directly, which, therefore, yields strong hydration shells enclosing the PEG-2000-AuNPs to prevent the near-surface contact of the nanoparticles with proteins.

The impact of SB, PEG-300, PEG-2000, and PEG-2000-AuNPs on the surface hydration of CaF_2 without the proteins was investigated for comparison. As shown in Figure 3.16, the spectrum taken with the presence of SB shows a strong band at 3200 cm^{-1} with a weak shoulder at 3400 cm^{-1}, whereas the signal intensity obtained with the presence of PEG-300 is much lower with a slightly stronger band at 3400 cm^{-1}. The water signal decreases to almost zero when PEG-2000 is present. Different from free PEGs, for PEG-2000-AuNP, the observed SFG signal at 3200 cm^{-1} is much stronger, indicating a majority of strongly hydrogen-bonded water at the interface. Therefore, the results obtained from the CaF_2 surface without the proteins are consistent with those obtained from the protein surfaces.

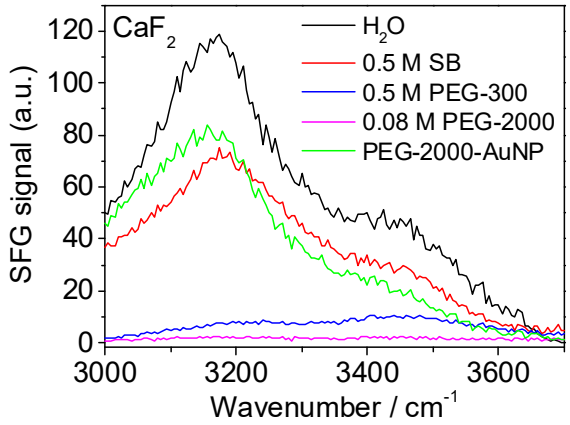

Figure 3.16 SFG spectra collected at a CaF_2 prism surface in contact with water and aqueous solutions of SB (0.5 M), PEG-300 (0.5 M), PEG-2000 (0.08 M), and PEG-2000-AuNPs (OD = 5).

Because PEG is a hydrogen bond acceptor, it is plausible to envision that upon adding the PEG chains into water, the hydrogen-bonding of water molecules will be broken to liberate free water molecules, which resembles hydrogen-bond disruption of chaotropic ions. On one hand, it weakens the hydration of proteins and thus facilitates the hydrophobic interaction between the proteins and PEG chains, when free PEG chains are present in water. In the case of PEG chains tethered on solid surfaces, on the other hand, the hydrophobic interaction between the PEG chains and the proteins is inhibited and, at the same time, the liberated water molecules may interact with the proteins via hydrogen bonding, which may offset the hydrogen-bond disruption impact of the PEG chains on the hydration of the proteins. Overall, one can conclude that the impact of PEG chains on the hydration of proteins is strongly dependent on their forms present in water (Figure 3.17). This dependence can well account for the difference between free PEG chains, pOEGMA brushes grafted on solid surfaces, and PEG-2000-AuNPs when they interact with the proteins. It also accounts for the nonfouling effect of pOEGMA brush surfaces and for the enhancement of protein hydration by PEG-2000-AuNPs (e.g. lysozyme in this work). In contrast to PEG, the interaction of SB with water and proteins is determined by its zwitterionic nature; it is always strongly hydrogen-bonded with water no matter whether it is present in water as free molecules or as surface-bound pSBMA coatings. The hydration of SB coatings (e.g. pSBMA) should be stronger than that of PEG (e.g. pOEGMA), because the latter can be disturbed by proteins.

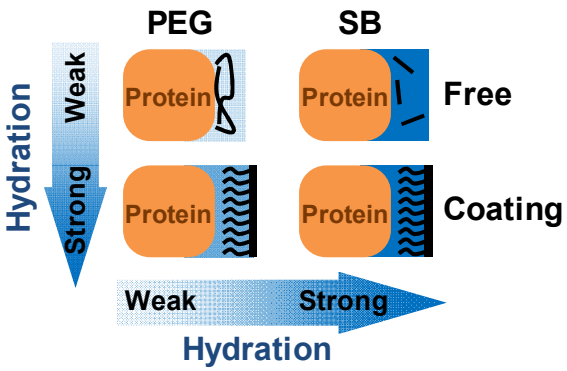

Figure 3.17 Schematic depiction of different hydration behaviors of PEG and SB (free or surface-bound) in contact with proteins.

3.2.4 Conclusions

In this work, the surface hydration behaviors of pSBMA and pOEGMA were in situ probed in contact with protein solutions using SFG spectroscopy. The polymer surfaces are well ordered in air and water, and most of the water molecules at the polymer/water interface are strongly hydrogen-bonded. The hydration layer at the pSBMA surface was not affected by proteins, whereas that at the pOEGMA surface was considerably disturbed. The effects of free SB and PEG on the surface hydration of proteins were also investigated. Whereas water was strongly bonded at the protein surfaces with the presence of free SB molecules in solution, a significant amount of weakly hydrogen-bonded water molecules was observed at the interface between proteins and free PEG solutions. Different from free PEG, when the proteins were in contact with PEG coated gold nanoparticles, a majority of strongly hydrogen-bonded water was observed which is similar to the pOEGMA surface. In summary, the study on the surface hydration of both polymers and proteins suggests that for PEG-coated surfaces and nanoparticles, although surface hydration is disrupted by proteins to a certain degree, it is still relatively strong and resists protein adsorption. However, free PEG binds to proteins,

reducing their hydration significantly. For SB-coated surfaces or free SB, surface hydration remains strong in contact with proteins.

3.3 Surface Hydration of Zwitterionic and PEG Materials Studied by Isotopic Dilution Spectroscopy

3.3.1 Introduction

Interpreting the SFG spectra of water is crucial to understanding the surface hydration of various materials. Over all, the water/vapor interface is the system with the least signal interference from other materials, and has been extensively studied.[40,84-86] Besides the O-H stretching signal at ~3700 cm^{-1} for the dangling O-H bonds, the SFG spectrum of the water/vapor interface mainly consists of two bands centered around 3200 cm^{-1} and 3400 cm^{-1}, which were classically assigned to contributions from "liquid-like" and "ice-like" water respectively based on the infrared spectra of liquid water and ice.[85] However, this assignment of the SFG bands of H_2O may raise controversy, because the mixing of the symmetric O-H stretching mode and the first overtone of the water bending mode results in Fermi resonance, and the symmetric stretch, asymmetric stretch, and Fermi resonance of H_2O vibration overlap heavily and cannot be easily deconvoluted.[86,87] Using HOD instead of H_2O can greatly simplify the water spectra by eliminating the Fermi resonance (The frequency of the overtone of the bending mode no longer matches that of the O-H stretching mode) and combining the symmetric and asymmetric stretches into one stretch mode.[88] With isotopic dilution, the structure of the water/vapor interface was revisited, which distinguished the contribution from Fermi resonance and confirmed the presence of strongly and weakly hydrogen-bonded water molecules.[84,89,90]

In this work, we applied SFG spectroscopy combined with isotopic dilution to study the surface hydration of nonfouling zwitterionic and PEG materials prepared on silica prisms (Figure 3.18A). The three zwitterionic polymers in question include two poly(carboxybetaine acrylamide)s with one or two carbon atoms between the positive and negative charges (pCBAA1 and pCBAA2) and poly(sulfobetaine methacrylate) (pSBMA), which were shown to have different nonfouling properties in response to pH.[12] The nonfouling poly(oligo ethylene glycol methacrylate) (pOEGMA) brush was compared with the zwitterionic counterparts. The hydration of two model polymers, PMMA and poly(ethylene terephthalate) (PET), which can form hydrogen bonds with water, were also investigated as controls. Further, with isotopic dilution, the effects of pH on the interfacial water structures of the nonfouling polymers were examined. The SFG results indicated that a majority of strongly hydrogen-bonded water formed at the nonfouling polymer surfaces compared to model polymers, and that the hydration properties of the materials were affected by the chemical structural formula as well as environmental factors such as pH.

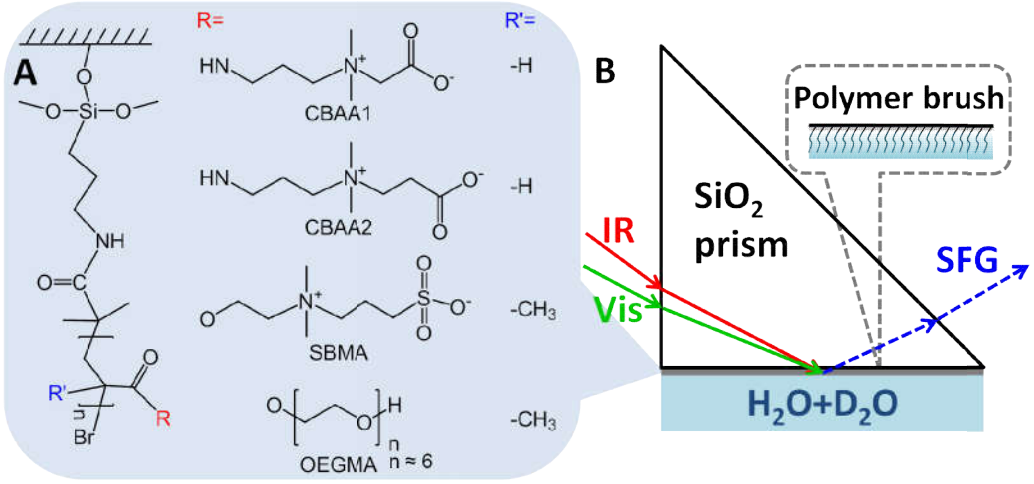

Figure 3.18 (A) Molecular structures of pCBAA1, pCBAA2, pSBMA, and pOEGMA brushes synthesized on silica substrates. These materials were provided by Prof. Shaoyi

Jiang's lab at the University of Washington. (B) SFG measurement of the polymer on a right angle silica prism in contact with isotopically diluted water

3.3.2 Experimental Section

Thin films of PMMA (M_n=75,000) and PET (M_n=30,000) were prepared by spin-coating a 1 % (w/w) solution at 3000 rpm for 30 s followed by annealing at 90 ^oC for 24 h. The zwitterionic and PEG polymer brushes were synthesized on silica prisms (Altos Photonics, Bozeman, MT) via atom transfer radical polymerization (ATRP) according to previous reports with thicknesses of 20-30 nm, and they showed good nonfouling properties.[12,63,64]

To probe the polymer/water interface, the surfaces of the polymers were placed in contact with water (Figure 3.18B). Isotopic dilution was performed by mixing H_2O and D_2O at different ratios (1:0, 1:1, 1:2, 1:3, and 0:1). Isotopically diluted water (H:D=1:3) was used to study the effects of pH. The pH was adjusted to 4 or 10 with HCl or NaOH. SFG spectra were collected from the polymer/water interfaces using the same SFG spectrometer and the same experimental parameters as presented above.

3.3.3 Results and Discussion

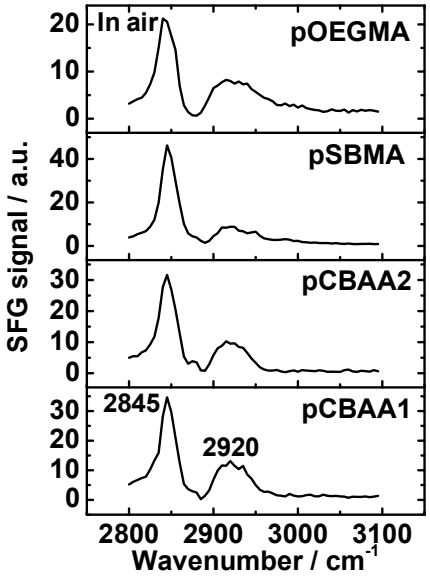

Figure 3.19 SFG spectra of (A) pCBAA1, (B) pCBAA2, (C) pSBMA, and (D) pOEGMA in air.

Before studying the polymer/water interfaces, the surface structures of the polymer brushes were characterized by SFG in air. We have presented the SFG spectra collected from zwitterionic polymer brushes in air previously;[91] these spectra in the C-H stretching frequency region are displayed here to compare to that detected from pOEGMA. All polymers show similar spectra in air, with a strong peak at 2845 cm^{-1} and a weaker peak at 2920 cm^{-1} (Figure 3.19), contributed from the symmetric and asymmetric stretches of CH_2 in the backbone and/or side chains.[39] Therefore, in air, all the polymer surfaces present substantial coverage of methylene groups.

Isotopically diluted water was used to study the surface hydration of the polymers. Ideally, pure HOD molecules should be used in the experiment which offers the neat spectrum of O-H stretching, but experimentally it is difficult to obtain pure HOD

molecules. Instead, H_2O was mixed with D_2O to acquire HOD. In the H_2O-D_2O mixture, in addition to the HOD molecules, there are also some H_2O and D_2O molecules. The percentage of each component in the mixture of H_2O and D_2O[84] was listed in Table 3.3. If H_2O is in excess, a significant amount of SFG signal will come from the O-H stretches of H_2O, which interferes with the SFG O-H stretching signal of HOD. As the percentage of D_2O increases from 50% to 100%, the ratio between HOD and H_2O increases but the absolute amount of HOD decreases, which results in less SFG signal interference from H_2O but weaker HOD signal at the same time. Low HOD SFG signal gives rise to spectral noise and impairs the accuracy of spectral data. Therefore, selection of the ratio of H_2O to D_2O is critical for acquiring as much HOD signal as possible to meet the sensitivity of the SFG system while reducing the interference from H_2O.

Table 3.3 The percentage of H_2O, HOD, and D_2O in mixtures of H_2O and D_2O at different ratios.

H_2O:D_2O	**H_2O**	**HOD**	**D_2O**	**HOD:H_2O**
1:0	1	0	0	0
1:1	1/4 (0.25)	2/4 (0.50)	1/4 (0.25)	2
1:2	1/9 (0.11)	4/9 (0.44)	4/9 (0.44)	4
1:3	1/16 (0.06)	6/16 (0.38)	9/16 (0.56)	6
1:4	1/25 (0.04)	8/25 (0.32)	16/25 (0.64)	8
1:5	1/36 (0.03)	10/36 (0.28)	25/36 (0.69)	10
0:1	0	0	1	N/A

To find the optimal isotopic dilution ratio, SFG spectra were taken when the polymers were placed in contact with water at different H_2O to D_2O ratios (Figure 3.20). As the ratio of H_2O to D_2O decreases from 1:0 to 1:3, the detected SFG signal band centered around 3200 cm^{-1} experiences a blue-shift due to less interference from the combination of symmetric and asymmetric stretches of O-H in H_2O, and the signal intensity of the O-H stretch decreases. It was noted that the intensity difference between the spectra at 1:2 and 1:3 is much less than that between 1:2 and 1:1, and that the spectral features of 1:2 and 1:3 are almost identical, which indicate that the decrease of the intensity from 1:2 to 1:3 is mostly caused by the decreased concentration of O-H bonds rather than the different interferences from H_2O signal. Therefore, the spectrum collected from the mixture at the H_2O to D_2O ratio of 1:3 here is a good representation of the HOD spectrum, which consists of only one O-H stretch without symmetric/asymmetric stretching and Fermi resonance.

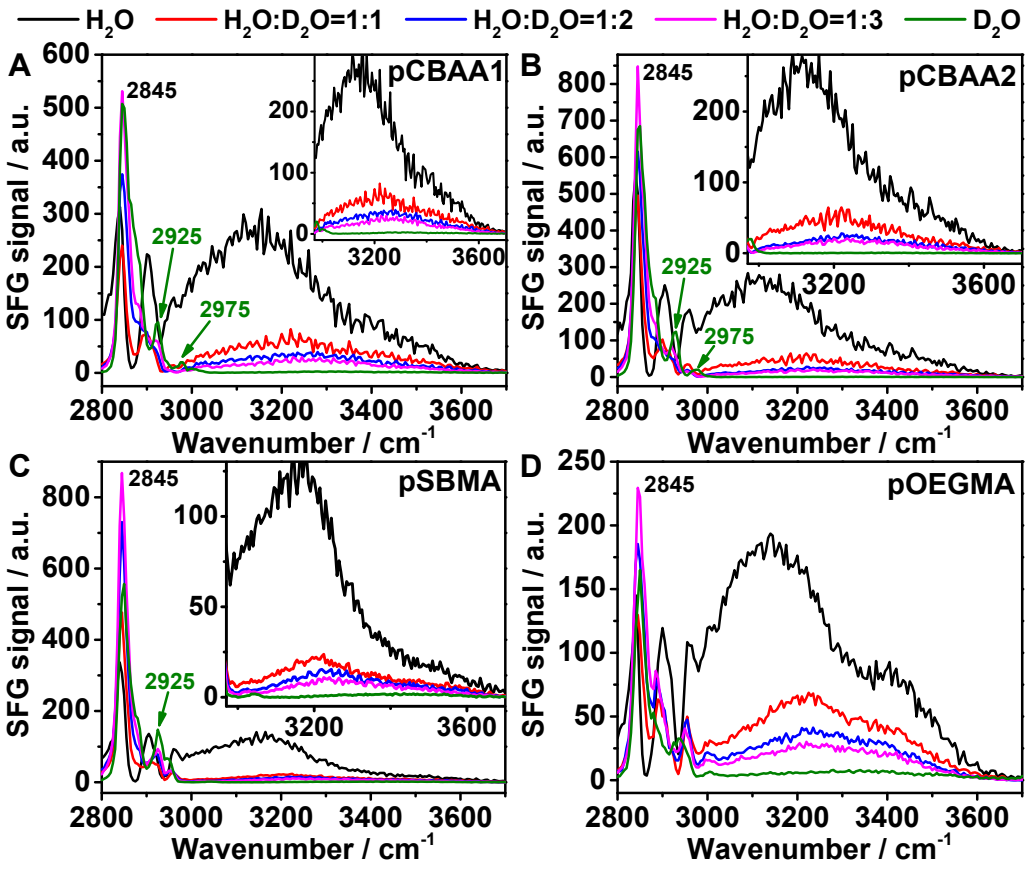

Figure 3.20 SFG spectra of (A) pCBAA1, (B) pCBAA2, (C) pSBMA, and (D) pOEGMA in contact with water with various isotopic dilution ratios. Insets of (A), (B), and (C): the corresponding enlarged water spectra.

Simplified SFG spectra offer a clearer view of the strongly and weakly hydrogen-bonded water, allowing for better interpretation of the SFG water signals. Pure water (without the addition of HCl, NaOH or salts) spectra (H:D=1:3) taken at different zwitterionic and pOEGMA polymer surfaces are enlarged in the insets of Figure 3.21A~D. For the zwitterionic materials, pCBAA1, pCBAA2, and pSBMA, the spectra are dominated by the band around 3200 cm^{-1}, indicating that the water molecules are strongly hydrogen-bonded[84,89] at the zwitterionic surfaces. Differently, the spectrum from the pOEGMA/water interface shows a strong band around 3200 cm^{-1} with a shoulder around 3400 cm^{-1}, indicating that some of the interfacial water molecules were weakly

hydrogen-bonded,[84,89] consistent with a previous report on the water structure at the surface of a polyethylene oxide containing coating.[28] Therefore, the majority of the water molecules form strong hydrogen bonds at both the zwitterionic and pOEGMA surfaces, but some water molecules form weak hydrogen bonds at the pOEGMA surface. The different water structures at the zwitterionic and pOEGMA surfaces result from the different hydrogen bonding mechanisms. Water molecules form hydrogen bonds with the hydrophilic charged groups in zwitterionic materials or the oxygen atoms in the repeating units of the OEG chains, while the former is enhanced by electrostatic attraction. Nevertheless, the surface dominating strongly hydrogen-bonded water molecules prevent biological molecules and organisms from directly interacting with the polymer surfaces, leading to excellent nonfouling performance of these surfaces.

In addition, the C-H signals of the polymers in water are easier to interpret than those presented in our previous report[91] due to the elimination of the interference between the signals of C-H and O-H when D_2O was used as a major component instead of H_2O (Figure 3.20, green curves). The signal intensity of the peak at 2845 cm^{-1} from the zwitterionic materials is higher than that from the pOEGMA surface, indicating that in water, the zwitterionic polymer surface methylene groups are better oriented towards the surface normal than those of pOEGMA. The peak at 2925 cm^{-1} which shows up in the zwitterionic polymer/D_2O interface is contributed from asymmetric stretch of CH_2 groups.[39] The peak at 2975 cm^{-1} observed at the CBAA1 and CBAA2 surfaces probably comes from the N-CH_3 of the quaternary amine.[92] Except the peak at 2845 cm^{-1}, the C-H signals of pOEGMA are different from the zwitterionic materials, which possibly contain some contributions from the OEG chains and indicate a different polymer conformation

in water. Since this study focuses on the interfacial water molecules, quantitative analysis on the SFG C-H stretching signals will not be performed.

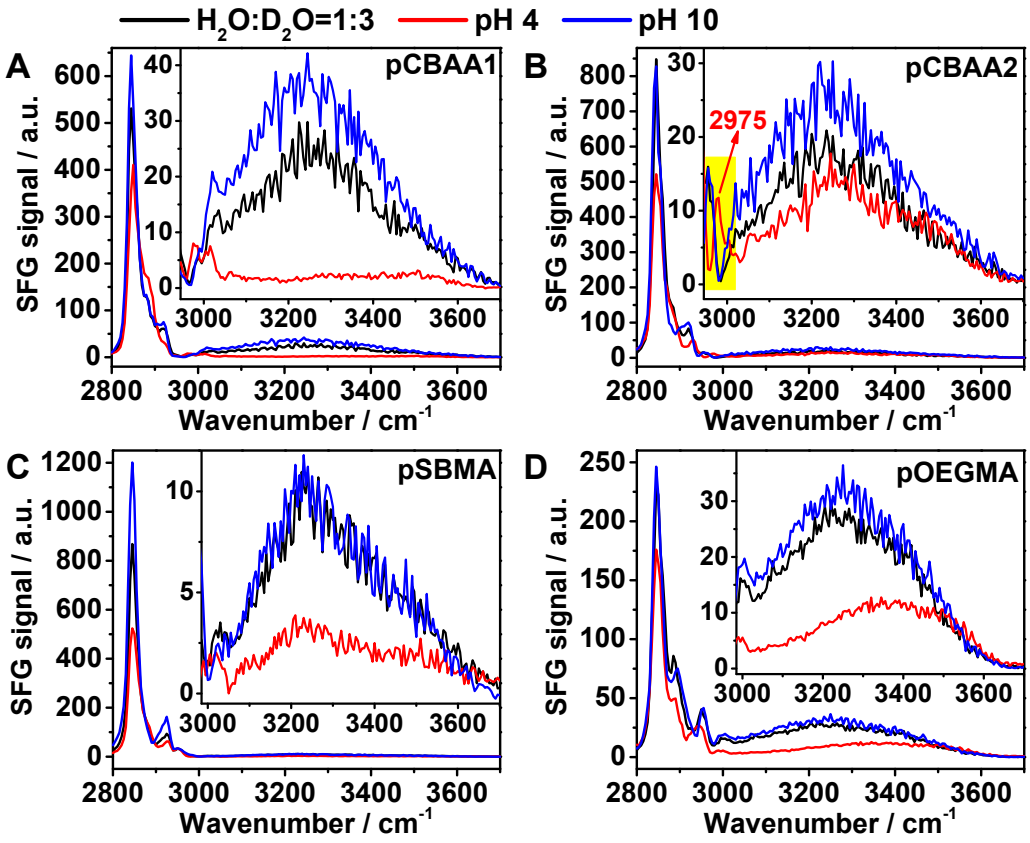

Figure 3.21 SFG spectra of (A) pCBAA1, (B) pCBAA2, (C) pSBMA, and (D) pOEGMA in contact with pure water, and water adjusted to pH 4 or pH 10 (H:D=1:3). Insets of (A), (B), (C), and (D) are the corresponding enlarged water spectra.

The surface hydration of PMMA and PET control films was compared to that of the above studied nonfouling surfaces. PMMA and PET can form hydrogen bonds with water, allowing for a better comparison with the nonfouling materials than other hydrophobic materials such as poly(dimethyl siloxane), polystyrene, polyethylene, or Teflon. The same trend of the water spectra was observed when the isotopic dilution ratio increased from 1:0 to 1:3 (H:D) (Figure 3.22A and B). At the ratio of 1:3, the spectra at both surfaces show a strong band at 3400 cm^{-1} in addition to the 3200 cm^{-1} band (Figure

3.22C), indicating that a significant amount of water molecules are weakly hydrogen-bonded at the polymer surfaces. As we discussed above, nonfouling performance of zwitterionic and pOEGMA polymers may be due to the strong surface hydration - whether the water molecules strongly bind to the surfaces. Under such a condition, it is difficult for biomolecules or organisms to replace the strongly hydrogen-bonded water to attach themselves to the surface. As shown above, for nonfouling zwitterionic and pOEGMA polymer surfaces, SFG signals from interfacial water molecules are dominated by the contribution from strongly hydrogen-bonded water at 3200 cm^{-1}. Differently, here for the two control polymer samples, SFG signals detected from the weakly hydrogen-bonded water centered at 3400 cm^{-1} were also very strong. Such water molecules on the surfaces may be easily replaced by biomolecules for fouling to occur. This result further demonstrates the importance of interfacial water molecules on the nonfouling behavior of the polymer materials.

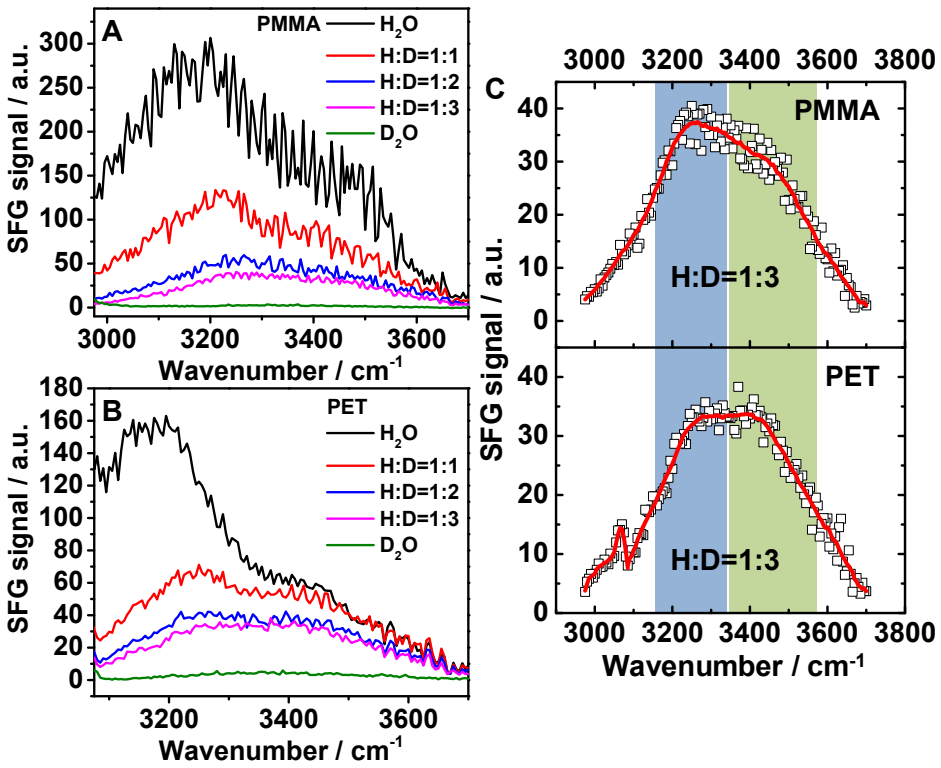

Figure 3.22 SFG spectra of (A) PMMA and (B) PET in contact with water with various isotopic dilution ratios. (C) A stack view of the SFG spectra of water (H:D=1:3) at the PMMA and PET surfaces. The red curves are included for eye guiding.

Because the nonfouling materials are expected to be used in complex environments such as seawater and body fluid, and they have shown different pH dependent properties,[11] we further investigated the effects of pH on their surface hydration with isotopic dilution. Pure water (H:D=1:3) was adjusted to pH 4 or pH 10 with a small amount of HCl or NaOH. We did not use buffer because we want to eliminate the effect of the ionic strength variation. The SFG spectra of water collected at the material surfaces are displayed in Figure 3.21.

For pCBAA1, the water signal decreased when pH decreased from 10 to 4 (Figure 3.21A) as a result of the reduced ordering of the interfacial water due to the protonation of the carboxylate group. Our previous report showed that the water retained some

ordering at pH 5.[91] Here at pH 4, the water signal decreases to almost zero indicating further loss of interfacial water ordering. Moreover, a small band at 3400 cm^{-1} shows up at pH 4 (Figure 3.21A, red curve), indicating the presence of weakly bonded water molecules.

For a different zwitterionic polymer, pCBAA2, our previous report showed that the water ordering decreased to zero from pH 9 to pH 5.[91] At pH 4 here, however, the water signal is strong (Figure 3.21B, red curve), indicating that the interfacial water regains ordering when the bulk aqueous medium changed from pH 5 to pH 4. Figure 3.21B also highlights (in yellow) the different interferences of the C-H stretching peak at 2975 cm^{-1} with the O-H stretching signal at different pH values. At pH 4, the interference is positive, whereas it is negative under neutral condition or at higher pH (e.g. at pH 10). Thus, we can deduce that the water molecules on the pCBAA2 surface flip the overall absolute orientation when the bulk aqueous medium changed from pH 7 to pH 4 (Figure 3.23). Positive interference at pH 4 means that the dipole moments of C-H and O-H have the same absolute direction.[93] If we assume that C-H points out of the polymer surface into the aqueous phase to generate SFG signal, which is true for the reported C-H/water interfaces,[29,93-95] O-H must also point towards the aqueous phase away from the polymer surface. Intuitively this is correct, because at pH 4, the pCBAA2 is positively charged, and the oxygen atom of water molecule is expected to associate with the polymer. At pH 5 of the bulk water medium, no SFG signal was detected from the water molecules on the pCBAA2 surface, as reported previously.[91] At this pH, the interfacial water molecules are randomly oriented, generating no SFG signal. Differently, when the pH of the bulk aqueous medium increased further to neutral and basic conditions, the dipole moments of

C-H and O-H have opposite directions, suggesting that the negatively charged headgroup plays a major role in orienting water molecules.[96] Besides, at pH 4, the intensity ratio between the water SFG bands at 3200 cm^{-1} and 3400 cm^{-1} becomes smaller than that at neutral (noticing the crossing of the spectra at pH 4 and at neutral above 3400 cm^{-1} (Figure 3.21B)), which again indicates the presence of more weakly bonded water at pH 4.

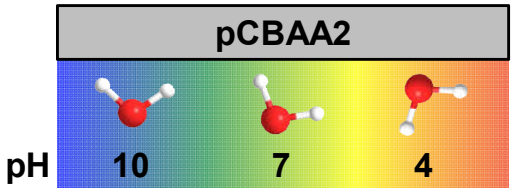

Figure 3.23 Schematic diagram of the water molecules flipping at pCBAA2 surface from pH 10 to pH 4.

For pSBMA, our previous research indicated that interfacial water structure does not change in the range of pH 9 to pH 5.[91] Here, using isotope dilution technique, we found that at pH 10, the water ordering is the same as that at pH 7 (Figure 3.21C), indicating no change of the surface state, agreed with our previous result. When we lowered the pH of the aqueous medium below 5, e.g. at pH 4, water signal decreased, indicating the loss of some ordering (Figure 3.21C, red curve). The reduced water ordering suggests that the sulfonate group starts to be protonated at pH 4.

For pOEGMA, the ordering of water at pH 7 and pH 10 is similar (Figure 4D). The ordering is reduced at pH 4 probably because a proton can bind to the oxygen atom on the OEG chain, which has lone pair electrons, and disturb the water structure. Besides, at pH 4, the band at 3400 cm^{-1} becomes stronger (Figure 3.21D, red curve), indicating a significant amount of weakly hydrogen-bonded water molecules.

Our current study shows similar results of the pH effect on the interfacial water structure to those reported previously for zwitterionic polymers at pH 7 and pH 10.[91] We further investigated the interfacial water structure at a low pH of 4 for the three zwitterionic polymers, showing that at this low pH value the interfacial water structures are varied for the materials. For the carboxybetaine containing materials, CBAA1 and CBAA2, the rise of the water signal contributed from weakly hydrogen-bonded water at pH 4 may be correlated to their weaker nonfouling ability at lower pH.[11] In addition, the pH effect on the surface hydration of pOEGMA has been examined for the first time, showing that at the pH of 4, the interfacial water signal is dominated by the contribution from weakly hydrogen-bonded water. Therefore, we predict that the nonfouling property of PEG materials may decrease at a lower pH.

3.3.4 Conclusions

In this work, we studied the hydration of three zwitterionic polymer surfaces and a PEG surface by SFG with isotopic dilution. The use of isotope diluted water greatly simplified the data analysis of SFG O-H stretching signal. Our results showed that the polymer surfaces are well-ordered in air and water. With the elimination of Fermi resonance, the strongly and weakly bonded water molecules were easily distinguished. Only strongly hydrogen-bonded water molecules were observed on the zwitterionic surfaces whereas the surface hydration of pOEGMA contained a small amount of weakly hydrogen-bonded water. For the two control polymer samples, the weakly hydrogen-bonded interfacial water molecules generated strong SFG signals. These results demonstrated that interfacial water structure is crucial in determining the nonfouling performance of the polymer materials. The effect of pH on the surface hydration of the

materials was also investigated under isotopic dilution. The surface hydration changes differently in response to pH due to the different structures of the materials. The flip of the water molecules at pCBAA2 surface from basic to acidic environment was observed for the first time. The pH dependent interfacial water structural variations of the polymer materials can be well correlated to their changes in nonfouling performance, further demonstrating that the interfacial water molecules play an important role in nonfouling behavior of polymer materials.

3.4 References

(1) Banerjee, I.; Pangule, R. C.; Kane, R. S. *Adv. Mater.* **2011**, *23*, 690-718.
(2) Lejars, M.; Margaillan, A.; Bressy, C. *Chem. Rev.* **2012**, *112*, 4347-4390.
(3) Rosenhahn, A.; Schilp, S.; Kreuzer, H. J.; Grunze, M. *Phys. Chem. Chem. Phys.* **2010**, *12*, 4275-4286.
(4) Rodriguez-Emmenegger, C.; Brynda, E.; Riedel, T.; Houska, M.; Šubr, V.; Alles, A. B.; Hasan, E.; Gautrot, J. E.; Huck, W. T. S. *Macromol. Rapid Commun.* **2011**, *32*, 952-957.
(5) Callow, J. A.; Callow, M. E. *Nat. Commun.* **2011**, *2*, 244 DOI:210.1038/ncomms1251.
(6) Grozea, C. M.; Walker, G. C. *Soft Matter* **2009**, *5*, 4088-4100.
(7) Jiang, S. Y.; Cao, Z. Q. *Adv. Mater.* **2010**, *22*, 920-932.
(8) Colak, S.; Tew, G. N. *Langmuir* **2012**, *28*, 666-675.
(9) Chen, S. F.; Li, L. Y.; Zhao, C.; Zheng, J. *Polymer* **2010**, *51*, 5283-5293.
(10) Vaisocherová, H.; Zhang, Z.; Yang, W.; Cao, Z. Q.; Cheng, G.; Taylor, A. D.; Piliarik, M.; Homola, J.; Jiang, S. Y. *Biosens. Bioelectron.* **2009**, *24*, 1924-1930.
(11) Mi, L.; Bernards, M. T.; Cheng, G.; Yu, Q. M.; Jiang, S. Y. *Biomaterials* **2010**, *31*, 2919-2925.
(12) Zhang, Z.; Vaisocherova, H.; Cheng, G.; Yang, W.; Xue, H.; Jiang, S. Y. *Biomacromolecules* **2008**, *9*, 2686-2692.
(13) Lambert, A. G.; Davies, P. B.; Neivandt, D. J. *Appl. Spectrosc. Rev.* **2005**, *40*, 103-145.
(14) Perry, A.; Neipert, C.; Space, B.; Moore, P. B. *Chem. Rev.* **2006**, *106*, 1234-1258.
(15) Hirose, C.; Akamatsu, N.; Domen, K. *Appl. Spectrosc.* **1992**, *46*, 1051-1072.
(16) Ji, N.; Zhang, K.; Yang, H.; Shen, Y. R. *J. Am. Chem. Soc.* **2006**, *128*, 3482-3483.
(17) Gracias, D. H.; Chen, Z.; Shen, Y. R.; Somorjai, G. A. *Acc. Chem. Res.* **1999**, *32*, 930-940.
(18) Fu, L.; Liu, J.; Yan, E. C. Y. *J. Am. Chem. Soc.* **2011**, *133*, 8094-8097.
(19) Howell, C.; Diesner, M. O.; Grunze, M.; Koelsch, P. *Langmuir* **2008**, *24*, 13819-13821.
(20) Kett, P. J. N.; Casford, M. T. L.; Yang, A. Y.; Lane, T. J.; Johal, M. S.; Davies, P. B. *J. Phys. Chem. B* **2009**, *113*, 1559-1568.

(21) Roy, S.; Covert, P. A.; FitzGerald, W. R.; Hore, D. K. *Chem. Rev.* **2014**, DOI: 10.1021/cr400418b.
(22) Tyrode, E.; Rutland, M. W.; Bain, C. D. *J. Am. Chem. Soc.* **2008**, *130*, 17434-17445.
(23) Tyrode, E.; Johnson, C. M.; Rutland, M. W.; Day, J. P. R.; Bain, C. D. *J. Phys. Chem. C* **2007**, *111*, 316-329.
(24) Hirose, C.; Bandara, A.; Katano, S.; Kubota, J.; Wada, A.; Domen, K. *Appl. Phys. B-Lasers O.* **1999**, *68*, 559-565.
(25) Hankett, J. M.; Liu, Y. W.; Zhang, X. X.; Zhang, C.; Chen, Z. *J. Polym. Sci., Part B: Polym. Phys.* **2013**, *51*, 311-328.
(26) Li, G. F.; Ye, S.; Morita, S.; Nishida, T.; Osawa, M. *J. Am. Chem. Soc.* **2004**, *126*, 12198-12199.
(27) Ye, S. J.; Liu, G. M.; Li, H. C.; Chen, F. G.; Wang, X. W. *Langmuir* **2012**, *28*, 1374-1380.
(28) Leung, B. O.; Yang, Z.; Wu, S. S. H.; Chou, K. C. *Langmuir* **2012**, *28*, 5724-5728.
(29) Uosaki, K.; Noguchi, H.; Yamamoto, R.; Nihonyanagi, S. *J. Am. Chem. Soc.* **2010**, *132*, 17271-17276.
(30) Anim-Danso, E.; Zhang, Y.; Alizadeh, A.; Dhinojwala, A. *J. Am. Chem. Soc.* **2013**, *135*, 2734-2740.
(31) Gopalakrishnan, S.; Liu, D. F.; Allen, H. C.; Kuo, M.; Shultz, M. J. *Chem. Rev.* **2006**, *106*, 1155-1175.
(32) Richmond, G. L. *Chem. Rev.* **2002**, *102*, 2693-2724.
(33) Shen, Y. R.; Ostroverkhov, V. *Chem. Rev.* **2006**, *106*, 1140-1154.
(34) Flores, S. C.; Kherb, J.; Cremer, P. S. *J. Phys. Chem. C* **2012**, *116*, 14408-14413.
(35) Nagata, Y.; Hsieh, C. S.; Hasegawa, T.; Voll, J.; Backus, E. H. G.; Bonn, M. *J. Phys. Chem. Lett.* **2013**, *4*, 1872-1877.
(36) Asanuma, H.; Noguchi, H.; Uosaki, K.; Yu, H. Z. *J. Phys. Chem. C* **2009**, *113*, 21155-21161.
(37) Zhang, Z.; Chao, T.; Chen, S. F.; Jiang, S. Y. *Langmuir* **2006**, *22*, 10072-10077.
(38) Leng, C.; Liu, Y. W.; Jenkins, C.; Meredith, H.; Wilker, J. J.; Chen, Z. *Langmuir* **2013**, *29*, 6659-6664.
(39) Wang, J.; Woodcock, S. E.; Buck, S. M.; Chen, C. Y.; Chen, Z. *J. Am. Chem. Soc.* **2001**, *123*, 9470-9471.
(40) Scatena, L. F.; Brown, M. G.; Richmond, G. L. *Science* **2001**, *292*, 908-912.
(41) Tang, C. Y.; Huang, Z. S.; Allen, H. C. *J. Phys. Chem. B* **2011**, *115*, 34-40.
(42) Tang, C. Y.; Huang, Z. S.; Allen, H. C. *J. Phys. Chem. B* **2010**, *114*, 17068-17076.
(43) Hu, D.; Yang, Z.; Chou, K. C. *J. Phys. Chem. C* **2013**, *117*, 15698-15703.
(44) Wurpel, G. W. H.; Sovago, M.; Bonn, M. *J. Am. Chem. Soc.* **2007**, *129*, 8420-8421.
(45) Covert, P. A.; Jena, K. C.; Hore, D. K. *J. Phys. Chem. Lett.* **2014**, *5*, 143-148.
(46) Dewan, S.; Yeganeh, M. S.; Borguet, E. *J. Phys. Chem. Lett.* **2013**, *4*, 1977-1982.
(47) Chen, X.; Yang, T. L.; Kataoka, S.; Cremer, P. S. *J. Am. Chem. Soc.* **2007**, *129*, 12272-12279.
(48) Shao, Q.; He, Y.; Jiang, S. Y. *J. Phys. Chem. B* **2011**, *115*, 8358-8363.
(49) Weers, J. G.; Rathman, J. F.; Axe, F. U.; Crichlow, C. A.; Foland, L. D.; Scheuing, D. R.; Wiersema, R. J.; Zielske, A. G. *Langmuir* **1991**, *7*, 854-867.
(50) Mi, L.; Giarmarco, M. M.; Shao, Q.; Jiang, S. Y. *Biomaterials* **2012**, *33*, 2001-2006.
(51) Shao, Q.; Jiang, S. Y. *J. Phys. Chem. B* **2013**, *117*, 1357-1366.

(52) Zhang, L.; Cao, Z. Q.; Bai, T.; Carr, L.; Ella-Menye, J. R.; Irvin, C.; Ratner, B. D.; Jiang, S. Y. *Nat. Biotechnol.* **2013**, *31*, 553-556.
(53) Keefe, A. J.; Jiang, S. Y. *Nat. Chem.* **2012**, *4*, 60-64.
(54) Welch, M.; Rastogi, A.; Ober, C. *Soft Matter* **2011**, *7*, 297-302.
(55) Wei, Q.; Becherer, T.; Angioletti-Uberti, S.; Dzubiella, J.; Wischke, C.; Neffe, A. T.; Lendlein, A.; Ballauff, M.; Haag, R. *Angew. Chem. Int. Ed.* **2014**, *53*, 8004-8031.
(56) Schlenoff, J. B. *Langmuir* **2014**, *30*, 9625-9636.
(57) Ma, H. W.; Hyun, J.; Stiller, P.; Chilkoti, A. *Adv. Mater.* **2004**, *16*, 338-341.
(58) Galvin, C. J.; Dimitriou, M. D.; Satija, S. K.; Genzer, J. *J. Am. Chem. Soc.* **2014**, *136*, 12737-12745.
(59) Gunkel, G.; Huck, W. T. S. *J. Am. Chem. Soc.* **2013**, *135*, 7047-7052.
(60) Shao, Q.; He, Y.; White, A. D.; Jiang, S. Y. *J. Chem. Phys.* **2012**, *136*, 225101-225106.
(61) Welsher, K.; McManus, S. A.; Hsia, C.-H.; Yin, S.; Yang, H. *J. Am. Chem. Soc.* **2015**, *137*, 580-583.
(62) Yang, W.; Liu, S. J.; Bai, T.; Keefe, A. J.; Zhang, L.; Ella-Menye, J. R.; Li, Y. T.; Jiang, S. Y. *Nano Today* **2014**, *9*, 10-16.
(63) Ma, H. W.; Li, D. J.; Sheng, X.; Zhao, B.; Chilkoti, A. *Langmuir* **2006**, *22*, 3751-3756.
(64) Yang, W.; Chen, S. F.; Cheng, G.; Vaisocherova, H.; Xue, H.; Li, W.; Zhang, J. L.; Jiang, S. Y. *Langmuir* **2008**, *24*, 9211-9214.
(65) Holmlin, R. E.; Chen, X.; Chapman, R. G.; Takayama, S.; Whitesides, G. M. *Langmuir* **2001**, *17*, 2841-2850.
(66) Sundaram, H. S.; Ella-Menye, J.-R.; Brault, N. D.; Shao, Q.; Jiang, S. Y. *Chem. Sci.* **2014**, *5*, 200-205.
(67) Bernards, M. T.; Cheng, G.; Zhang, Z.; Chen, S. F.; Jiang, S. Y. *Macromolecules* **2008**, *41*, 4216-4219.
(68) Chen, S. F.; Jiang, S. Y. *Adv. Mater.* **2008**, *20*, 335-338.
(69) Azzaroni, O.; Brown, A. A.; Huck, W. T. S. *Angew. Chem. Int. Ed.* **2006**, *45*, 1770-1774.
(70) Huang, C.-J.; Li, Y. T.; Krause, J. B.; Brault, N. D.; Jiang, S. Y. *Macromol. Rapid Commun.* **2012**, *33*, 1003-1007.
(71) Li, L. Y.; Chen, S. F.; Zheng, J.; Ratner, B. D.; Jiang, S. Y. *J. Phys. Chem. B* **2005**, *109*, 2934-2941.
(72) Yuan, J.; Huang, X.; Li, P.; Li, L.; Shen, J. *Polym. Chem.* **2013**, *4*, 5074-5085.
(73) Nguyen, A. T.; Baggerman, J.; Paulusse, J. M. J.; van Rijn, C. J. M.; Zuilhof, H. *Langmuir* **2011**, *27*, 2587-2594.
(74) Kobayashi, M.; Terayama, Y.; Yamaguchi, H.; Terada, M.; Murakami, D.; Ishihara, K.; Takahara, A. *Langmuir* **2012**, *28*, 7212-7222.
(75) Tang, L.; Lee, N. Y. *Lab Chip* **2010**, *10*, 1274-1280.
(76) Wu, J.; Lee, N. Y. *Lab Chip* **2014**, *14*, 1564-1571.
(77) Cantini, M.; Sousa, M.; Moratal, D.; Mano, J. F.; Salmeron-Sanchez, M. *Biomater. Sci.* **2013**, *1*, 202-212.
(78) Zhang, Z.; Chen, S. F.; Chang, Y.; Jiang, S. Y. *J. Phys. Chem. B* **2006**, *110*, 10799-10804.

(79) Ladd, J.; Zhang, Z.; Chen, S. F.; Hower, J. C.; Jiang, S. Y. *Biomacromolecules* **2008**, *9*, 1357-1361.
(80) Wang, J.; Chen, C. Y.; Buck, S. M.; Chen, Z. *J. Phys. Chem. B* **2001**, *105*, 12118-12125.
(81) Kim, J.; Somorjai, G. A. *J. Am. Chem. Soc.* **2003**, *125*, 3150-3158.
(82) Wang, J.; Buck, S. M.; Even, M. A.; Chen, Z. *J. Am. Chem. Soc.* **2002**, *124*, 13302-13305.
(83) Wu, J.; Wang, Z.; Lin, W. F.; Chen, S. F. *Acta Biomater.* **2013**, *9*, 6414-6420.
(84) Nihonyanagi, S.; Ishiyama, T.; Lee, T.; Yamaguchi, S.; Bonn, M.; Morita, A.; Tahara, T. *J. Am. Chem. Soc.* **2011**, *133*, 16875-16880.
(85) Ji, N.; Ostroverkhov, V.; Tian, C. S.; Shen, Y. R. *Phys. Rev. Lett.* **2008**, *100*, 096102.
(86) Sovago, M.; Campen, R. K.; Wurpel, G. W. H.; Muller, M.; Bakker, H. J.; Bonn, M. *Phys. Rev. Lett.* **2008**, *100*, 173901.
(87) Falk, M.; Ford, T. A. *Can. J. Chem.* **1966**, *44*, 1699-1707.
(88) Black, S. B.; Chang, Y.; Bae, C.; Hickner, M. A. *J. Phys. Chem. B* **2013**, *117*, 16266-16274.
(89) Tian, C. S.; Shen, Y. R. *J. Am. Chem. Soc.* **2009**, *131*, 2790-2791.
(90) Stiopkin, I. V.; Weeraman, C.; Pieniazek, P. A.; Shalhout, F. Y.; Skinner, J. L.; Benderskii, A. V. *Nature* **2011**, *474*, 192-195.
(91) Leng, C.; Han, X. F.; Shao, Q.; Zhu, Y. H.; Li, Y. T.; Jiang, S. Y.; Chen, Z. *J. Phys. Chem. C* **2014**, *118*, 15840-15845.
(92) Leng, C.; Gibney, K. A.; Liu, Y. W.; Tew, G. N.; Chen, Z. *ACS Macro Lett.* **2013**, *2*, 1011-1015.
(93) Sagle, L. B.; Cimatu, K.; Litosh, V. A.; Liu, Y.; Flores, S. C.; Chen, X.; Yu, B.; Cremer, P. S. *J. Am. Chem. Soc.* **2011**, *133*, 18707-18712.
(94) Chen, C. Y.; Wang, J.; Chen, Z. *Langmuir* **2004**, *20*, 10186-10193.
(95) Wang, J.; Paszti, Z.; Even, M. A.; Chen, Z. *J. Am. Chem. Soc.* **2002**, *124*, 7016-7023.
(96) Shao, Q.; He, Y.; White, A. D.; Jiang, S. Y. *J. Phys. Chem. B* **2010**, *114*, 16625-16631.

CHAPTER 4 MOLECULAR UNDERSTANDING OF ADHESION MECHANISMS OF BIOFOULING

4.1 Surface Dehydration Effect on Mussel Adhesion

4.1.1 Introduction

Marine organisms such as mussels and barnacles can deposit adhesive mixtures in order to attach themselves onto various surfaces in wet environments which lead to biofouling.[1-3] On one hand, because marine biofouling causes many issues in the naval industry, antifouling materials that resist the adhesion of marine organisms are highly desired.[4] Probing the adhesive interfaces of marine organisms leads to an understanding of the adhesion mechanisms, which aids in the design of effective antifouling materials. On the other hand, underwater glue is challenging to prepare. By probing the biofouling interfaces, the principles of underwater adhesion can be learned, which will inspire and guide the development of novel adhesive materials for underwater applications.[5,6]

As a typical example of underwater adhesion, mussel adhesives have been extensively investigated, and mussel foot proteins (MFP) have been extracted and purified to study their adhesion mechanisms.[1,7-10] It is believed that the abundance of a special amino acid, L-3,4-dihydroxyphenylalanine (DOPA), in MFPs is responsible to the strong adhesion of the proteins[11,12] due to the crosslinking and reactions of the catechol groups in DOPA.[13-15] Recently, adhesion mechanisms other than DOPA-mediated

adhesion have been discovered, including thiol-mediated redox reactions,[16] adaptive hydrophobic interaction,[17,18] and synergistic cationic effect.[19] However, the adhesion mechanisms in these reports were mainly proposed from force measurements, which did not offer direct molecular structural information at the adhesion interfaces. In addition, the purified MFPs may not behave or react in exactly the same ways as the native proteins secreted by live mussels.

In situ probing the interfaces between native mussel adhesives and the substrates offers an opportunity to reveal the adhesion mechanisms that otherwise could not be elucidated by studying purified MFPs. Previously reported methods to study the adhesion mechanisms including force measurements,[10] electrochemistry,[18] and various spectroscopies[12,14] could not provide molecular information at buried interfaces. Alternatively, sum frequency generation (SFG) vibrational spectroscopy is a powerful technique to probe buried interfaces in situ, providing information about chemical structures at the molecular level.[20] It has been extensively used to study buried polymer interfaces, polymer/water interfaces, and interfacial biomolecules.[21-23] Furthermore, the detailed structural information of interfacial water can be extracted from SFG data.[24-26]

In this work, SFG spectroscopy was applied to probe the interfaces between mussel adhesives and various substrates in water (Figure 4.1). The substrates used in this work covered a wide range of materials including CaF_2, SiO_2, poly(methyl methacrylate) (PMMA), polystyrene (PS), poly(dimethyl siloxane) (PDMS), poly(oligo ethylene glycol methacrylate) (pOEGMA), and poly(sulfobetaine methacrylate) (pSBMA). Among the substrates, CaF_2 and SiO_2 provide analogs to natural rock and earth surfaces; PMMA and PS represent widely used plastics; and PDMS, pOEGMA, and pSBMA are the most

promising antifouling coatings. SFG signals at the buried interfaces were compared to those collected at the substrates without the mussel proteins. Interfacial H/D exchange was also applied to investigate the access of water into the buried interfaces. On various substrates, surface dehydration by mussel proteins was observed using SFG spectroscopy. Surface dehydration was found to a lesser extent on the antifouling surfaces, pOEGMA and pSBMA. In addition, different functional groups on the polymer surfaces were found to interact differently with the mussel proteins.

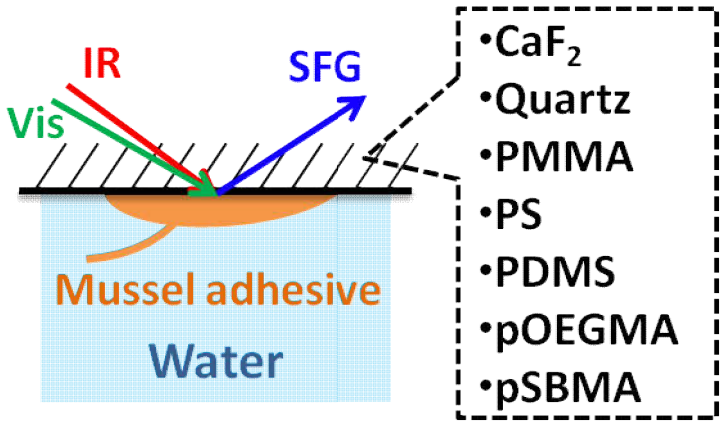

Figure 4.1 SFG sample geometry used to probe the buried interfaces between mussel adhesive plaques and various substrates in water.

4.1.2 Experimental Section

Quartz slides (1 inch x 1 inch, 1 mm thick) were purchased from VWR International. CaF_2 and SiO_2 prisms (right angle) were purchased from Altos Photonics. PMMA (M_w=75,000 g/mol), PS (M_w=280,000 g/mol), and toluene were purchased from Sigma-Aldrich. Deuterated PMMA (d8PMMA) (M_n=150,000 g/mol, M_w=180,000 g/mol) and deuterated PS (d8PS) (M_n=165,000 g/mol, M_w=198,000 g/mol) were purchased from Polymer Source Inc. Sylgard 184 silicone elastomer kit was purchased from Dow Corning Corporation.

Thin films of PMMA, d8-PMMA, PS, and d8-PS were prepared by spin-coating a 1% (w/w) toluene solution on a clean quartz slide at 3000 rpm for 40 s using a P-6000 spin coater (Speedline Technologies) followed by annealing at 95 ^{o}C for 24 h. To prepare the PDMS thin film, the base and curing agents of Sylgard 184 silicone elastomer kit were thoroughly mixed in 10:1 ratio and diluted to 1% (w/w) using toluene. The toluene solution was immediately spin-coated on a plasma-cleaned quartz slide at 3000 rpm for 90 s, followed by curing at 110 ^{o}C for 35 min. The brushes of pOEGMA and pSBMA were prepared by Prof. Shaoyi Jiang's group at the University of Washington on quartz slides via atomic transfer radical polymerization (ATRP) according to the previous report.[27] The thicknesses of the identical polymer brushes prepared on silicon wafers were measured to be 25-30 nm by an alpha-SE ellipsometer (J. A. Woollam).

To prepare the mussel adhesive plaques on various substrates, live mussels were fixed by rubber bands on the substrates until they deposit the plaques. This was dones by Prof. Jonathan Wilker's lab at Purdue University. Figure 4.2 shows the photographs of a mussel adhesive plaque deposited on a quartz slide taken with a Mighty Scope 5M USB Digital Microscope (Aven Inc). The size of a mussel plaque is around 1 mm in diameter and the average thickness is around 0.1 mm.

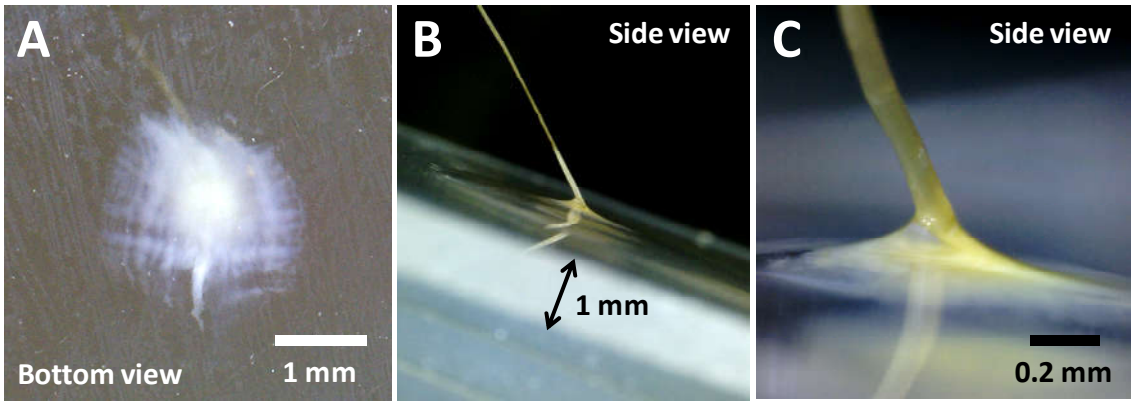

Figure 4.2 Photographs of a mussel adhesive plaque on a quartz slide: (A) bottom view, (B) side view, and (C) enlarged side view.

Total internal reflection Fourier Transform infrared (TIR-FTIR) spectroscopy experiments[28] were carried out using a Nicolet Magna 550 FTIR spectrometer. A mussel adhesive plaque was deposited on the surface of a CaF_2 prism and the interface between the mussel plaque and the CaF_2 substrate was probed using the IR beam (Figure 4.3A).

The SFG spectroscopy was implemented according to the protocol reported previously.[29] The visible and infrared (IR) input beams were overlapped spatially and temporally at the interfaces between mussel adhesive plaques and the substrates immersed in water, or the interfaces between the substrates and water without the plaques. All SFG spectra were collected using the ssp (s-polarized sum frequency output, s-polarized visible input, and p-polarized IR input) polarization combination.[30]

4.1.3 Results and Discussion

4.1.3.1 Mussel plaque/CaF_2 interface

Before SFG measurements were taken at the mussel adhesive interface, a TIR-FTIR spectrum was collected between a mussel adhesive plaque and the CaF_2 surface to reveal the major component at the interfacial region (with a thickness of several hundred

nanometers around the interface) . Figure 4.3B shows that the peaks from the amide (C=O and N-H) groups dominate the spectra, indicating the presence of a large amount of proteins at the interfacial region.

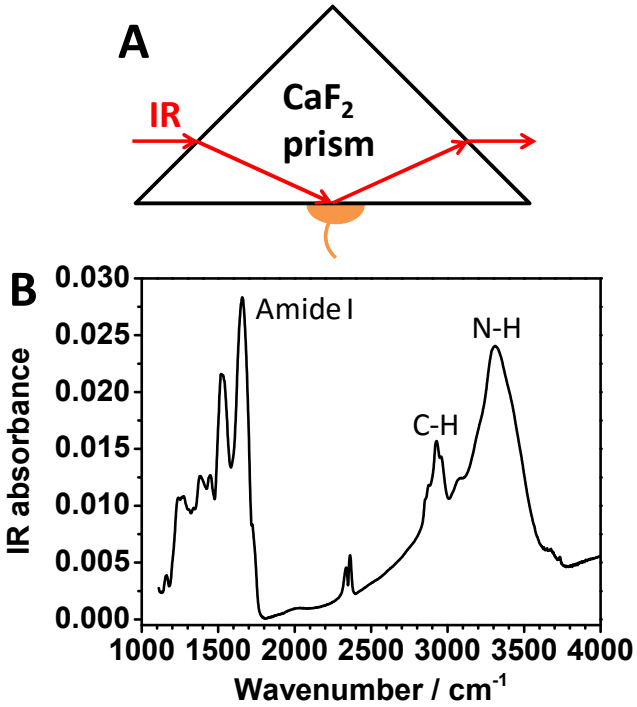

Figure 4.3 (A) TIR-FTIR experiment of a mussel adhesive plaque on a CaF_2 prism and (B) the corresponding spectrum.

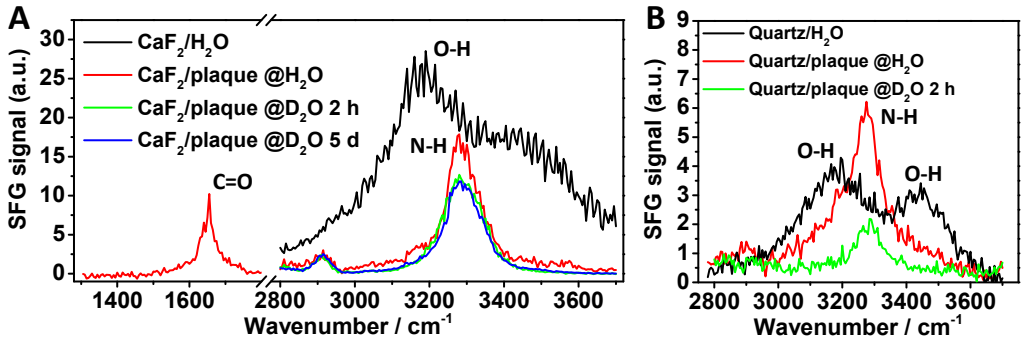

Figure 4.4 SFG spectra of mussel plaques at (A) CaF_2 and (B) quartz interface in water (H_2O or D_2O).

To investigate the interfacial structure of mussel adhesives on the CaF_2 surface, SFG spectra were collected at the CaF_2 surface in water with or without the mussel plaque. (Because the mussel adhesives deposited on the CaF_2 surface do not cover the entire surface, the surface is inhomogeneous with regions with or without adhesive.) As shown in Figure 4.4A, at the buried interface between the mussel adhesive plaque and CaF_2, strong protein signals from amide I (contributed mainly from the C=O group) and N-H stretching were observed, indicating strong ordering of the MFPs at the interface. No discernible water O-H stretching signal was observed, indicating that no ordered water molecules were present at the CaF_2/mussel adhesive plaque interface. In contrast, at the CaF_2/water interface, strong water O-H stretching signal was detected, indicating the presence of strongly ordered water molecules. Comparing the SFG signals detected from the interfaces between CaF_2 and mussel adhesive plaque, and between CaF_2 and water, we believe that during the adhering process of MFPs, the initial hydration layer consisting of ordered water molecules on the CaF_2 surface was replaced by adhesive proteins (Figure 4.5). Therefore, the elimination of the surface hydration layer on a surface is crucial for bio-adhesion to occur on the CaF_2 surface in water.

As mentioned above, a strong SFG signal of N-H stretching was detected from the buried interface between mussel adhesive plaque and CaF_2. The N-H bond of an amide group in a protein can be transformed to an N-D bond if the N-H bond is able to directly contact D_2O molecules around/inside the protein. Whether N-H bond can be transformed to N-D and how fast the transformation occurs can reveal the exposure of the N-H bond to water. Such information can be used to deduce structural information of a protein.[31] Here we performed H/D exchange experiment to study the mussel adhesive plaque on a

CaF_2 substrate (Figure 4.4A). After the mussel adhesive sample was immersed in D_2O for 2 h, N-H signal at 3280 cm^{-1} collected from the mussel adhesive plaque/CaF_2 interface in D_2O decreased by about 1/4 compared to that collected in H_2O before replacing the H_2O with D_2O. After the sample was immersed in D_2O for five days, the N-H signal did not further decrease. Because SFG signal intensity is proportional to the square of the number of the functional groups, we believe that about 15% of the N-H groups transformed to N-D groups, indicating that the majority of the amide bonds of the interfacial proteins were not exposed to water molecules. Water could not reach the interfacial protein amide bonds even after five days, suggesting limited access of water to the buried adhesive interface. The non-permeability of water to the biofouling interface may be critical for bio-adhesion underwater.

4.1.3.2 Mussel plaque/quartz interface

The SFG spectra of a mussel plaque deposited on a quartz slide were obtained (Figure 4.4B). On a clean quartz surface without the mussel plaques, strong SFG signals of O-H bonds indicate the strong ordering of the interfacial water structure. At a mussel plaque/quartz interface, similar to the mussel adhesive/CaF_2 interface, strong N-H signal was observed instead of the O-H signals. Therefore, surface dehydration also happened on the quartz surface due to the adhesion of the MFPs. H/D exchange experiment was performed to evaluate the water permeability of the mussel plaque/quartz interface. After H_2O was replaced by D_2O for 2 h, the N-H peak decreased to about 1/3. The percentage decrease of the N-H signal is more significant at the quartz interface than CaF_2, indicating that water can penetrate more easily to the mussel plaque/quartz interface. Although surface dehydration still plays an important role in the adhesion on quartz,

other mechanisms may also contribute to mussel adhesion on quartz such as the hydrogen bonding and electrostatic attraction between the MFPs and the $-O^-$ groups on the quartz surface (Figure 4.5).[32]

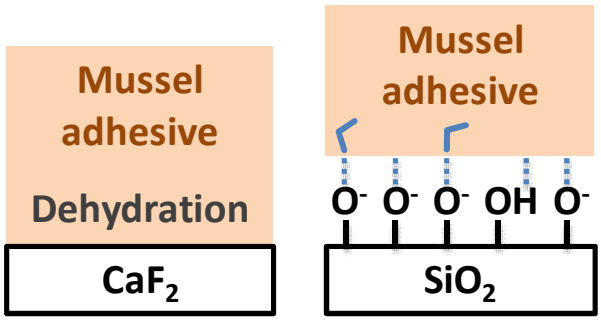

Figure 4.5 Schematic showing the mussel adhesion mechanisms on CaF_2 and quartz surfaces.

4.1.3.3 Mussel plaque/plastic interfaces: PMMA and PS

The SFG spectra were taken at the interface between a mussel plaque and PMMA or PS (Figure 4.6). At the PMMA/water interface without mussel plaques, SFG signals contributed from the PMMA O-CH_3 group and H_2O dominated the spectra (Figure 4.6A), indicating that the O-CH_3 group tilted on the surface in water and the interfacial water molecules are ordered. At the d8PMMA/water interface, the water spectrum is the same (Figure 4.6B). However, at the mussel plaque/PMMA interface in water, the water signals significantly decreased, while the N-H signal dominated the spectra, indicating surface dehydration on the PMMA surfaces by the MFPs. Further, with the presence of the mussel plaque, the O-CH_3 signal disappeared, showing that the O-CH_3 group lied down at the adhesive interface (Figure 4.7) probably due to the unfavorable interaction between the O-CH_3 group and MFPs. In addition, H/D exchange experiment performed at the plaque/d8PMMA interface showed that the majority of the N-H signal remained (Figure 4.6B), indicating low penetration of water into the interface.

At the PS/water interface without mussel plaques, only weak SFG signals of water were observed (Figure 4.6C), indicating that the phenyl ring on PS lied down at the water interface and the water molecules are weakly ordered, due to the unfavorable interaction between the hydrophobic PS surface and water. At the d8PS/water interface, the water spectrum is the same (Figure 4.6D). However, at the mussel plaque/PS interface in water, both the N-H signal from the mussel plaque and the phenyl signal from the PS were observed, indicating the favorable interaction between the hydrophobic PS surface and the MFPs (Figure 4.7). Further, H/D exchange experiment performed at the plaque/d8PS interface showed that the majority of the N-H signal remained (Figure 4.6D), indicating low penetration of water into the interface, similar to the plaque/PMMA interface.

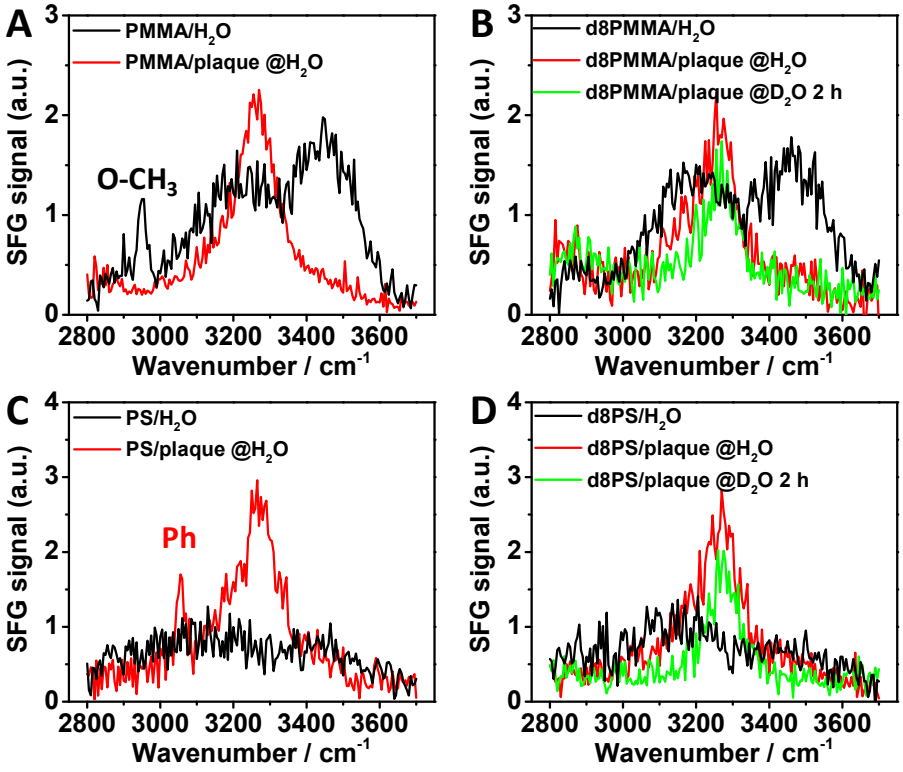

Figure 4.6 SFG spectra of mussel plaques at (A) PMMA, (B) d8PMMA, (C) PS, (D) d8PS interfaces in water (H_2O or D_2O).

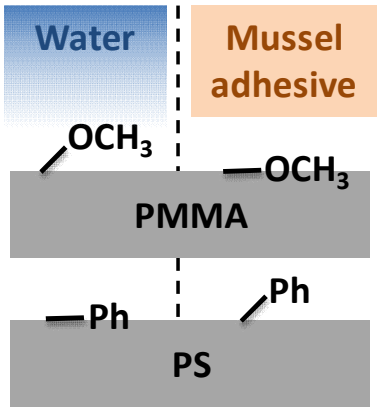

Figure 4.7 Schematics showing the molecular interactions between mussel adhesives and PMMA or PS.

4.1.3.4 Mussel plaque/antifouling polymer interfaces: PDMS, pOEGMA, and pSBMA

PDMS is widely used as a fouling release material.[33] Mussel plaques could be deposited on PDMS surfaces, although the adhesion force is low. SFG spectra taken from the PDMS/water interface showed Si-CH_3 peaks and very weak water signal, indicating the weak ordering of interfacial water molecules. At the mussel plaque/PDMS interface in water, both signals decreased, and no signal from the MFPs were observed (Figure 4.8A), indicating the surface dehydration and hydrophobic interaction at the plaque/PDMS interface. Further, the Si-CH_3 unfavorably interacts with MFPs which could not adopt a certain interfacial ordering to maintain strong adhesion (Figure 4.9).

At the pOEGMA surface, strong water signal at 3200 cm^{-1} was observed, indicating strongly hydrogen bonded water at the polymer surface (Figure 4.8B). At the pOEGMA/plaque interface in water, different from all the surfaces mentioned previously, water signal dominated the spectra above 3000 cm^{-1}, showing a less extent of dehydration at the pOEGMA surface by MFPs (Figure 4.9). Further, after H/D exchange at the plaque/pOEGMA interface, neither the O-H signal nor the N-H signal was observed, indicating good penetration of water into the interface.

At the pSBMA, surface, strong water signal at 3200 cm^{-1} was observed, indicating strongly hydrogen bonded water at the polymer surface (Figure 4.8C), similar to the pOEGMA surface. At the pSBMA/plaque interface in water, the water signal almost did not decrease, indicating hardly any dehydration at the pSBMA surface by MFPs (Figure 4.9). This agrees with our previous study that the surface hydration of pSBMA is strong and is not disrupted by proteins.[27] Further, after H/D exchange at the plaque/pOEGMA

interface, neither the O-H signal nor the N-H signal was observed, indicating good penetration of water into the interface.

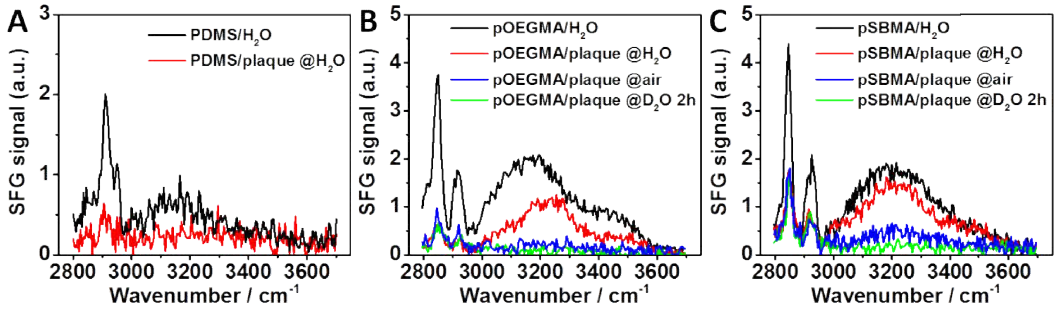

Figure 4.8 SFG spectra of mussel plaques at (A) PDMS, (B) pOEGMA, (C) pSBMA interfaces in water (H_2O or D_2O).

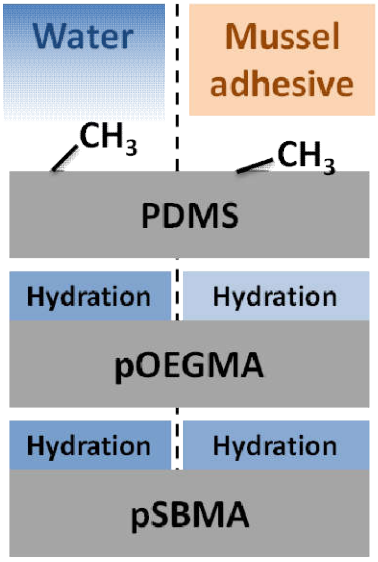

Figure 4.9 Schematic showing the molecular interaction and hydration at the interfaces between mussel adhesives and PDMS, pOEGMA, or pSBMA.

4.1.4 Conclusions

In this work, SFG was applied to probe the buried interfaces between mussel adhesives and different substrates in water in situ. FTIR data showed the dominating presence of MFPs in the interfacial region. On the surfaces of CaF_2, quartz, PMMA, PS, and PDMS, SFG data taken at the mussel adhesion interfaces combined with interfacial

H/D exchange experiments indicate surface dehydration after the attachment of the mussel adhesive plaques. The polymers interact differently with MFPs. The phenyl groups interact more strongly with MFPs than the methyl groups. For the hydrophilic antifouling polymers, pOEGMA and pSBMA, however, surface dehydration is to a less extent, and water can penetrate into the interface. On the pSBMA surface, in particular, surface hydration is almost unaffected by the mussel adhesives. Overall, this study suggests that surface dehydration is crucial for underwater adhesion and biofouling, and strong surface hydration is crucial to anti-biofouling.

4.2 Interfacial Structure of a DOPA-Inspired Adhesive Polymer

4.2.1 Introduction

Marine organisms such as barnacles[34] and mussels[2,35] are able to deposit adhesive protein mixtures and attach themselves to various surfaces even in wet environments.[36-40] Hence there is a need for understanding the origins of such strong adhesion. Although the exact mechanism of adhesive protein-surface interaction has not yet been completely revealed, the amino acid 3,4-dihydroxyphenylalanine (DOPA) has been proven essential for mussel adhesion[11,37] due to its cross-linking capability. The proposed DOPA cross-linking mechanisms include chemical oxidation[11,41], enzymatic oxidation[42], metal chelation[14,43] and disulfide formation[16]. Given that purification of such natural proteins tends to be difficult, DOPA has inspired the development of numerous bio-mimic synthetic polymers.[5,44-46] The simplest of these adhesive polymers, poly[(3,4-dihydroxystyrene)-*co*-styrene] (PDHSS) (Figure 4.10A), was reported to have a convenient synthetic route and strong adhesive bonding.[44] The effects of PDHSS composition and substrates on adhesion were investigated in detail recently.[47] It was

found that when the molar ratio of styrene to 3,4-dihydroxystyrene is 2:1, adhesive bonding is optimized. The polymer bonds well to a variety of surfaces including aluminum, steel, red oak and plastics with adhesion strength comparable to commercial glues. Mussel mimicking polymers with other applications in mind including anti-fouling[48-50] and surface modification[5,51] are also being developed with catechol groups at one end of the polymer chains for anchoring to surfaces.

Fundamental understanding of the adhesion mechanism for a simplified polymeric mimic will provide insights on DOPA-adhesion and help to guide the design of future high performance polymers. The pendant catechol group of PDHSS (i.e. the 3,4-dihydroxystyrene monomer) is believed to be essential for adhesion.[52] A prior report described the adhesion of catechol groups on organic and inorganic surfaces using atomic force microscopy (AFM).[10] Hydrogen bond formation between the catechol hydroxyl or quinone carbonyl group and the primary amine of a modified substrate, as well as covalent Michael addition reactions between the quinone and amine groups were proposed to explain adhesion.[10] Moreover, a recent simulation study of catechol adhesion on silica surfaces showed that both the hydroxyls and phenylene ring of catechol groups can contribute to strong surface binding due to hydrogen bonds and dispersion forces.[53] To date, however, there has not been any direct experimental evidence for these proposed mechanisms of adhesion. In order to understand the detailed, interfacial structures of such adhesive materials, we have used sum frequency generation vibrational spectroscopy (SFG) to study PDHSS.

The SFG theory has been reported in detail elsewhere.[54-57] In this current work, SFG spectroscopy was applied to study the structure of the PDHSS, a DOPA-inspired

polymer at different interfaces, including surfaces in air, water and polymeric substrates. Fourier transform infrared spectroscopy (FTIR) was also applied to provide analogous spectroscopic signals from the bulk sample. The catechol phenylene ring and the quinone ring of PDHSS were found to be ordered underwater, poised for adhesion. With buried polymer interfaces, benzene π-π stacking at the polystyrene (PS) (Figure 4.10B) interface, and hydrogen bonding between catechols and amines or reactions between quinones and amines at the poly(allylamine) (PAA) (Figure 4.10C) interface, are proposed to be the origins of adhesion.

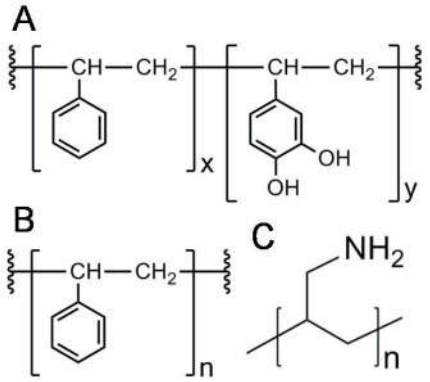

Figure 4.10 Structural formulas of (A) poly[(3,4-dihydroxystyrene)-co-styrene] (PDHSS) (x:y~2:1), (B) polystyrene (PS) and (C) poly(allylamine) (PAA)

4.2.2 Experimental Section

Polystyrene (PS) (M_w = 35,000 g/mol) and poly(allylamine) (PAA) solution (M_w = 17,000 g/mol, 20% w/w in H_2O) were purchased from Sigma-Aldrich. Tetrabutylammonium periodate $[(C_4H_9)_4N](IO_4)$ was synthesized following a protocol from literature[58] and confirmed by ultraviolet-visible absorption spectroscopy, ^1H NMR spectroscopy and melting point determinations. Deuterated polystyrene (d8PS) (Mw~207,500 g/mol) was purchased from Polymer Source Inc. $[(C_4H_9)_4N](IO_4)$ was

used for a cross-linking oxidant. PDHSS with a 2:1 molar ratio between styrene and 3,4-dihydroxystyrene was synthesized according to our method published previously.[44]

CaF_2 prisms (right angle) and windows (25 mm in diameter and 2 mm in thickness) were purchased from Altos Photonics (Bozeman, MT) and used for depositing the polymers. Prisms were used in SFG spectroscopy and windows in FTIR spectroscopy experiments. The CaF_2 substrates were dried in N_2 and plasma cleaned before use. Solvent for the PDHSS and $[(C_4H_9)_4N](IO_4)$ was 1:1 (v/v) acetone/dichloromethane. To prepare a thin film of PDHSS, 0.5% (w/w) PDHSS was spin-coated on a CaF_2 prism or window. For cross-linked PDHSS, a solution containing 0.5% PDHSS and 0.2% (w/w) $[(C_4H_9)_4N](IO_4)$ was used for spin-coating. Toluene cannot dissolve PDHSS thus could be used as a selective solvent for d8PS. To prepare the polymer double layer, a thin film of PDHSS was first spin-coated and after drying, another thin film of d8PS was then spin-coated from a 1% (w/w) toluene solution on top of the PDHSS film. Water was used for a selective solvent for PAA. Similarly a PDHSS-PAA double layer was prepared by spin-coating PDHSS and then PAA from a 1% (w/w) aqueous solution on top. Every solution was freshly prepared just prior to use. All samples except PAA were spin-coated at 3000 rpm for 30 s using a P-6000 spin coater (Speedline Technologies). PAA was spin-coated at 3000 rpm for 60 s. The thicknesses of the PDHSS, d8PS and PAA films were similar, around 40 nm, measured by a Dektak 6M surface profilometer (Veeco Instruments). Samples were dried in vacuum overnight prior to testing.

For these studies we used the same SFG spectroscopy system as reported previously.[59] Briefly, the visible and infrared (IR) input beams penetrate through a CaF_2 substrate and overlap spatially and temporally at the sample surface/interface, where the

pulse energies of the visible and IR beams are 10 and 100 μJ, respectively. The reflected SFG signal is collected by a monochromator along with a photomultiplier tube (PMT). In this research, we used a right angle CaF_2 prism for the solid support of the thin film sample, with a near critical angle geometry (Figure 4.11) for stronger reflected SFG signal. Here, the incident angles of the visible and IR beams are 60° and 54° with respect to the surface normal, respectively. All SFG spectra were collected using the ssp (sum frequency output, visible input, and IR input) polarization combination.

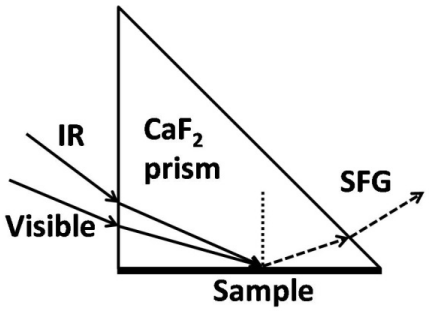

Figure 4.11 SFG spectroscopy experiment with a near critical angle geometry.

The FTIR spectroscopy experiments were carried out using a Nicolet Magna 550 FTIR spectrometer. All sample films were prepared on CaF_2 windows. Static water contact angle measurements were performed with a CAM 100 contact angle goniometer (KSV Instruments). At least three samples of each polymer type were used. Contact angles were measured on five different spots on each sample.

4.2.3 Results and Discussion

4.2.3.1 FTIR spectra

Prior to analyzing the SFG spectroscopy results, we collected IR spectra from various materials for proper peak assignments. Figure 4.12 shows the FTIR spectra of PS and PDHSS before and after cross-linking with periodate. All spectra show the 1600 cm^{-1}

peak due to C=C stretching from the phenyl ring. Before cross-linking, PDHSS shows a broad band from 3300-3600 cm^{-1} contributed from the catechol hydroxyl groups. Almost no signal could be found from the quinone carbonyl group. The spectrum detected from the cross-linked PDHSS shows a strong 1663 cm^{-1} peak contributed from the carbonyl group[60], but no signal from the catechol hydroxyl groups. Therefore, the FTIR spectra show oxidation of the catechol hydroxyl groups to quinone carbonyl groups resulting from the periodate cross-linking. Given that FTIR detects signals from the sample bulk, this oxidation reaction occurred in the entire sample. According to prior literature, cross-linking enhances the cohesion of this adhesive polymer system.[44,47]

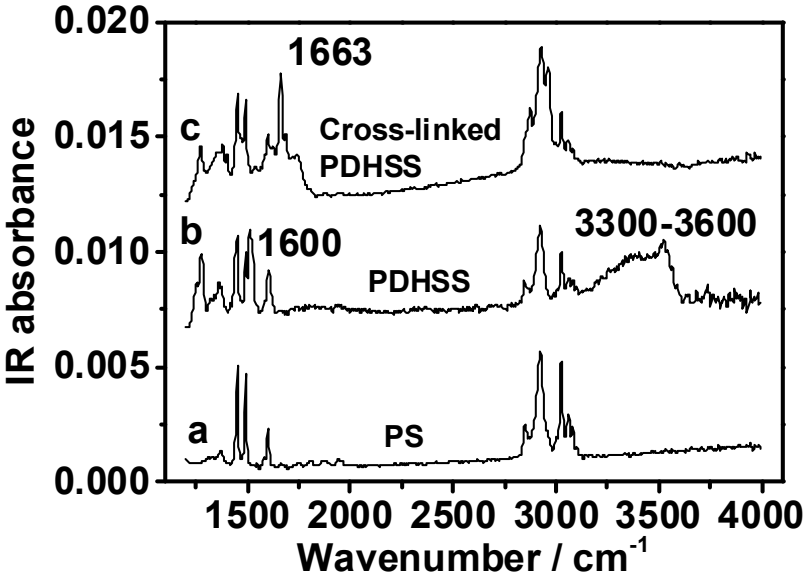

Figure 4.12 IR spectra of (a) PS, (b) PDHSS and (c) cross-linked PDHSS.

4.2.3.2 Air interface

SFG spectra were first taken in air for comparison with other interfaces. Figure 4.13 shows the SFG spectra detected from surfaces of PS, PDHSS and cross-linked PDHSS in air. Between 3000 and 3100 cm^{-1}, all three materials showed the same signal

from the benzene C-H stretching modes (Figure 4.13B), indicating that the phenyl rings were ordered. However, PS showed no signal between 1500 and 1800 cm^{-1}, indicating that the C=C stretching from the styrene was not detectable in SFG spectroscopy (Figure 4.13A, Curve a). In contrast, PDHSS before cross-linking showed a strong peak around 1610 cm^{-1} and a weak peak at 1663 cm^{-1} (Figure 4.13A, Curve b). The former peak was contributed by C=C stretching from the catechol ring, which has a different resonance structure from the styrene phenyl ring. The latter peak was from the quinone carbonyl group, which is also Raman active.[61] The carbonyl groups at the surface of PDHSS before cross-linking are likely from spontaneous oxidation of some catechol groups in air. After cross-linking the PDHSS, the SFG signal at 1663 cm^{-1} became stronger (Figure 4.13A, Curve c) owing to an increase in quinone carbonyl groups at the surface.

We sought to determine if the signals detected here were obtained from the surface in air and not from the interface between the CaF_2 and the polymer. Thick films of PDHSS, before and after cross-linking, were prepared by solvent casting PDHSS on CaF_2 prisms. The IR beam could not penetrate these thick films. Consequently, any signals that are observed should be from the interface between the CaF_2 and the polymer. In this experiment, no signal was observed between 1500 and 1800 cm^{-1}, indicating that at least most of the signals we obtained in Figure 4.13 were contributed from the surfaces in air.

These SFG results indicate that before cross-linking, the catechol ring was ordered and that some carbonyl groups already existed on the film surface due to partial oxidation of surface catechol groups in air. But for the sample bulk, formation of quinone

carbonyl groups required cross-linking. After cross-linking, the catechols were completely transformed to quinones, both on the surface and within the bulk material.

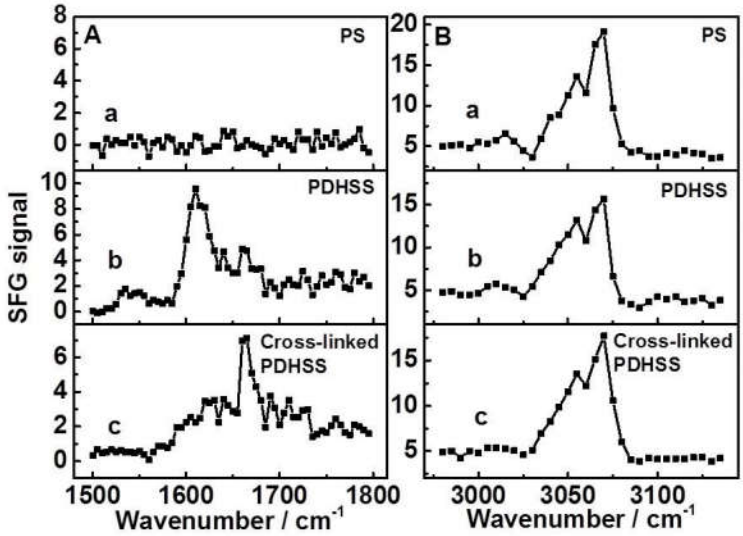

Figure 4.13 SFG spectra of (a) PS, (b) PDHSS and (c) cross-linked PDHSS in air in two different frequency regions.

4.2.3.3 Water interface

DOPA-based polymers can adhere strongly underwater.[37,38] Here we applied SFG spectroscopy to reveal the interfacial structure of PDHSS in water. Deuterated water (D_2O) was used in the experiment in order to avoid signal interference from H_2O. Figure 4.14 shows SFG spectra of the PS, PDHSS and cross-linked PDHSS surfaces when in contact with water. The PS did not exhibit any signal between 1500 and 1800 cm^{-1} (Figure 4.14A, Curve a). For PDHSS, there was a strong peak at 1610 cm^{-1} when in contact with D_2O. The signal was more intense than in air, indicating greater ordering of the catechol rings in D_2O than air due to interactions between phenolic hydroxyl groups and water (Figure 4.14A, Curve b). If the catechol ring also contributed to the signal between 3000 and 3100 cm^{-1} (Figure 4.13B, Curve b), we would likely have observed an analogous signal in water due to substantial ordering. However, the signal between 3000

and 3100 cm^{-1} of all three materials disappeared upon coming in contact with water (Figure 4.14B). Therefore, the lack of signal between 3000 and 3100 cm^{-1} is likely a contribution from styrene, not from the phenylene ring of the catechol. In fact, a previous SFG study of a catechol containing polymer showed that the catechol ring only has very weak signal around 3040 cm^{-1}, quite different from what we obtained in Figure 4.13B.[62] This result could be further explained by the fact that in PDHSS, the ratio of styrene and catechol is 2:1 and there are more C-H bonds per styrene than catechol. This assignment of the SFG signal is also consistent with a previous detailed analysis of vibrational modes of phenyl groups.[63] The disappearance of the signal was attributed to the unfavorable interaction between the hydrophobic phenyl ring on the styrene with water. After cross-linking, PDHSS showed a slightly weaker peak at 1663 cm^{-1} in water than in air, indicating that the quinone group was still stable and ordered. The SFG spectroscopy results discussed here suggest that both the catechol and quinone groups in the polymer were ordered underwater, ready for adhesion to surfaces.

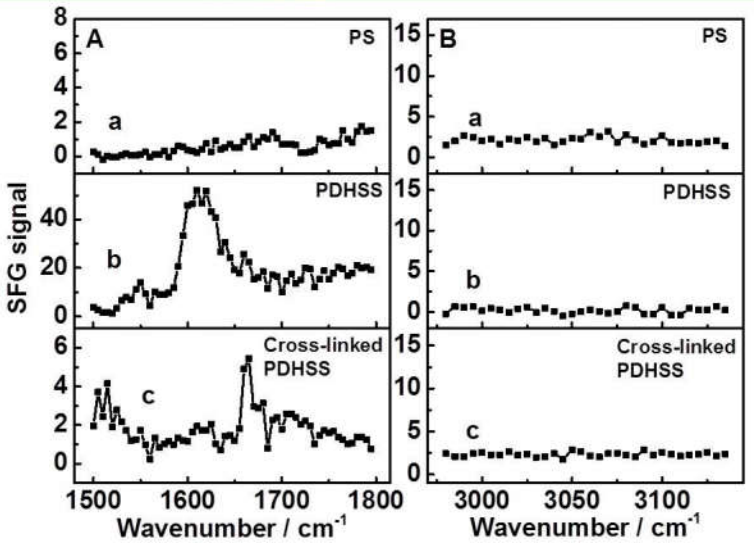

Figure 4.14 SFG spectra of (a) PS, (b) PDHSS and (c) cross-linked PDHSS in contact with D_2O in two different frequency regions.

4.2.3.4 Polymer interface

The PDHSS polymer is known to adhere to plastics[47] and DOPA can bind organic substrates with amino end groups.[10] Thus we probed the molecular structure of the polymer at buried interfaces between PDHSS and the model plastic d8PS and PAA films. Figure 4.15 shows SFG spectra of PDHSS before and after cross-linking, when sandwiched between a CaF_2 prism and a d8PS or PAA film.

The d8PS had no signal between 1500 and 1800 cm^{-1} (Figure 4.15A, Curve a), much like PS, therefore there should be no interference with the signals from the PDHSS/d8PS interface. The PDHSS/d8PS interface generated a stronger peak around 1610 cm^{-1} (Figure 4.15A, Curve b) than the PDHSS surface in air (Figure 4.13A, Curve b) due to better ordering of the catechol rings. For the cross-linked PDHSS/d8PS interface, when compared to the cross-linked PDHSS surface in air, the peak intensity at 1663 cm^{-1} remained constant but the band around 1610 cm^{-1} from quinone C=C stretching increased (Figure 4.15A, Curve c), indicating enhanced ordering of the quinone rings. This observation could be explained by π-π stacking between the catechol or quinone rings in PDHSS and the phenyl rings in d8PS. Such a π-π interaction can be one type of adhesive forces present in this system.[64]

To demonstrate that the SFG signals came from buried interfaces and that there was no PDHSS exposed to the double layer sample surface, water contact angles were measured for d8PS, PDHSS and PDHSS-d8PS double layer samples (Table 4.1). The same contact angles were observed for d8PS and PDHSS-d8PS double layer surfaces. The PDHSS sample has a smaller contact angle owing to the hydroxyl and/or carbonyl groups on the surface. This contact angle result showed that the PDHSS layer was

completely protected by the d8PS layer. Furthermore, thick film SFG spectroscopy experiments discussed previously showed no signal from the CaF_2/PDHSS interface. Therefore, the signals here are likely derived from the PDHSS/d8PS interface.

Table 4.1 Water contact angles of polymer samples prepared on CaF_2 windows

Sample	Contact angle (degree)
CaF_2-d8PS	89.4±1.2
CaF_2-PDHSS	77.3±1.7
CaF_2-PDHSS-d8PS	89.4±1.0

The PDHSS/PAA interface exhibits SFG signals that differ from those found for the PDHSS/d8PS interface (Figure 4.15B). The PAA film shows a very weak band around 1590 cm^{-1} (Figure 4.15B, Curve a) from -NH_2 bending[65,66], therefore this signal will not interfere with that of PDHSS. The PDHSS/PAA interface displays a strong peak at 1610 cm^{-1} (Figure 4.15B, Curve b) and looks very similar to the spectrum of PDHSS in water (Figure 4.14A, Curve b). This result indicates enhanced ordering of the catechol rings at the interface due to hydrogen bonding between the phenolic hydroxyl groups in PDHSS and the primary amine groups in PAA[10,53,67,68]. The cross-linked PDHSS/PAA interface shows a stronger 1610 cm^{-1} band and a weaker 1663 cm^{-1} peak (Figure 4.15B, Curve c) than the cross-linked PDHSS in air (Figure 4.13A, Curve c) or water (Figure 4.14A, Curve c). Here the stronger 1610 cm^{-1} band could be either from a C=N formed during a Schiff base reaction between amine and quinone[69-71] or a better ordered quinone ring resulting from a reaction or hydrogen bonding. The weakened carbonyl signal at 1663 cm^{-1} may also imply the presence of a Schiff base reaction which consumes the carbonyl groups.[72] Since the vibrational frequency of C=N in a Schiff base could overlap with C=C stretching, C=O stretching or -NH_2 bending, our results and prior reports[10,11,72]

provide no direct evidence of a Schiff base. However, the SFG spectroscopy results do suggest that such quinone + amine → Schiff base reaction is likely contributing here to adhesion.

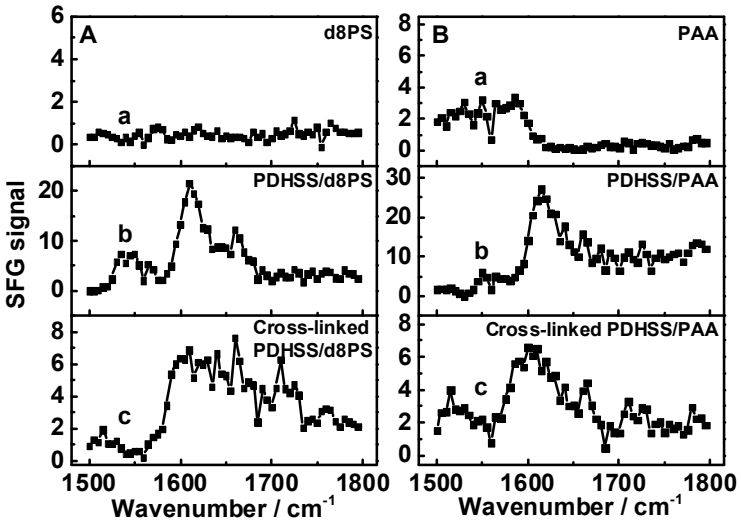

Figure 4.15 (A) SFG spectra of (a) d8PS film, (b) PDHSS/d8PS and (c) cross-linked PDHSS/d8PS double layer in air. (B) SFG spectra of (a) PAA film, (b) PDHSS/PAA and (c) cross-linked PDHSS/PAA double layer in air.

4.2.4 Conclusions

In this work, we have gained insight on the structure of a DOPA-inspired adhesive polymer at air, water and buried polymer interfaces by SFG spectroscopy. These SFG results show that in air, both the catechol and quinone rings were well-ordered. When contacting water, the catechol rings exhibited enhanced ordering and the quinone rings were still stable and ordered. These orderings appear to contribute to adhesion underwater. Two kinds of buried polymer interfaces were also investigated. Data from SFG spectroscopy indicate that at a PDHSS/d8PS interface, π-π stacking could be the primary adhesive force. At a PDHSS/PAA interface, phenolic hydroxyl groups appear to hydrogen bond whereas quinone carbonyl groups react to generate covalent bonds. These

molecular insights on the mechanisms of surface bonding may help us design future generations of biomimetic adhesive materials.

4.3 References

(1) Danner, E. W.; Kan, Y. J.; Hammer, M. U.; Israelachvili, J. N.; Waite, J. H. *Biochemistry* **2012**, *51*, 6511-6518.
(2) Coyne, K. J.; Qin, X. X.; Waite, J. H. *Science* **1997**, *277*, 1830-1832.
(3) Gohad, N. V.; Aldred, N.; Hartshorn, C. M.; Jong Lee, Y.; Cicerone, M. T.; Orihuela, B.; Clare, A. S.; Rittschof, D.; Mount, A. S. *Nat. Commun.* **2014**, *5*, 4414, doi:4410.1038/ncomms5414.
(4) Grozea, C. M.; Walker, G. C. *Soft Matter* **2009**, *5*, 4088-4100.
(5) Lee, H.; Dellatore, S. M.; Miller, W. M.; Messersmith, P. B. *Science* **2007**, *318*, 426-430.
(6) Sedó, J.; Saiz-Poseu, J.; Busqué, F.; Ruiz-Molina, D. *Adv. Mater.* **2013**, *25*, 653-701.
(7) Yu, J.; Wei, W.; Menyo, M. S.; Masic, A.; Waite, J. H.; Israelachvili, J. N. *Biomacromolecules* **2013**, *14*, 1072-1077.
(8) Lu, Q. Y.; Hwang, D. S.; Liu, Y.; Zeng, H. B. *Biomaterials* **2012**, *33*, 1903-1911.
(9) Hwang, D. S.; Harrington, M. J.; Lu, Q. Y.; Masic, A.; Zeng, H. B.; Waite, J. H. *J. Mater. Chem.* **2012**, *22*, 15530-15533.
(10) Lee, H.; Scherer, N. F.; Messersmith, P. B. *Proc. Natl. Acad. Sci. USA* **2006**, *103*, 12999-13003.
(11) Yu, M. E.; Hwang, J. Y.; Deming, T. J. *J. Am. Chem. Soc.* **1999**, *121*, 5825-5826.
(12) Harrington, M. J.; Masic, A.; Holten-Andersen, N.; Waite, J. H.; Fratzl, P. *Science* **2010**, *328*, 216-220.
(13) Yu, J.; Wei, W.; Danner, E.; Israelachvili, J. N.; Waite, J. H. *Adv. Mater.* **2011**, *23*, 2362-2366.
(14) Sever, M. J.; Weisser, J. T.; Monahan, J.; Srinivasan, S.; Wilker, J. J. *Angew. Chem. Int. Ed.* **2004**, *43*, 448-450.
(15) Zeng, H. B.; Hwang, D. S.; Israelachvili, J. N.; Waite, J. H. *Proc. Natl. Acad. Sci. USA* **2010**, *107*, 12850-12853.
(16) Yu, J.; Wei, W.; Danner, E.; Ashley, R. K.; Israelachvili, J. N.; Waite, J. H. *Nat. Chem. Biol.* **2011**, *7*, 588-590.
(17) Yu, J.; Kan, Y. J.; Rapp, M.; Danner, E.; Wei, W.; Das, S.; Miller, D. R.; Chen, Y. F.; Waite, J. H.; Israelachvili, J. N. *Proc. Natl. Acad. Sci. USA* **2013**, *110*, 15680-15685.
(18) Wei, W.; Yu, J.; Broomell, C.; Israelachvili, J. N.; Waite, J. H. *J. Am. Chem. Soc.* **2013**, *135*, 377-383.
(19) Maier, G. P.; Rapp, M. V.; Waite, J. H.; Israelachvili, J. N.; Butler, A. *Science* **2015**, *349*, 628-632.
(20) Chen, Z. *Prog. Polym. Sci.* **2010**, *35*, 1376-1402.
(21) Hankett, J. M.; Liu, Y. W.; Zhang, X. X.; Zhang, C.; Chen, Z. *J. Polym. Sci., Part B: Polym. Phys.* **2013**, *51*, 311-328.
(22) Zhang, C.; Myers, J. N.; Chen, Z. *Soft Matter* **2013**, *9*, 4738-4761.
(23) Roy, S.; Covert, P. A.; FitzGerald, W. R.; Hore, D. K. *Chem. Rev.* **2014**, *114*, 8388-8415.

(24) Richmond, G. L. *Chem. Rev.* **2002**, *102*, 2693-2724.
(25) Shen, Y. R.; Ostroverkhov, V. *Chem. Rev.* **2006**, *106*, 1140-1154.
(26) Lis, D.; Backus, E. H. G.; Hunger, J.; Parekh, S. H.; Bonn, M. *Science* **2014**, *344*, 1138-1142.
(27) Leng, C.; Hung, H.-C.; Sun, S. W.; Wang, D. Y.; Li, Y. T.; Jiang, S. Y.; Chen, Z. *ACS Appl. Mater. Interf.* **2015**, *7*, 16881-16888.
(28) Myers, J. N.; Zhang, C.; Lee, K.-W.; Williamson, J.; Chen, Z. *Langmuir* **2014**, *30*, 165-171.
(29) Leng, C.; Han, X. F.; Shao, Q.; Zhu, Y. H.; Li, Y. T.; Jiang, S. Y.; Chen, Z. *J. Phys. Chem. C* **2014**, *118*, 15840-15845.
(30) Wang, J.; Chen, C. Y.; Buck, S. M.; Chen, Z. *J. Phys. Chem. B* **2001**, *105*, 12118-12125.
(31) Fu, L.; Xiao, D. Q.; Wang, Z. G.; Batista, V. S.; Yan, E. C. Y. *J. Am. Chem. Soc.* **2013**, *135*, 3592-3598.
(32) Sulpizi, M.; Gaigeot, M.-P.; Sprik, M. *J. Chem. Theory Comput.* **2012**, *8*, 1037-1047.
(33) Liu, Y. W.; Leng, C.; Chisholm, B.; Stafslien, S.; Majumdar, P.; Chen, Z. *Langmuir* **2013**, *29*, 2897-2905.
(34) Dougherty, W. J. *Tissue Cell* **1990**, *22*, 463-470.
(35) Waite, J. H. *J. Biol. Chem.* **1983**, *258*, 2911-2915.
(36) Deming, T. J. *Curr. Opin. Chem. Biol.* **1999**, *3*, 100-105.
(37) Danner, E. W.; Kan, Y.; Hammer, M. U.; Israelachvili, J. N.; Waite, J. H. *Biochemistry* **2012**, *51*, 6511-6518.
(38) Shafiq, Z.; Cui, J.; Pastor-Pérez, L.; San Miguel, V.; Gropeanu, R. A.; Serrano, C.; del Campo, A. *Angew. Chem. Int. Ed.* **2012**, *51*, 4332-4335.
(39) Crisp, D. J.; Walker, G.; Young, G. A.; Yule, A. B. *J. Colloid Interf. Sci.* **1985**, *104*, 40-50.
(40) Lin, Q.; Gourdon, D.; Sun, C.; Holten-Andersen, N.; Anderson, T. H.; Waite, J. H.; Israelachvili, J. N. *Proc. Natl. Acad. Sci. U.S.A.* **2007**, *104*, 3782-3786.
(41) Monahan, J.; Wilker, J. J. *Langmuir* **2004**, *20*, 3724-3729.
(42) Suci, P. A.; Geesey, G. G. *J. Colloid Interf. Sci.* **2000**, *230*, 340-348.
(43) Zeng, H.; Hwang, D. S.; Israelachvili, J. N.; Waite, J. H. *Proc. Natl. Acad. Sci.* **2010**, *107*, 12850-12853.
(44) Westwood, G.; Horton, T. N.; Wilker, J. J. *Macromolecules* **2007**, *40*, 3960-3964.
(45) Yu, M.; Deming, T. J. *Macromolecules* **1998**, *31*, 4739-4745.
(46) Holten-Andersen, N.; Harrington, M. J.; Birkedal, H.; Lee, B. P.; Messersmith, P. B.; Lee, K. Y. C.; Waite, J. H. *Proc. Natl. Acad. Sci.* **2011**, *108*, 2651-2655.
(47) Matos-Perez, C. R.; White, J. D.; Wilker, J. J. *J. Am. Chem. Soc.* **2012**, *134*, 9498-9505.
(48) Brault, N. D.; Gao, C.; Xue, H.; Piliarik, M.; Homola, J.; Jiang, S.; Yu, Q. *Biosens. Bioelectron.* **2010**, *25*, 2276-2282.
(49) Statz, A. R.; Meagher, R. J.; Barron, A. E.; Messersmith, P. B. *J. Am. Chem. Soc.* **2005**, *127*, 7972-7973.
(50) Li, G.; Xue, H.; Gao, C.; Zhang, F.; Jiang, S. *Macromolecules* **2009**, *43*, 14-16.
(51) Ye, Q.; Zhou, F.; Liu, W. *Chem. Soc. Rev.* **2011**, *40*, 4244-4258.
(52) Wilker, J. J. *Nat. Chem. Biol.* **2011**, *7*, 579-580.

(53) Mian, S. A.; Saha, L. C.; Jang, J.; Wang, L.; Gao, X.; Nagase, S. *J. Phys. Chem. C* **2010**, *114*, 20793-20800.
(54) Lambert, A. G.; Davies, P. B.; Neivandt, D. J. *Appl. Spectrosc. Rev.* **2005**, *40*, 103-145.
(55) Zhuang, X. W.; Miranda, P. B.; Kim, D.; Shen, Y. R. *Phys. Rev. B* **1999**, *59*, 12632-12640.
(56) Perry, A.; Neipert, C.; Space, B.; Moore, P. B. *Chem. Rev.* **2006**, *106*, 1234-1258.
(57) Chen, Z.; Shen, Y. R.; Somorjai, G. A. *Annu. Rev. Phys. Chem.* **2002**, *53*, 437-465.
(58) Santaniello, E.; Manzocchi, A.; Farachi, C. *Synthesis-Stuttgart* **1980**, 563-565.
(59) Zhang, C.; Hankett, J.; Chen, Z. *ACS Appl. Mater. Interf.* **2012**, *4*, 3730-3737.
(60) Bagli, J. F. *J. Am. Chem. Soc.* **1962**, *84*, 177-180.
(61) Palmö, K.; Pietilä, L. O.; Mannfors, B.; Karonen, A.; Stenman, F. *J. Mol. Spectrosc.* **1983**, *100*, 368-376.
(62) Han, H.; Wu, J.; Avery, C. W.; Mizutani, M.; Jiang, X.; Kamigaito, M.; Chen, Z.; Xi, C.; Kuroda, K. *Langmuir* **2011**, *27*, 4010-4019.
(63) Lu, X. L.; Spanninga, S. A.; Kristalyn, C. B.; Chen, Z. *Langmuir* **2010**, *26*, 14231-14235.
(64) Chirdon, W. M.; O'Brien, W. J.; Robertson, R. E. *J. Biomed. Mater. Res., Part B* **2003**, *66B*, 532-538.
(65) Lio, K.; Minoura, N. *J. Polym. Sci., Part A: Polym. Chem.* **1992**, *30*, 2071-2073.
(66) Rivas, B. L.; Seguel, G. V. *Polym. Bull.* **1996**, *37*, 463-468.
(67) Loch, C. L.; Ahn, D.; Chen, C.; Wang, J.; Chen, Z. *Langmuir* **2004**, *20*, 5467-5473.
(68) Qin, Z.; Buehler, M. *Appl. Phys. Lett.* **2012**, *101*, 083702-083704.
(69) Zhang, Y.; Thomas, Y.; Kim, E.; Payne, G. F. *J. Phys. Chem. B* **2012**, *116*, 1579-1585.
(70) Rothschild, K. J.; Roepe, P.; Lugtenburg, J.; Pardoen, J. A. *Biochemistry* **1984**, *23*, 6103-6109.
(71) Rothschild, K. J.; Marrero, H. *Proc. Natl. Acad. Sci. U.S.A.* **1982**, *79*, 4045-4049.
(72) Chen, H. Y.; McClelland, A. A.; Chen, Z.; Lahann, J. *Anal. Chem.* **2008**, *80*, 4119-4124.

CHAPTER 5 CONCLUSIONS AND FUTURE OUTLOOK

5.1 Conclusions

In this thesis, the molecular-level surface structures and/or hydration of various novel antifouling materials, such as biocide modified PDMS coatings, amphiphilic polymers, and zwitterionic materials, have been investigated using SFG spectroscopy supplemented by other techniques. Surface restructuring behaviors of the polymers in water have been elucidated and correlated to their antifouling and other applications. The effects of polymer structure, pH, salt, and proteins on the surface hydration of zwitterionic polymers have been investigated to reveal their nonfouling properties. The buried interfacial structures of adhesion interfaces relevant to biofouling have also been investigated to get a molecular understanding of bio-adhesion underwater. The adhesion mechanisms have been revealed by in situ probing the adhesion interfaces of mussel adhesives and the buried interfaces of a mussel inspired polymer. These research results will greatly facilitate the design and development of new antifouling and adhesive materials with improved properties.

SFG spectroscopy was applied to investigate the surface structures of PDMS materials incorporated with QAS-based biocides in situ for antifouling and fouling release applications. Polymers prepared from TES-QAS showed better antifouling performance, which generated stronger SFG signals from the alkyl groups in sea water.

This shows that the different reaction dynamics of methoxysilane and ethoxysilane can lead to different surface structures of QAS-tethered PDMS, resulting in different antifouling activities. In addition, coatings prepared from QAS-tethered 18K-PDMS generated stronger SFG signals from the QAS alkyl chains than those prepared from the QAS-tethered 49K-PDMS, because 18K-PDMS could provide more end groups for QAS tethering. The surface orientation of the alkyl chains in QAS plays an important role in preventing bacterial biofilm growth. This study provides a general set of guidelines to follow when designing PDMS materials incorporated with QAS to generate antifouling coatings: The QAS groups need to aggregate to the surface and the QAS alkyl chains need to extend fully into the aqueous environment. As a result, the long alkyl chains can penetrate into the cell membrane and kill microorganisms.

In addition to the modified PDMS coatings, the surface structures of environmentally benign amphiphilic polymers were studied to reveal their antifouling mechanisms. Three polybetaines with different side chains were investigated, which showed different surface structures in water. The SFG results showed that the side chains of the three polymers were all present on the surfaces in air. In water, the OEG and alkyl chains remained on the coating surfaces, while the fluorocarbon chains withdrew from the water interface. For polybetaines with the fluorocarbon chains, both the quaternary amine groups and the carboxylate groups were present at the water interface, where the carboxylate groups formed hydrogen bonds with water molecules. The structural information obtained from the SFG data provided direct experimental evidence of the antifouling mechanisms of the amphiphilic materials: The good antifouling properties of the material with the OEG chains were due to the surface presence of the OEG groups; it

has been extensively shown that the surface OEG groups lead to improved antifouling activity. The poor antifouling performance of the material with the alkyl chains was due to the surface presence of the alkyl side chains in water, which resulted in protein adsorption via hydrophobic interactions. The material with the fluorocarbon chains also exhibited good antifouling performance, because the fluorocarbon groups retreated into the bulk of the coating in water so that the zwitterionic groups were exposed to the water interface. It has been demonstrated that zwitterionic materials can be good antifouling materials. This research indicates that side chains can greatly influence the polymer surface structures in water, resulting in different antifouling properties.

Besides the amphiphilic polybetaines, the surface structures and hydration of a series of sequence-specific amphiphilic polypeptoids were investigated with SFG spectroscopy and correlated to their antifouling and fouling release performances. SFG spectra of the polymer surfaces in air revealed the sequence-dependent surface coverage of the hydrophilic peptoid units as a function of the number and position of the hydrophobic fluorinated peptoid units in the polymer chain. The surface coverage of the hydrophilic units is inversely correlated to the surface fluorine concentration. The SFG results of the polymer/water interfaces showed that the ability of the polymer surfaces to orient and form strongly hydrogen bonded water is sensitively dependent on the sequence of the peptoids, which determines their hydrophilicity and surface restructuring rate underwater. The surface coverage of the hydrophilic peptoid units and the strong interaction between the polymers and water are well-correlated to their antifouling properties. The surface restructuring rate of the polypeptoids upon contact with water is also well-correlated with their fouling-release properties.

Coatings that can resist oil adhesion in water can be utilized for oil/water separation. An oil/water separation film was prepared using PDDA/PSS multilayers. The molecular mechanism for oil/water separation was elucidated using SFG spectroscopy. Oil stick to the PDDA-capped surface in water because the methyl groups on the quaternary amine groups tilted on the surface which bind oil molecules. The PSS-capped surface repelled oil completely due to the strong hydration of the sulfonate groups. Further, the correlation between the surface wetting behavior of polyeletrolyte multilayers (PEM) and their surface local structures will shed light on the study of PEM internal structures, which are still under debate. Due to the operational simplicity and versatility of layer-by-layer deposition, our success in using $(PDDA/PSS)_4$-coated meshes for efficient oil-water separation also endorses the technical significance of PEMs in self-cleaning applications.

In addition to polymer structures, surface hydration of the polymers also plays a critical role in determining their nonfouling properties. Strong hydration has been proved as a key contributor to the nonfouling performance of zwitterionic materials. The effects of ions and pH on the surface hydration of three zwitterionic polymer brushes were examined using SFG spectroscopy. The SFG results indicated the presence of strongly hydrogen bonded water at polymer/water interfaces. Ions have different binding affinities to the polymers as indicated by the reduced ordering of interfacial water due to ion binding. For example, pCBAAs bind Na^+ more strongly than K^+ while pSBMA binds K^+ more strongly than Na^+. All three materials bind divalent cations more strongly than monovalent cations and pCBAA2 binds Mg^{2+} and Ca^{2+} more strongly than pCBAA1. Furthermore, for pCBAAs, lower pH of water leads to weaker ordering of the interfacial

water molecules. At pH 5, water was still ordered at the pCBAA1/water interface but was completely random at the pCBAA2/water interface. Different from pCBAAs, the ordering of water at the pSBMA/water interface was not affected by pH in the same range.

The surface hydration of pSBMA and pOEGMA were further studied in contact with protein solutions using SFG spectroscopy. The hydration layer at the pSBMA surface was not affected by proteins, whereas that at the pOEGMA surface was considerably disturbed. The effects of free sulfobetaine and PEG on the surface hydration of proteins were also investigated. Whereas water was strongly bonded at the protein surfaces with the presence of free sulfobetaine molecules in solution, a significant amount of weakly hydrogen-bonded water molecules was observed at the interface between proteins and free PEG solutions. Different from free PEG, when the proteins were in contact with PEG coated gold nanoparticles, a majority of strongly hydrogen-bonded water was observed, which is similar to the pOEGMA surface. In summary, the study on the surface hydration of both polymers and proteins suggests that for PEG-coated surfaces and nanoparticles, although surface hydration is disrupted by proteins to a certain degree, it is still relatively strong and resists protein adsorption. However, free PEG binds to proteins, reducing their hydration significantly. For sulfobetaine-coated surfaces or free sulfobetaine, surface hydration remains strong in contact with proteins.

The surface hydration of the zwitterionic and PEG materials was revisited using isotopic dilution spectroscopy. The use of isotopic diluted water greatly simplified the data analysis of SFG O-H stretching signal. With the elimination of Fermi resonance, the strongly and weakly bonded water molecules were easily distinguished. Only strongly

hydrogen-bonded water molecules were observed on the zwitterionic surfaces whereas the surface hydration of pOEGMA contained a small amount of weakly hydrogen-bonded water. For the two control polymer samples, PMMA and PET, the weakly hydrogen-bonded interfacial water molecules generated strong SFG signals. These results demonstrated again that the interfacial water structure is crucial in determining the nonfouling performance of the polymer materials.

While a variety of materials have been developed and studied to resist biofouling, we can learn from biofouling to develop underwater adhesive materials. Buried interfaces between mussel adhesives and different substrates in water were probed in situ using SFG. On the surfaces of CaF_2, quartz, PMMA, PS, and PDMS, SFG data taken at the mussel adhesion interfaces combined with interfacial H/D exchange experiments indicated surface dehydration after the attachment of the mussel adhesive plaques. The polymers were found to interact differently with the mussel proteins. The phenyl groups interact more strongly with proteins than the methyl groups. For the hydrophilic antifouling polymers, pOEGMA and pSBMA, however, surface dehydration was to a less extent, and water could penetrate into the interface. On the pSBMA surface, in particular, surface hydration was almost unaffected by the mussel adhesives. Overall, this study suggests that surface dehydration is crucial for underwater adhesion and biofouling, and strong surface hydration is crucial to anti-biofouling.

Further, the interfacial structures of a mussel inspired adhesive polymer (PDHSS) were investigated using SFG spectroscopy. The SFG results showed that in air, both the catechol and quinone rings were well-ordered. When contacting water, the catechol rings obtained enhanced ordering and the quinone rings were still stable and ordered. These

orderings appeared to contribute to adhesion underwater. Two kinds of buried polymer interfaces were also examined. At the PDHSS/d8PS interface, π-π stacking could be the primary adhesive force. At the PDHSS/PAA interface, phenolic hydroxyl groups appeared to hydrogen bond whereas quinone carbonyl groups reacted to generate covalent bonds. These molecular insights to the mechanisms of surface bonding may help us design future generations of biomimetic adhesive materials.

Table 5.1 Molecular mechanisms of antifouling materials and underwater adhesives

	Samples	**Antifouling/adhesion mechanisms**	**Interactions with proteins**	**At mussel adhesive interface**
Antifouling Materials	QAS modified PDMS	Surface alkyl chains sticking out		
	Amphiphilic polymers	Strong hydration		
	Zwitterionic polymers	Strong hydration	Strong hydration unaffected by proteins	Strong hydration
	PEG	Strong hydration	Hydration disturbed by proteins	Strong hydration
Underwater adhesives	Mussel adhesive proteins	Interfacial dehydration		Dehydration on CaF_2, SiO_2, PMMA, and polystyrene
	DOPA	Hydrogen bonding or reaction with primary amine, phenyl π-π interaction		

As summarized above, our studies focused on two aspects of biofouling. Biofouling causes many issues, so we aimed to understand and develop antifouling materials. We also learned from biofouling to develop underwater adhesive materials. The research in this thesis provides profound knowledge about the molecular mechanisms of various antifouling materials. At the polymer/water interfaces, both the

polymer structures and water structures are important to their antifouling performances. In addition, bio-adhesive interfaces underwater were revealed to understand the molecular mechanisms of biofouling, which helps to better develop both adhesive materials and antifouling materials. The most important results of this thesis about the molecular mechanisms and design rules for antifouling materials and underwater adhesives are summarized in Table 5.1. For example, a good antifouling amphiphilic or hydrophilic material must bind water molecules very strongly in contact with an aqueous environment. The water binding property of the material can be evaluated using SFG spectroscopy by characterizing the signal at 3200 cm^{-1} generated by the interfacial water molecules. A good underwater glue should possess the ability to dehydrate an underwater surface to adhere to the surface.

5.2 Future Outlook

Although this thesis presented substantial progress in understanding biofouling and anti-biofouling, much is remained to be investigated in the future.

For antifouling materials, mixed charged polymers are potential candidates in addition to zwitterionic polymers. The structure of a sulfobetaine based mixed charged polymer (Figure 5.1) is similar to pSBMA, but the charged functional groups are randomly distributed in the polymer.[1] Mixed charged polymers are of interest to study because they are easier to synthesize. There is no need to synthesize zwitterionic monomers first. Besides, there are more variations of charged monomers to be tested. For the mixed charged polymer shown in Figure 5.1, the charge ratio can be controlled via synthesis and characterized using XPS by quantifying the amount of N and S elements. We hypothesized that when the positive and negative charge ratio equals one, the mixed

charged polymer should have similar strong hydration and antifouling property as pSBMA although the charged groups are not necessarily on the same side chain, unlike pSBMA. The hydration of mixed charged polymers as a function of the charge ratio will be investigated in the future. The effects of pH and salts on the interfacial water structure on mixed charged polymer surfaces will also be studied using SFG. The hydration behavior of the mixed charged polymers in response to environmental changes (e.g. pH, ionic strength) will be compared to pSBMA with samples of different thicknesses.

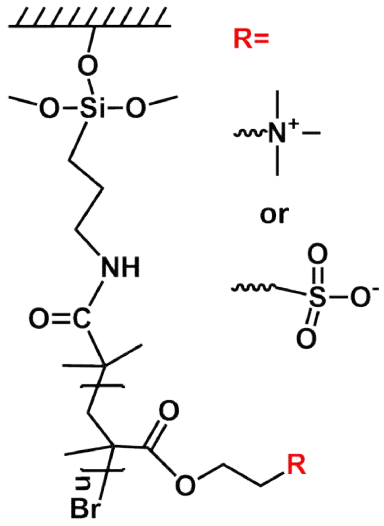

Figure 5.1 Molecular structure of a mixed charged polymer synthesized on a silica substrate.

In addition to antifouling purposes, mixed charged materials have great potential in biomedical applications. Mixed charged gold nanoparticles have been tested for cell endocytosis and the charge ratio of the nanoparticle surfaces affects their interaction with cells in different pH environments.[2] We hypothesized that in addition to the charge effect, the hydration layer around the particles in response to pH also plays a critical role in modulating their interactions with cells (Figure 5.2). The hydration of the mixed charged gold nanoparticles will be investigated as a function of charge ratio and pH. The effect of

the nanoparticles on the surface hydration of hydrophilic and hydrophobic surfaces will also be studied. Then, the interaction between biomolecule (e.g. sugar, receptor) modified mixed charged gold nanoparticles and model lipid bilayer will be monitored using SFG spectroscopy to understand such interactions and how nanoparticles enter into cells.

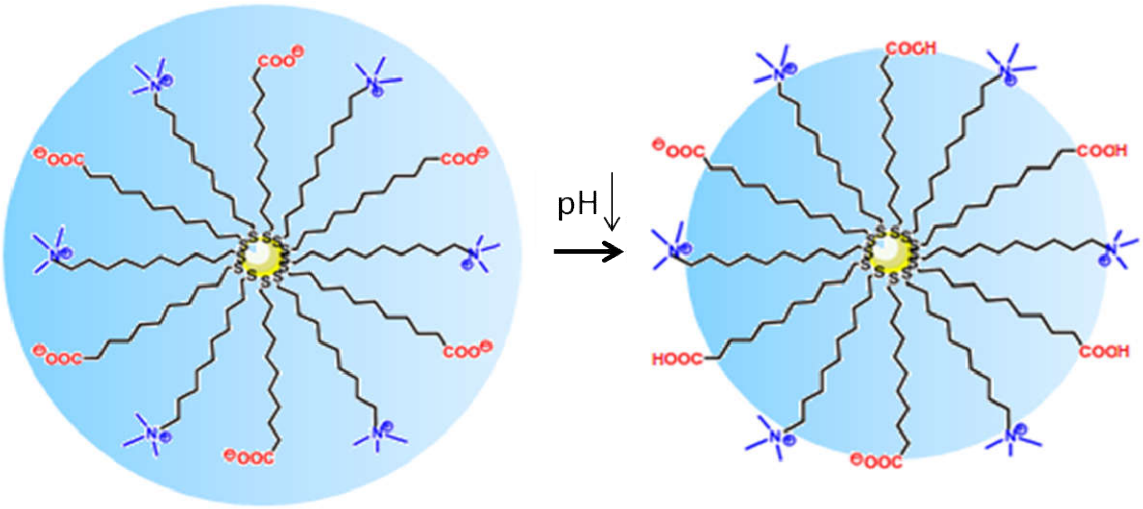

Figure 5.2 Surface hydration of a mixed charged nanoparticle in response to pH. The charged molecules on the particle surface contain quaternary amine and carboxyl groups. When pH decreases, some of the carboxyl groups are protonated and the hydration on the particle decreases.

In this thesis, the strong surface hydration of zwitterionic polymers has been proved to be critical to their nonfouling properties. Some biomolecules like peptides and proteins are zwitterionic in nature and may have similar properties. For example, bovine serum albumin (BSA) has been widely used in bio-assays to resist nonspecific binding of biomolecules. It is commonly believed that this is due to the inertness of BSA.[3] In this thesis, strong hydration of BSA has been observed, and we believe that other than inertness, strong hydration is the key to resist nonspecific binding. We also hypothesize that strong hydration is a universal property of various albumins. The surface hydration of a wide spectrum of albumin molecules will be studied in comparison with other

protein molecules. In addition, casein and fish gelatin have similar properties and will be investigated as well. The effect of these proteins on the hydration of zwitterionic and PEG materials will be further examined.

On the adhesion mechanisms of mussel proteins, the SFG data will be correlated to the adhesion strength on different substrates. Different surfaces with large surface areas will be prepared for mussels to deposit adhesive proteins in our collaborator's lab. The number of the protein plaques on each surface will be counted to show the preference of mussels to stick to these surfaces. Then, the adhesion force of the mussel proteins on the substrates will be measured. The effect of surface hydration/dehydration and surface chemistry of the substrates will be correlated to the adhesion strength on these substrates. Such a study will provide in-depth understanding of the adhesion mechanisms of mussels. In addition to mussels, the adhesion mechanisms of other marine animals causing biofouling such as barnacles and oysters will be investigated in the future.

5.3 References

(1) Bernards, M. T.; Cheng, G.; Zhang, Z.; Chen, S. F.; Jiang, S. Y. *Macromolecules* **2008**, *41*, 4216-4219.
(2) Liu, X.; Chen, Y.; Li, H.; Huang, N.; Jin, Q.; Ren, K.; Ji, J. *ACS Nano* **2013**, *7*, 6244-6257.
(3) Zhang, B.; Wang, X.; Liu, F.; Cheng, Y.; Shi, D. *Langmuir* **2012**, *28*, 16605-16613.